# Non-continuous porous media flow. November 1965.

**Author:**
Watson, K. K.

**Publication details:**
Report No. UNSW Water Research Laboratory Report No. 84

**Publication Date:**
1965

**DOI:**
https://doi.org/10.4225/53/5796c73fa7789

**License:**
https://creativecommons.org/licenses/by-nc-nd/3.0/au/
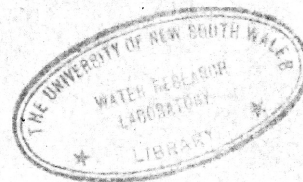Link to license to see what you are allowed to do with this resource.

# THE UNIVERSITY OF NEW SOUTH WALES

## WATER RESEARCH LABORATORY
### Manly Vale, N.S.W., Australia

**REPORT No. 84**

# Non-Continuous
# Porous Media Flow

by

## K. K. Watson

**NOVEMBER, 1965**

The University of New South Wales

WATER RESEARCH LABORATORY.

NON-CONTINUOUS POROUS MEDIA FLOW

The measurement and analysis of aspects
of the non-continuous unsteady flow of
water in an initially saturated sand column.

by

K. K. Watson

Report No. 84

November, 1965.

- - - - - - - - - - - - - -

# Preface.

The research reported in this document was sponsored by the Water Research Foundation of Australia.

It was carried out under the general direction of Professor C. H. Munro, Foundation Professor of Civil Engineering and Head of the Department of Water Engineering.

R. T. Hattersley,
Senior Lecturer in Civil Engineering,
Officer-in-Charge,
Water Research Laboratory.

22. 11. 65

## ABSTRACT

Non-continuous unsteady flow in unsaturated porous materials is defined and it is shown that time-dependent problems of this type, having varying boundary conditions, are representative of many commonly occurring, yet complex, field situations. The exacting experimental requirements for the comprehensive measurement of this type of flow in laboratory columns are then discussed and the relevant literature reviewed.

The design and construction of the traversing mechanism is considered and detailed descriptions given of the methods used for the simultaneous measurement with rapid response of the soil-water suction and the water content. Calibration and correction procedures for these methods are also considered in detail.

The draining of an initially saturated sand column to atmosphere at its base is then studied from an experimental and analytical viewpoint and particular attention paid to the nature of the hydrologic characteristics of the sand fraction under dynamic conditions. The differential equation of flow is solved numerically using a digital computer and comparisons made between the measured and computed moisture profiles.

Finally, the form of the hysteresis behaviour of the sand fraction under wetting and drying is measured and the effect of pore-air compression, during rewetting under excess surface water, on both infiltration and drainage is considered. A numerical approach for the solution of this latter problem is suggested.

# TABLE OF CONTENTS

# CHAPTER 1

## INTRODUCTION

The general objectives of this study and the philosophy behind the ordered development of the work may be introduced most clearly by a consideration of the sub-title:

"The Measurement and Analysis of Aspects of

the Non-Continuous Unsteady Flow of Water in

an Initially Saturated Sand Column."

The principal operative words in this title are found in the expression 'non-continuous', which has reference to the lack of continuity in the supply of water to the upper boundary of the system. The most commonly occurring field example of such flow is the infiltration-redistribution sequence and its cyclic repetition. In this, and similar non-continuous systems, there will occur at times during the cycle a wetting-up or draining of a previously drained or wet section of the soil profile. Because of the hysteresis effect in the relationship between soil-water suction and water content during wetting and drying it is not possible to approach such non-continuous flow problems using any method which assumes the soil suction to be a single-valued function of the water content. On the contrary, it is necessary for both these variables to be measured simultaneously and with rapid response by non-destructive means. When this is achieved the pressure and moisture changes in the column during any cyclic treatment of water application are able to be followed.

The nature of most non-continuous systems is such that, in addition to the complication of hysteresis, a further complication occurs due to changes in the pressure of the pore air. This also may be illustrated from infiltration-redistribution where pore-air pressure

changes occur during the second and subsequent infiltration cycles. This results from the air, which enters the pore space during redistribution, being unable to escape (or in some cases, hindered in escaping) due to the very wet region lower down the column; accordingly, as the wet front descends the air becomes compressed with consequent effects on the infiltration rate and drainage movement in the lower part of the column.

The design and construction of measuring equipment to allow investigation in laboratory columns of this type of hitherto intractable time-dependence problem involving the complex interrelation of changes in the water content, soil suction and pore-air pressure becomes therefore, the first requirement of the study. In addition, calibration procedures require careful consideration and dynamic correction techniques need development for those situations where the variables change very rapidly.

The particular non-continuous system examined is that of a saturated column of porous material (a sand fraction) which, firstly drains to atmosphere at its base and then is wetted at its upper surface with water in excess of the infiltration capacity. The initial saturation of the sand has decided advantages in these early experiments in this complex field for it makes possible, at the commencement of the test, a fully interpretable series of pressure measurements. This would not be the case with a column of initially dry material. In addition, initial saturation permits comparison of the draining moisture characteristics determined under unsteady state and equilibrium conditions. The use of the sand fraction as the porous material is also advantageous because its low air-entry value (approx. 40 cm. of water) obviates the necessity for long columns in obtaining measurements during the drainage cycle. Notwithstanding this, the traversing

equipment has been designed to accommodate columns up to 180 cm. in length.

The scope of the experimentation and analysis is such that reference could be made to a large body of published material. However, in this written presentation the review of literature, which forms the substance of the next chapter, has been purposely restricted to cover only those papers which are particularly relevant to the various facets of the work.

It is of interest to note that the significant nature of flow in unsaturated porous materials has been highlighted in the recent report (Linsley (1964)) of the American Geophysical Union Committee on Status and Needs in Hydrology. The Committee listed sixty-three areas of research in Hydrology in approximately priority order. The first area of research was as follows:

"Flow in Unsaturated Porous Media. This study covers the development of the mechanics of water movement, in liquid and vapour form, through the unsaturated zone including the soil, subsoil and other Earth materials, and it covers infiltration from the land surface, seepage of surface water, capillary rise and vapour transport."

## CHAPTER 2

## REVIEW OF LITERATURE

The published material which is of significant value in this study has been considered in the following pages under a series of headings relating to the principal experimental and analytical aspects.

### 2.1   Measurement of Water Content

There is a vast literature available on water content measurement but most of this can assist little in the present work because of the demanding nature of the experimental requirements.  The full specification for water content measurements in column experiments of the non-continuous unsteady flow type is as follows:-

(a)   Accurate measurement over a small thickness of the sample to approximate as closely as possibly a planar measurement.

(b)   Determination by non-destructive means and in such a way that flow in the column is not impeded.

(c)   Measurement over a short time interval.

(d)   Rapid means of making measurements at different parts of the soil column.

(e)   Provision for an automatically obtained record of readings with time.

For those soils where the water content changes occur quickly the above specification is in no way excessive, each aspect being a necessity for accurate measurement.  The exacting nature of the specification is such that only one published technique is capable of satisfactorily meeting it.

Ferguson (1959) seems to have been the first to show that the principle of gamma-ray absorption could be used to accurately infer the moisture content of a soil from changes in the soil density, for those soils in which the pore geometry remains unchanged during water content variations. In the study, the low energy isotope $Cs^{137}$ (20 mc.) was used as a gamma-ray emitter, because of the poor absorption properties of water for high energy gamma rays and the greater ease of collimating and counting efficiently the low energy radiation. The equipment lacked a discriminator facility and, accordingly, the thickness of sample measurement was limited solely by collimation. In addition, this prevented the attenuation equation from being used to calculate water contents and made it necessary to use empirical calibration procedures. The above study has been more briefly reported by Ferguson and Gardner (1962).

Rawlins (1961) extended the above equipment by including a ratemeter and recorder and using a $Cs^{137}$ source of greater intensity (100 mc.). Such an arrangement enabled more rapidly changing moisture contents to be measured and facilitated the recording of readings at several column positions. Although this arrangement was more sophisticated no comment was made on whether electrical means were used to limit the energy band measured and it must be presumed that again reliance was placed on collimation for sample volume restriction.

Gurr (1962) used the method to measure the water movement and permeability of a short column of a loam soil, which was wetted at the bottom and then evaporated at the top. The rate of change of water content in this experiment was very slow allowing a scaler to be used for measuring the gamma radiation. In addition, Gurr (1964) has described a method suitable for calculating the water contents from gamma-ray readings for a column of an undisturbed field soil with

unknown initial moisture conditions.

The use of a pulse height analyser allowed Davidson et al. (1963) to limit the energy band measured and thus eliminate from the radiation measurement all scattered and secondary radiation. With the measurement of almost entirely monoenergetic gamma radiation the empirical calibration procedures could be dispensed with and the attenuation equation used directly in determining the water content.

Since the gamma-ray method with an appropriate traversing mechanism can adequately meet all aspects of the water content specification for non-continuous unsteady flow it has been used in this study. Watson (1963) has given a brief report of the early stages of the work. One essential feature of the method, detailed in Chapter 5 and absent from the literature, concerns the correction procedure for ratemeter lag; this is necessary when the ratemeter readings change very rapidly (as in the drainage of a saturated column) and the accuracy requirements of the experiment do not permit a small time constant to be used.

## 2.2   Measurement of Soil-Water Suction

In considering the general question of the type of device to be used for the soil-water suction measurements it is important to remember that the gamma-ray absorption method for water content measurements, as mentioned in section 2.1, is strictly applicable only to non-shrinking soils. This means that equipment capable of measuring suctions up to approximately one atmosphere will satisfactorily meet the needs of most of the porous materials which could be used. These considerations clearly point to the tensiometer as the preferred instrument.

A tensiometer system for the measurement of rapidly changing suctions in column experiments should have the following features :

(a)　A high gauge sensitivity.

(b)　A response time of the order of a few seconds or less.

(c)　Rapid means of reading at least ten tensiometers.

(d)　The convenience of recording the suction changes with time.

It must be noted that the achievement of a very rapid response in the tensiometer system to suction changes in the soil inherently implies a negligibly small exchange of water between the soil and the tensiometer.

Miller (1951) described equipment for measuring rapidly changing suctions. Essentially it was a null method in which a suction change was detected by an optical lever system attached to a sylphon bellows. By means of a second bellows arrangement the manometer in a manometric system was adjusted until no deflection of the optical system occurred with the tensiometer connected to one side of the sylphon bellows and the manometer to the other. The system was rather ingenious and inexpensive but the manipulations necessary would preclude its use for very rapidly changing systems. In addition the arrangement did not lend itself to ease of recording.

Croney (1952) adapted a suction plate apparatus in a manner that resulted in an almost null system. The small water-filled reservoir below the suction plate was connected to a horizontal flow tube in which the water meniscus was clearly visible. A vacuum was applied to the open end of the tube and so regulated that the meniscus was held in a constant position. Such an arrangement could be used with a tensiometer. The technique was a simple one but would have the limitations of precise vacuum control for several tensiometers and the difficulty of recording.

The method used by Graecen (1960) was similar in principle to that of Miller (1951). The tensiometer cup was connected through a

capillary tube with bubble to a variable mercury manometer. Any tendency for movement of the bubble was corrected by changing the balancing pressure by means of a metal bellows.

Leonard and Low (1962) have recently developed a self-adjusting null point tensiometer. This instrument represents the natural development of the more rudimentary system of Miller (1951). However, as the authors state, there could be limitations to the system when measuring rapidly changing suctions; no investigations to date have been conducted on minimum response time. It is not apparent how a recording system could be easily linked with the instrument. In addition, there would be delays during adjustments when switching from tensiometer to tensiometer.

Klute and Peters (1962) have reported the satisfactory use of a pressure transducer of the diaphragm type for soil suction measurements. Although a pressure transducer requires some movement of water from the soil to displace the diaphragm the volume displacement-pressure characteristics of these instruments are such that the volume of water transfer across the cup is very small particularly for the low suctions involved in measurements with sand columns. With appropriate ancillary equipment the tensiometer-pressure transducer system is able to meet fully the specification listed at the beginning of this section; accordingly, it has been used in the present equipment, as discussed by Watson (1963).

## 2.3 Pore-Air Compression

It has been realized for a considerable time (Powers (1934), Free and Palmer (1940)) that a reduction occurs in the infiltration rate when the pore air which is normally allowed to escape to atmosphere through the base of the column is prevented from doing so due to an impervious base or saturated layer of soil. The above studies were

valuable but the conclusions assisted little in providing an understanding of the physical mechanisms involved.

Recently Wilson and Luthin (1963) have reported a series of comprehensive tests in which three conditions of obstruction were examined: the more usual ideal laboratory condition of no obstruction, partial obstruction as occurs during infiltration into a stratified column with the lower zone of lesser air permeability and complete obstruction. The theoretical and practical implications of the experiments were detailed, particular reference being made to the limitations of diffusion theory when there is pore-air compression.

Adrian (1964) reformulated the flow equations by making a number of simplifying assumptions so that the changes in infiltration brought about by air resistance could be more easily examined. The assumptions were that during infiltration the saturation of the wetted zone was constant and that a sharp wetting front existed. The capillary forces assisting infiltration were assumed to act at this definite air-water interface. As would be expected, for uniform fine materials the approximate model yielded good agreement between predicted and experimental values. However, the agreement was not so good for coarser mediums and those having a wide grain size distribution. In addition, attention was given to instability of the porous medium during pressure build-up and predictions were made concerning when column breakage would occur.

Youngs and Peck (1964) have presented a theoretical treatment of infiltration into a horizontal column with pore-air pressure changes in a form using reduced variables. The vertical case was also considered but could not be posed in terms of reduced variables due to the gravity term. Detailed comments were also made concerning the history of wetting and drying along the profile during the uptake of water.

Continuing the work, Peck (1965 a, b) has reported results of experimental studies on horizontal and vertical soil columns including theoretically derived comparisons. For the horizontal bounded column Peck (1965 a) developed an approximate model on the assumption that the uptake of a small increment of volume of water took place as if the pore-air pressure had remained constant at the value at the beginning of the uptake. A stepwise method was then developed for calculating the time dependence of the pore-air pressure and the moisture profiles. The calculated data agreed well with the experimental results at early times. The flow behaviour in the column after air began to escape was also investigated. The measured pore-air pressures and moisture profiles in the vertical bounded columns (Peck (1965 b)) of the slate dust during early stages of infiltration were very similar to those obtained in the horizontal case. In the bounded columns the rates of infiltration were reduced by a factor of up to 9 for the slate dust and 500 for the sand, indicating a 'freezing' of the water for that case.

## 2.4   The Vertical Drainage Problem

A thorough and theoretically sound treatment of the problem of the drainage of a vertical saturated sand column was made by Day and Luthin (1956). Using a fine sand column the capillary conductivity under steady state conditions at various water application rates was determined. This was followed by the actual drainage experiment using the same column when the pressure readings down the column were taken with tensiometers connected to fine bore capillary tubing. The relationship between water content and suction was determined on a duplicate column from the equilibrium readings taken after one week's drainage. The experimentally derived pressure distributions during drainage at various times were compared with those obtained by calculation using the

hydrologic characteristics of the material and the differential equation of flow. This equation was solved by a fairly lengthy numerical means and the general trend of the drainage process was predicted.

Youngs (1960) described the yield of a liquid at a given time for a draining column by a capillary tube model. Experiments were carried out with a range of liquids, column lengths and inclinations of column, and it was found that the approximate analysis agreed with the experimental results up to a yield of 60% but thereafter the deviations were quite marked.

Another approximate solution was given by Gardner (1962) who argued that above the capillary fringe, the relation between hydraulic head and water content was very nearly linear for the narrow range of suctions involved. This enabled the differential equation of flow to be simplified and the fairly amenable solution to be utilized. The agreement with experimentally determined outflow data was reasonable, but exact water content distributions could not be calculated.

Recently Fujioka and Kitamura (1964) presented an approximate analysis similar to that of Gardner (1962) with the exception that the case of ponded surface water under decreasing head was also considered. The solutions were given in terms of dimensionless quantities and presented in graphical form. Again there was reasonable agreement between the theoretical and experimental results.

Wang et al. (1964) have presented a numerical approach called the 'moving section method' which utilizes a digital computer for the computational work. The authors state that the method is applicable to the drainage problem but illustrate the procedure with an infiltration example in which a non-uniform initial moisture profile was chosen. Good agreement on later profiles was achieved between the new method

and the numerical procedure of Philip (1957). However, one of the basic assumptions of the method was that parabolic arcs could adequately approximate the distribution of moisture and other variables. Where the initial moisture distribution is uniform (as in the vertical drainage case) the parabolic distribution assumption is invalidated and the method, in its present form, is unable to be successfully used.

Remson et al.(1965) have presented digital computer programmes for the vertical drainage of an unsaturated soil based on the diffusion form of the differential equation of flow. The equation was solved for a 400 cm. thick well-drained unsaturated zone draining to the water table (from an initial condition of saturation) and evaporating from an unvegetated surface. The computed solutions are of definite interest although there is no experimental information presented which allows the comparison of predicted and actual moisture profiles. It would appear that for non-continuous flow, with the accompanying hysteresis complications, computational procedures using the diffusion form of the flow equation show less promise than those utilizing the basic pressure form of the equation.

## 2.5   Capillary Conductivity Determination

In this brief summary of the present experimental status of this determination only those methods applicable to laboratory columns as distinct from outflow type experiments have been considered.

Undoubtedly, the classical experiment in this work was that reported by Childs and Collis-George (1950). In this experiment not only was the capillary conductivity-water content relation for porous materials determined under steady state conditions but, in addition, by varying the gravitational potential by inclination of the column it was possible to show that Darcy's Law was applicable to unsaturated materials.

Day and Luthin (1956), as mentioned in section 2.4, determined the capillary conductivity-suction relationship by steady state methods from hydraulic gradient measurements taken with tensiometers.

Whereas Childs and Collis-George (1950) determined the water content of the constant moisture region, which existed in their experiments, by observing the change in capacitance of a small cell, Youngs (1960) in infiltration experiments obtained the water content from the progress of the wet front and the rate of infiltration. It was found that extremely low infiltration rates using a drip-feed arrangement were impracticable. In a more recent paper Youngs (1964) has again used an infiltration method for measuring the capillary conductivity. In this experiment the necessary unsaturated conditions were obtained either by maintaining an air pressure greater than atmospheric in the dry material with the surface at saturation or by maintaining the surface at a constant suction. The results from the various wetting and drying methods used for determining the capillary conductivity of the slate dust were also compared. The scatter of the results in this graphical comparison makes reliable conclusions on the possibility of hysteresis in the capillary conductivity-water content relation rather difficult to form.

# CHAPTER 3

## MEASURING EQUIPMENT AND EXPERIMENTAL ARRANGEMENT

### 3.1  The Traversing Mechanism

In order to be able to investigate experimentally most infiltration-redistribution and drainage problems for the range of soils in which the pore geometry remains constant during water content changes it is necessary to be able to accommodate soil columns up to approximately 200 cm. in length. In the present equipment provision has been made in the design both of the column and traversing mechanism for a column length of 180 cm.

The use of the principle of gamma-ray absorption for the non-destructive measurement of water content necessitates, external to the soil column, a radioactive source on one side and a scintillation counter on the other. This assembly of source and detector must then be positioned at the elevation where the measurement of water content change is desired.

The general design requirements of the traversing mechanism then emerge as follows:

(a)    The mechanism must be sufficiently robust to move the source and detector, together with the heavy shielding involved, up and down the column with a minimum of vibration and with accurate horizontal positioning of the collimation slit relative to the column centre line.

(b)    The range of this movement must be 180 cm.

(c)    The source and detector assembly must be

able to be stopped precisely at any graduation mark on the column. These marks are spaced at 1 cm. intervals. Due to the height of the column this requirement implies a remote control method.

(d)  The movement from one elevation to another must be as rapid as possible keeping in mind the accuracy of positioning required by (c).

A general view of the column in relation to the entire experimental arrangement may be seen in Figure 3.1. In this photograph it was not possible to include the full column length; however, this is shown in Figure 3.2. Figure 3.3 presents a detailed view of the traversing arms.

Essentially this section of the traversing mechanism consists of a 3" dia. bright mild steel tube 1/8" wall thickness 7'10" long to which is attached a 3/8" x 1/4" key. The traversing arms are welded to a 9" long mild steel sleeve which is machined to slide freely on the mild steel tube yet with a minimum clearance. The traversing arms and sleeve are driven by a 1" dia. Whitworth threaded screw of high tensile steel. The drive is transmitted from the screw to the traversing arms through a universal unit, thus minimizing the vibration and drag which inevitably occur with such a long drive screw. The cylindrical lead shielding on the source and detector is shown in Figures 3.1 and 3.3. It will be noticed that this places a large eccentric load on the column, thus requiring the incorporation of the counterweight system visible in Figure 3.2.

The motor drive and control mechanism are shown in Figures 3.4 and 3.5. The basic unit consists of a 1/3 H.P., 3 phase, 50 cycle, 1425 RPM, 415 volt electric motor connected to a solenoid released,

spring loaded, magnetic brake assembly and thence through a flexible coupling to a 10:1 ratio gearbox with horizontal input and vertical output. This equipment is rigidly mounted on an inner frame which in turn is mounted on rubber bushes within the outer frame.

The accurate control of the traversing arms allowing precision positioning at any graduation mark is achieved in the following manner. The output shaft from the gearbox not only drives the main Whitworth screw but in addition, through a small gear connected to the base of the screw, the chain of gears visible in Figures 3.4 and 3.5. The gear ratios are so arranged that the final gear in the chain completes one revolution for exactly 1 cm. rise of the traversing arms. Two adjustable cams are attached to this final gear to provide control for upward and downward movement. A microswitch with a rolling type contact arm makes contact with this gear and cam assembly and is wired so that the circuit is broken when the cam operates the switch. The remote control is achieved by operation of the mill type push button station shown in the foreground in Figure 3.4. The starter for the electric motor, and the reversing controller, which governs the direction of travel of the traversing arms, are mounted on the front panel of the base assembly and are clearly visible in this figure.

Electrically the system operates in the following manner. On pressing the push button all the electrical components are brought into operation. The electric motor is started via the starter and the magnetic brake is held in the open position. Whilst the push button is in the depressed position the microswitch is overriden; however, as soon as the button is released the microswitch becomes the control unit and on actuation by the cam, breaks the circuit causing the motor to be switched off and the magnetic brake to clamp on the drum stopping the rotation very quickly. In practice the push button is released from the depressed
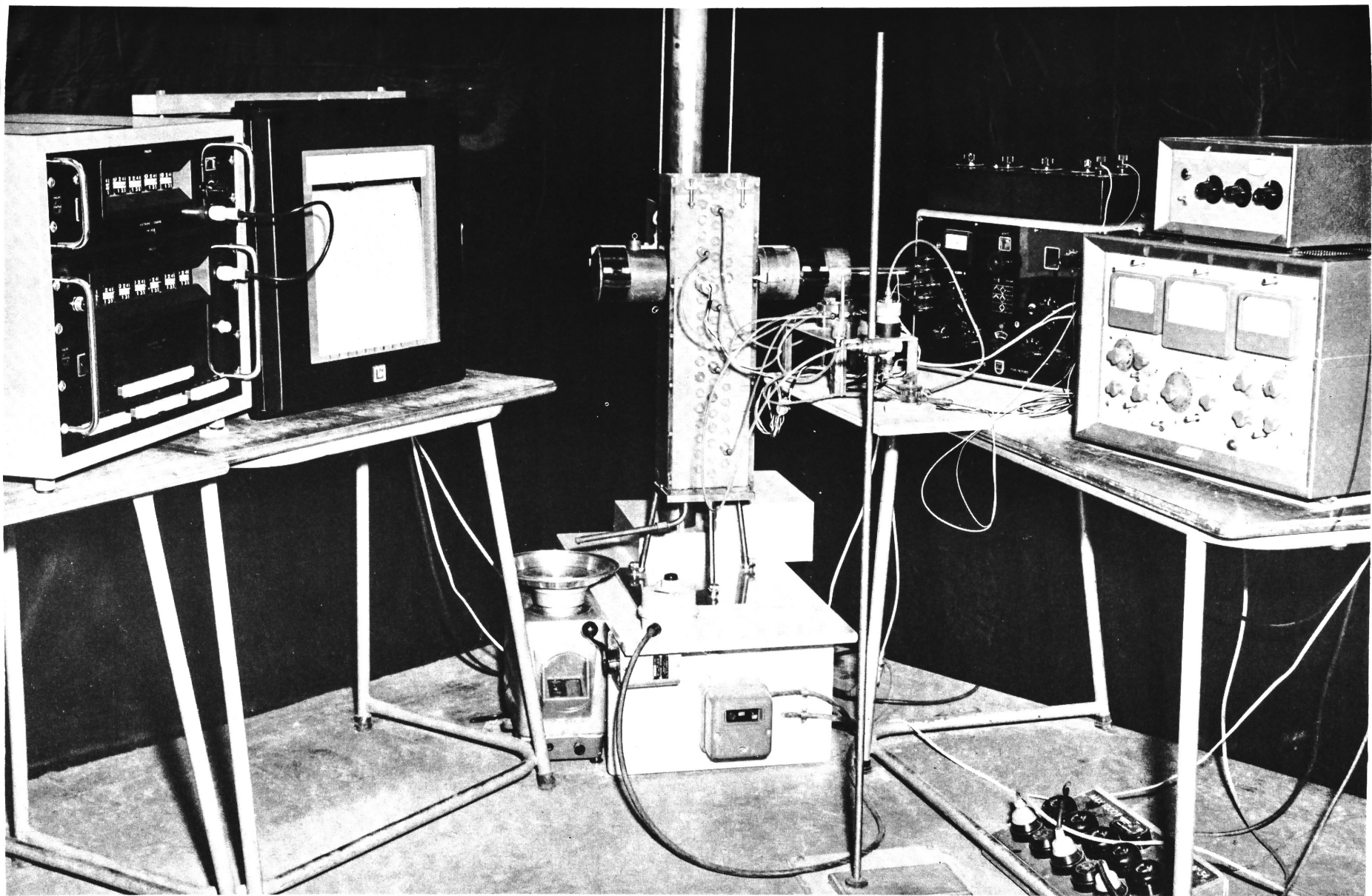
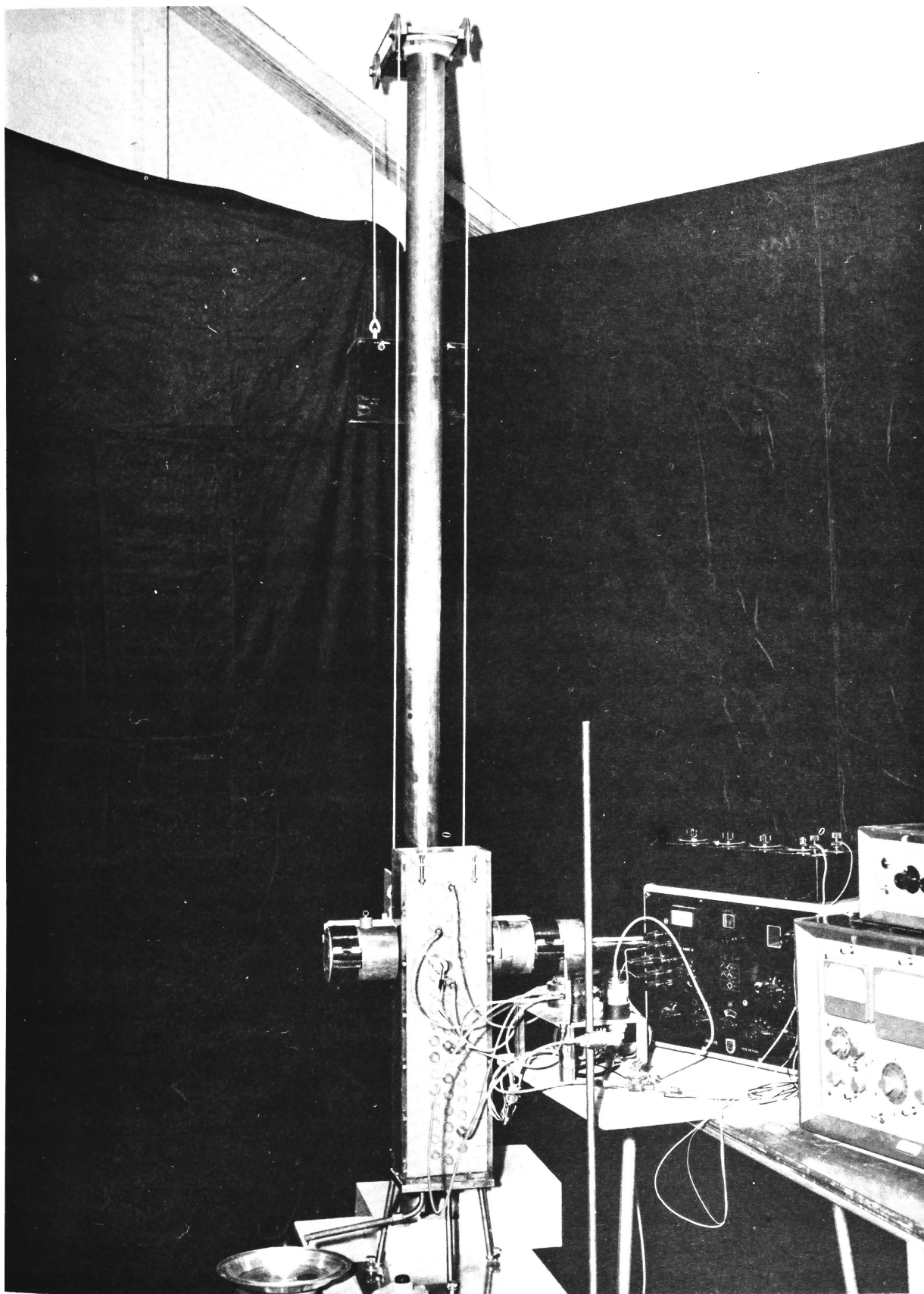Figure 3.1:   General View of Measuring Equipment.
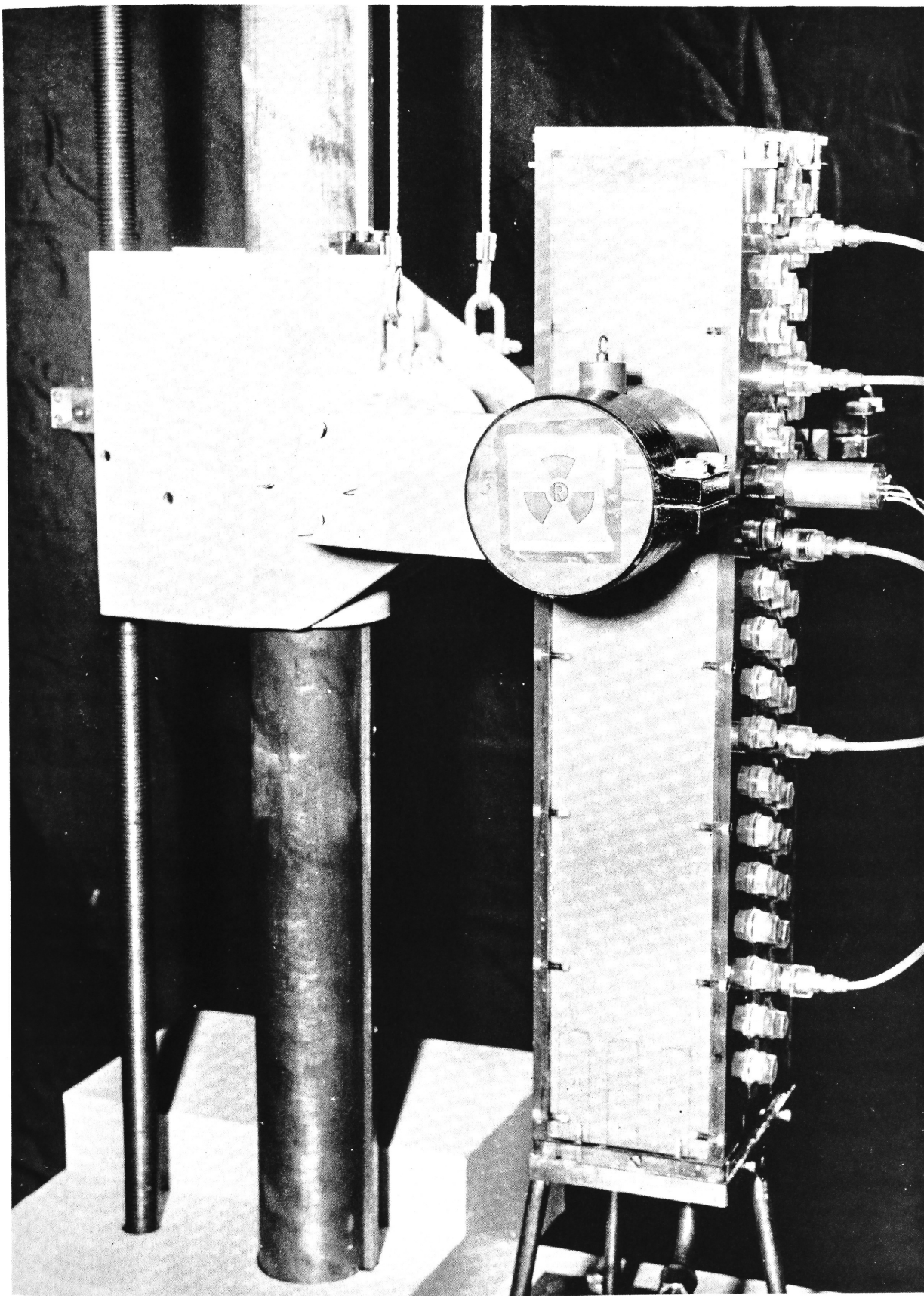
Figure 3.2:  The Column Assembly.
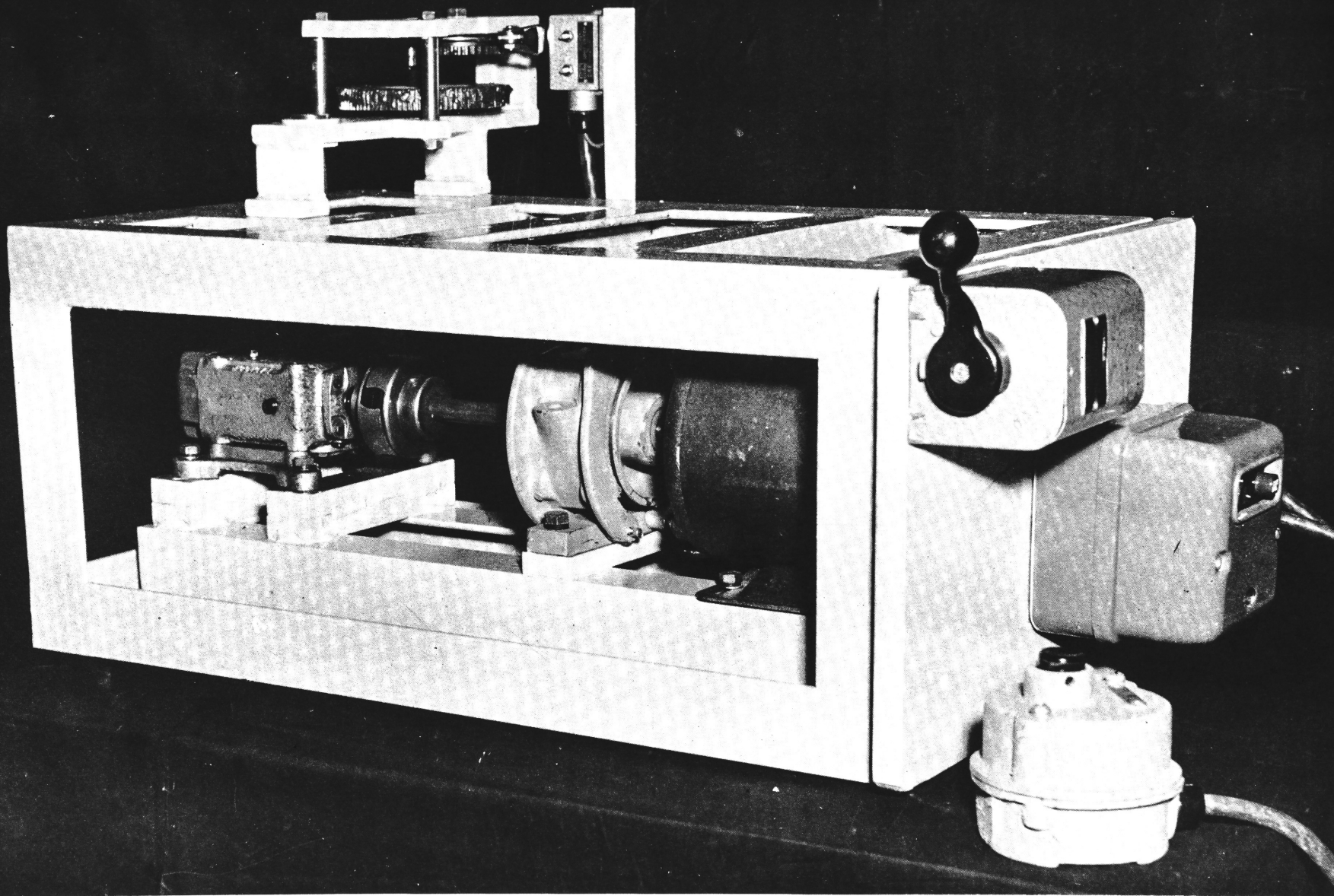
Figure 3.3:    The Traversing Arms.

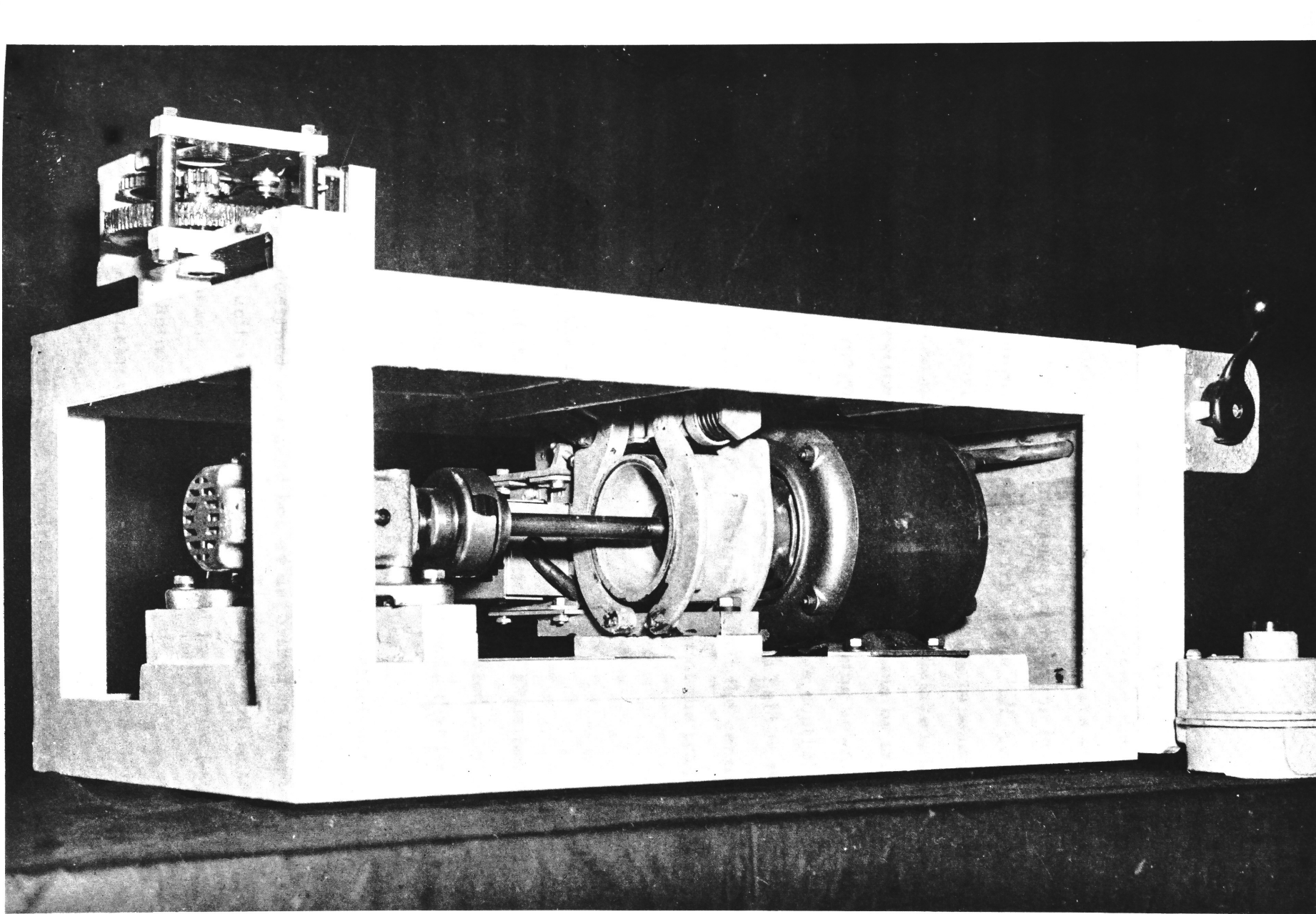Figure 3.4: Motor Drive and Control Mechanism.

Figure 3. 5:    The Base Unit showing the Magnetic Brake.

position after passing the centimetre mark immediately before the
required position.  The cam-microswitch reaction and the overrun on
applying the brake are so regulated that on releasing the push button the
traversing arms are positioned at the centimetre mark with an accuracy
of .02 cm.  The latest release point of the push button for stopping at any
centimetre mark is 3 mm. before the mark.  The 'off' position on the
reversing controller provides a means of stopping in some intermediate
position between the centimetre marks if this is desired; however, this is
not subject to microswitch control and must be done by trial and error.
The efficiency of the magnetic brake and the gearing down of the drive
enable this to be done quite accurately.  The above control mechanism
works extremely well.  The push button station is held in the hand and
the only additional requirement for control is that the centimetre marks
must be visible.  The rate of vertical movement of the traversing arms
is 0.77 cm. per second.

## 3.2   Gamma-Ray Absorption Arrangement

A study of the attenuation equation (see Equation 5.1 and
following equations) for a moist soil and a collimated monoenergetic
beam with a fixed source-detector distance reveals that its use in
determining the water content requires

(a)   Values of the mass attenuation coefficients.  These
are conveniently determined using a specially
designed sectioned box as described in Chapter 5.

(b)   A uniform initial bulk density of the soil in the
column.  This can be achieved by careful packing
techniques.

(c)   A constant thickness dimension along the length of
the column.  This is dependent upon the column
construction and requires fabrication with fine
tolerances.

Figure 3.6 shows the source-detector assembly. The source is 100 mc. of $Cs^{137}$ attached to a 1 inch diameter lead plug which can be raised to remove the source from the collimation slit. This slit is 5 cm. long with cross section dimensions of 2.5 cm. x 3 mm. The overall source housing is a 4 inch diameter lead cylinder. This cylinder is placed as closely as possible to the soil column which is made from 3/8 in. clear acrylic sheeting (Perspex) and has internal cross-section dimensions of 15 cm. (in direction of the gamma-ray emission) by 10 cm. The maximum height of this column is 180 cm. comprising a base unit of 60 cm. in length and three other units each of 40 cm. in length. The units are located on each other by precisely positioned dowels and then clamped together by bolts through side brackets. The bottom 60 cm. unit only is shown in Figure 3.1. The column was fabricated with great care to fine tolerances.

The scintillation counter[*] and the thallium-activated sodium iodide crystal[+] are also housed in a 4 inch diameter lead cylinder with the collimation slit of dimensions 5 cm. x 2.5 cm. x 1 mm. The heavy scintillation housing has two advantages; firstly, from the mechanical viewpoint it balances what would otherwise be a continuous lateral eccentric load on the column, and secondly, it decreases the background count to a negligible quantity of 1/3 - 1/2 pulse/second.

The scintillation counter is connected directly to the ratemeter[**] which incorporates a HV-amplifier unit, a pulse height analyser unit and a ratemeter unit. The analyser is most important

---

[*]   ECKO type N 618, eleven stage photo-multiplier tube.

[+]   ECKO type N 632, crystal dia. 13/16 in., crystal depth 1 in.
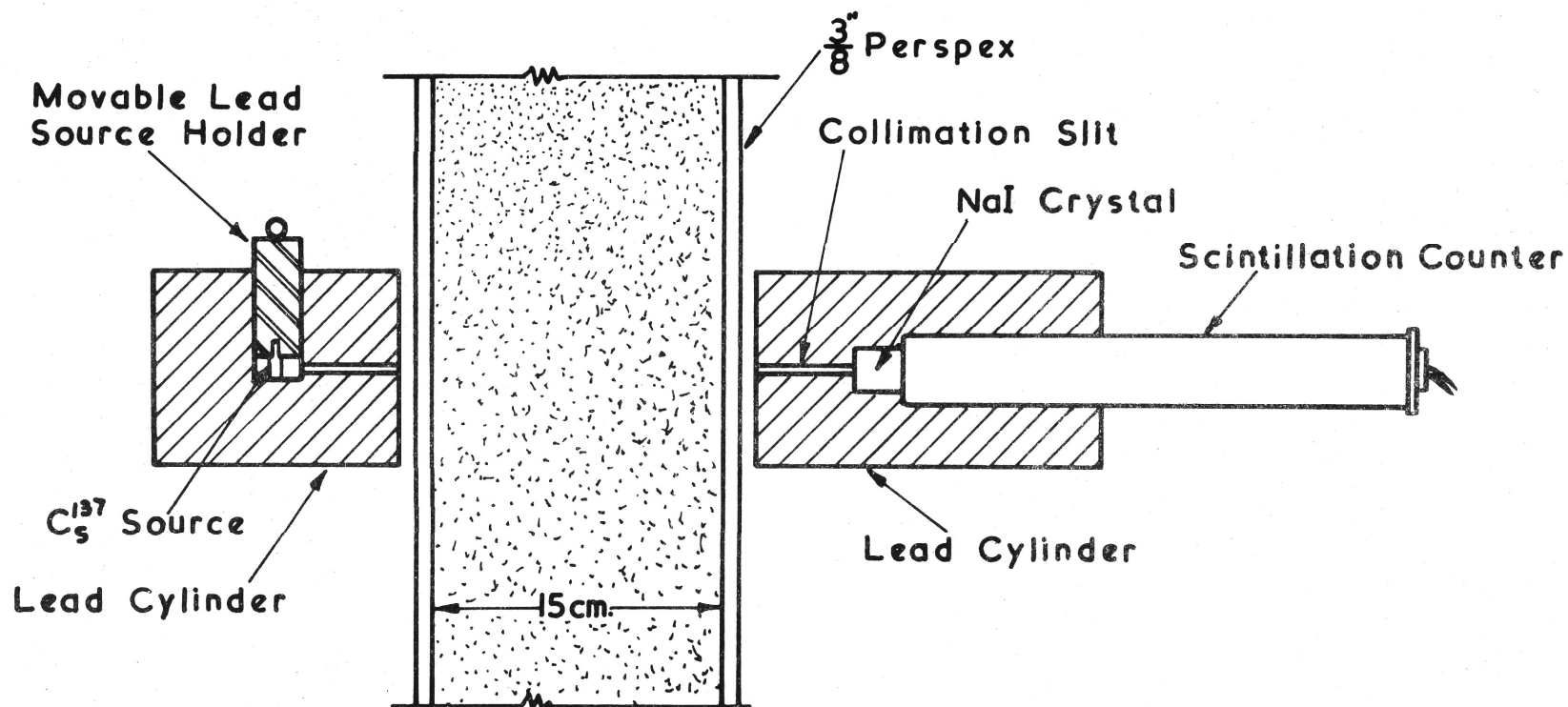
[**]  ECKO Ratemeter, Type N 600.

Figure 3.6:  Source, Column and Counter Assembly.

as it selects for measurement the high energy peaks only. The output from the ratemeter is fed to one channel of a dual channel DC potentio-metric recorder* where a continuous record of radiation changes against a time base is obtainable. The response time of the recorder is 1 second and a dot record for each channel is set down every 4 seconds exactly. To check the accuracy of the ratemeter at periodic intervals and to accurately control the uniformity of the initial packing of the soil in the column a slave scaler[+] is also incorporated. This is driven by the ratemeter and receives all pulses coming from the analyser unit. The scaler is extremely fast and, by using two binary stages a resolution of 1/2 microsecond is obtained. An electronic timer[**] is connected to the scaler so that the time intervals over which the count is determined will be accurate. At times it is necessary to observe accurately small moisture variations even at high moisture contents. For this purpose a zero suppression unit is connected to the ratemeter. The selection of the best operating conditions is described in Chapter 5. In order to be able to correct for electronic drift during an experiment and to set the ratemeter controls at a standard level for day to day operation a standard lead absorber of comparable absorption to the saturated sand column is used.

## 3.3 The Tensiometer-Transducer System

Figure 3.7 illustrates the provision in the column at 1 cm. intervals for tensiometer connection. 5/8" diameter tapped holes (26 threads per inch) are staggered to form three vertical rows 2.5 cm. apart. At the desired elevations the Perspex plugs are removed and

---

* Leeds and Northrup, Speedomax G, 0-100mV.

+ Phillips, Universal Counter, Type PW 4032.

** Phillips, Electronic Timer, Type PW 4062.

replaced by brass inserts into which the tensiometers can be easily pushed and sealed with a rubber ring. The design details of the tensiometer are given in Figure 3.8. It should be noted that the push-fit tensiometer assembly is of decided benefit since the hydraulic connections do not have to be disconnected when it is desired to move the tensiometer to a new position. The grade of ceramic used in making the porous cups depends on the maximum suction likely to be expected during the experiment. A ceramic with as large a pore size as possible, yet with an air-entry value greater than the maximum suction to be encountered, should be used to increase the response of the measuring system. A ceramic with a 5 micron pore size has an air-entry value of 400 cm. head of water and that with pores varying in size between 25-30 microns, 86 cm. In order to measure suctions over a depth of soil comparable to the moisture measurement the bottom and top of the porous cup are sealed off with epoxy resin and a 3 mm. wide strip in the middle is left for contact with the soil. With the present equipment up to 12 tensio-meters may be connected to the column. 1/8" bore nylon tubing with very strong walls is used for the hydraulic leads. This has the decided advantages of transparency (for sighting air bubbles) and flexibility. However, for long term experiments air diffusion through the tube walls could be troublesome. The hydraulic leads connect to a specially constructed multi-inlet — single outlet valve which allows, without any undesirable pumping effects, rapid selection of any tensiometer line. The valve is detailed in Figure 3.9 and is visible in Figure 3.7. The single outlet from the valve is connected to a pressure transducer[*] of capacity 0-20 lb/in.[2] absolute. The deflection of the diaphragm of this transducer is measured by a fully active unbonded strain gauge bridge

---

[*] Statham, Pressure Transducer, Type PA731TC-20-350.
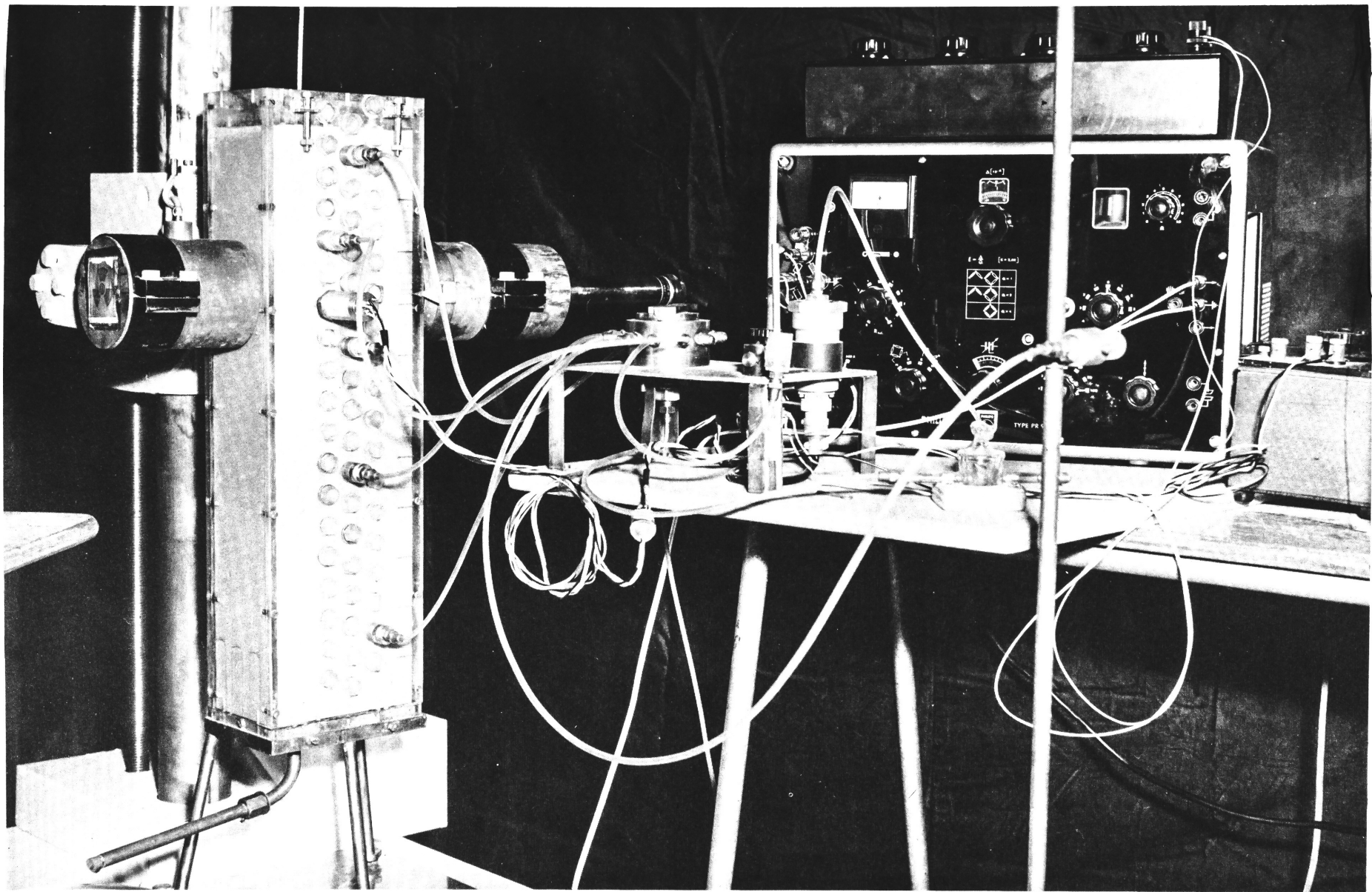
Figure 3.7:   Detailed View of Pressure Measuring Equipment.

Figure 3. 8: Tensiometer Arrangement.

Handle

Mild Steel

Precision Lapped

$3\frac{1}{2}''$ dia

$\frac{1}{8}''$ gas thread

Brass

12 outlets
Spaced
Circumferentially

Series of 3 Sleeves
and 2 Rubber Rings
for Seal
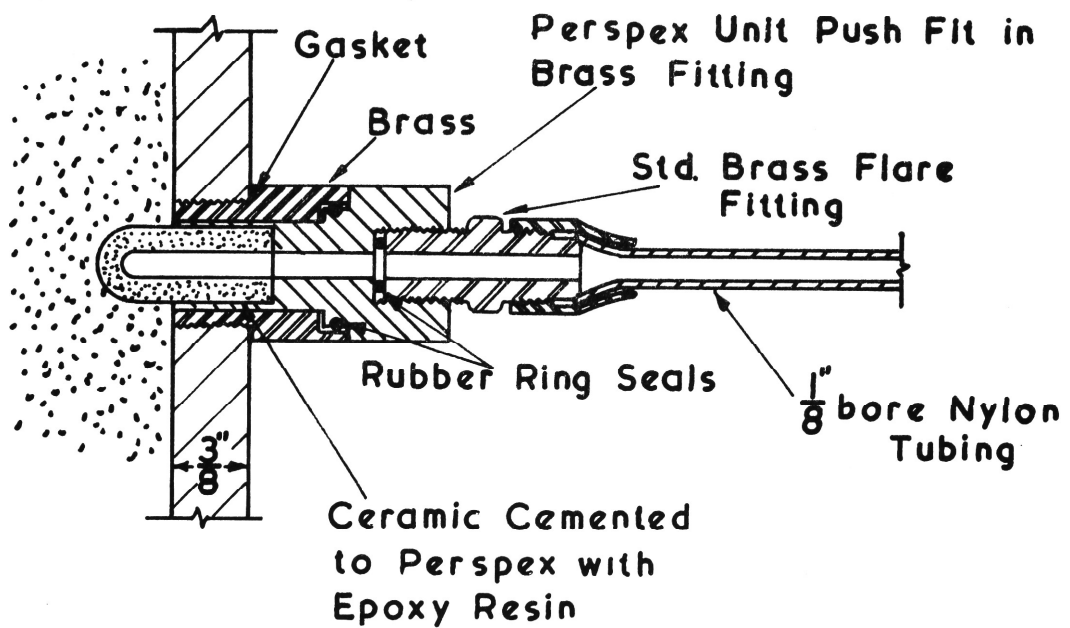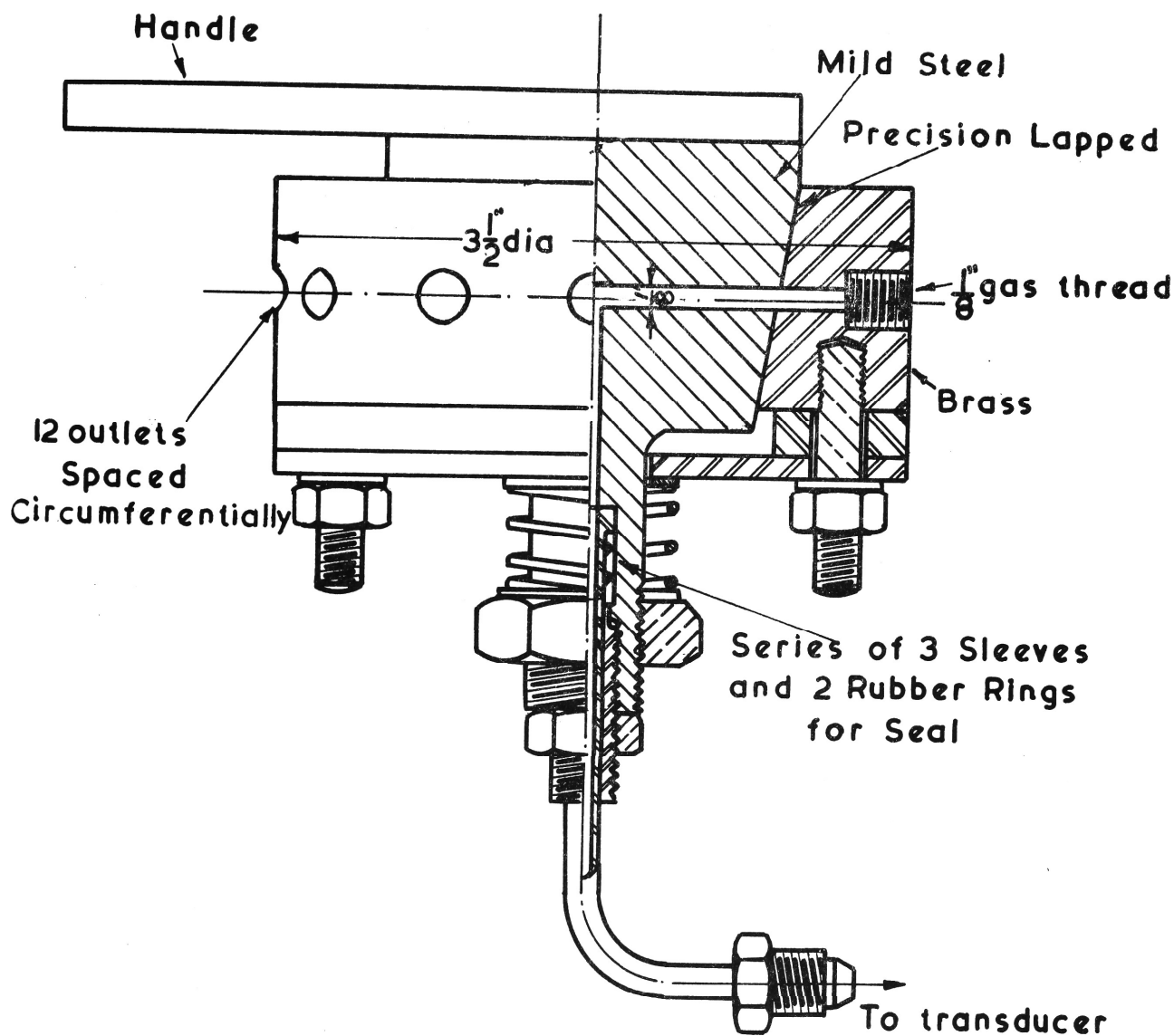
To transducer

Figure 3.9:   The Multi-inlet Selection Control.

which utilizes the "zero-length" principle in its design. This results in excellent stability. Both the input voltage to the bridge of the transducer and the output voltage from the bridge are supplied and measured respectively by a strain gauge measuring bridge[*]. This instrument has the facility of recorder output and hence provides the signal for the second channel of the potentiometric recorder.

The transducer has excellent volume displacement-pressure characteristics and when used in conjunction with the 25-30 micron ceramic cup it provides a measuring system with a response time of less than 1 second. When finer ceramic tips are used the response time will be greater and corrections must be applied to the measured readings as discussed in Chapter 4.

Because the transducer is calibrated on the basis of absolute pressure it is necessary to continuously monitor atmospheric pressure changes. This is best achieved by connecting one of the multi-inlet valve positions to a constant level water source, which is open to atmosphere, and taking readings on the source at regular intervals. In addition, a graduated rod fitted with a movable tensiometer, that can be precisely set at any graduation on the rod, provides a rapid and convenient calibration system (see Figure 3.7).

The sensitivity of the suction measuring system is such that it is possible to detect pressure changes of 1 mm. head of water.

The pore-air pressure is very conveniently measured by mounting a second transducer directly into a specially drilled and tapped Perspex plug which is screwed into one of the tensiometer outlets on the column face. A fine brass screen is bonded to the inner face of the plug

---

[*] Phillips, Strain Gauge Measuring Bridge, Type PR9302.

with epoxy resin. The mounted transducer is clearly visible in Figure 3.7. Such an arrangement has the advantage of ease of mounting and positioning with an almost negligible volume of air in the measuring system. A two-way, four-pole switch enables either transducer to be switched to the strain gauge measuring bridge. The response of the transducer to the air pressure changes is extremely rapid. An alternative procedure, when all the tensiometer connections on the multi-inlet valve are not required, is to connect to one of the nylon leads a Perspex unit exactly the same as the tensiometer unit shown in Figure 3.8 with the exception that the porous ceramic is replaced at the end of the plug by a fine brass screen, again bonded with epoxy resin. The hydraulic line is filled with water to within 1/4 inch of this screen thus minimizing the volume of air in the measuring system. Such an arrangement has the advantage of one transducer calibration serving both suction and air pressure measurements.

The outflow from the bottom of the column (in those experiments where this is required) is conveniently and accurately measured by piping it to the pan of an automatic balance and recording the balance reading at suitable times from the start of the experiment.

## 3.4  General

The equipment detailed on the previous pages facilitates the measurement with rapid response of the only three physical quantities that change magnitude during unsteady flow in unsaturated soil of rigid structure. Accordingly, any one-dimensional flow problem is capable of investigation. As has been mentioned, the present study is concerned with the drainage of an initially saturated sand column to atmosphere at its base. Following the drainage cycle the column is wetted at its top surface at a rate in excess of the infiltration capacity. During the wetting up each elevation in the column wets up along its appropriate

scanning curve. In addition, the saturated depth of sand at the bottom
of the soil column prevents the escape of the pore air, which is then
compressed as the wet front descends. This change of air pressure
has two effects, firstly, it lowers the infiltration rate and secondly,
due to the increased pressure difference across the air-water interfaces
it causes drainage of a part of the hitherto saturated section in the lower
profile of the column.

In a similar manner the equipment can be used to study the
infiltration-redistribution problem for any water application treatment
at the upper boundary. This includes the case where water is applied
in excess of the infiltration capacity and that in which the application
rate is less than the infiltration capacity. Investigation of layered
systems or systems having non-uniform initial moisture profiles can
also be readily carried out.

Recently Poulovassilis (1962) and Phillip (1964) have presented
analyses in which the scanning curves within the hysteresis loop are
calculable from the main wetting and draining arms. At this stage only
one set of experimental data has been published for the comparison of
the predicted curves and those experimentally obtained. However, using
the equipment detailed in this chapter in conjunction with a small Perspex
box containing a porous plate through which any desired suctions from an
external suction source may be applied to the soil it is possible to follow
quite rapidly the entire wetting and draining pattern of a material and
hence build up the hysteresis behaviour of a wide range of soils and
porous materials.

# CHAPTER 4

## PRESSURE MEASUREMENTS - CALIBRATION AND CORRECTION PROCEDURES

### 4.1 Calibration

Since the pressure change at the face of the tensiometer cup is converted by the pressure transducer into an electrical signal, which is finally presented in recorded form on the strip chart, it is essential to be able to easily and rapidly relate by calibration the chart reading to the appropriate pressure. In section 3.3 the calibrating column used for this purpose was described. The calibration is achieved by balancing the strain gauge measuring bridge with the calibrating tensiometer placed at any convenient elevation, and then, from this zero setting, obtain the recorded outputs for other elevations of the calibrating tensiometer. Both positive and negative pressures (with respect to the zero setting) may be applied to the transducer diaphragm in this way.

By placing a decade resistance box in parallel with the transducer terminals it is possible, by varying the box resistance, to adjust the recorded deflection for a given applied pressure. Such an adjustment has been made for some of the present experiments, so that 20 divisions on the strip chart represent 10 cm. head of water. The chart record for suction pressures (relative to the zero elevation) of 10, 20, 30 and 40 cm. is given in Figure 4.1. The output from the strain gauge measuring bridge is linear up to approximately 90 divisions on the chart; accordingly, the zero setting is made such that chart records beyond this magnitude are avoided.

Another calibration check of an 'in-situ' nature is also
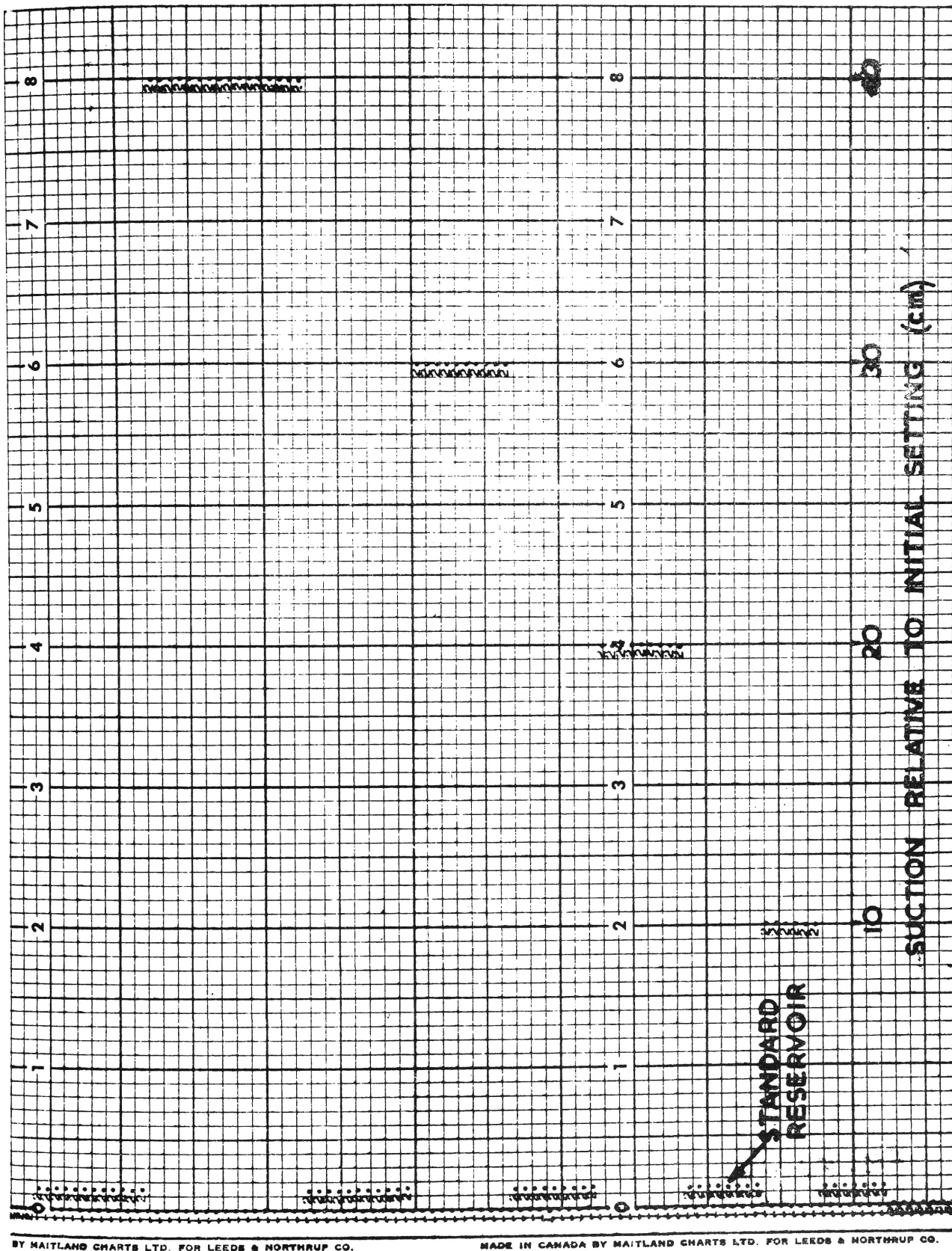
Figure 4.1: Chart record of pressure calibration.

Note: All chart records read from right to left.

possible with drainage experiments on saturated columns. Upon the completion of drainage, when equilibrium is established, the suction pressure at any point is equal to the height of that point above the base of the column. Hence a chart reading for a given tensiometer can be related to the corresponding pressure in cm. of water.

The calibrating tensiometer is made from a very porous ceramic such that the response to the pressure change is extremely rapid as may be seen in Figure 4.1. Such rapid response allows the calibration to be regularly checked during an experiment.

In section 3.3 attention was drawn to the necessity of allowing for atmospheric pressure changes during the test. Such changes, together with any instrument drift, can also be regularly checked during an experiment by connecting the transducer to the open-ended reservoir, whose upper surface is placed at the same elevation as the transducer diaphragm. The transducer is mounted vertically giving a horizontal position of the diaphragm. It is then convenient to balance the strain gauge measuring bridge against the pressure of the open-ended reservoir (that is, atmospheric pressure at transducer diaphragm elevation). With this arrangement positive hydrostatic pressures and suction pressures can both be accommodated on the chart by simply changing the plug position at the recorder output terminals as the pressure changes from positive to negative (or vice versa). Allowance must also be made in calculating pressures for the elevation of the transducer diaphragm relative to the particular tensiometer.

## 4.2   Operating Characteristics

Richards (1949) summarized the tensiometer cup and pressure measuring device characteristics which enable the general

operating characteristics of the tensiometer-transducer system to be suitably defined. The essential characteristics are:

(a) Cup conductance K. This is defined as the volume of water passing through the cup wall per unit of time per unit of pressure difference. Convenient dimensions for present usage are cc./sec./p.s.i. For a given time and pressure difference the cup conductance depends primarily on the area of ceramic in contact with the soil and the pore size of the ceramic material.

(b) Air-Entry Value. The air pressure difference required to cause an air leak when the cup wall is saturated with water is known as the air-entry value. This naturally decreases as the pore size of the ceramic increases. In designing an experiment a ceramic should be chosen so that its air-entry value will be somewhat greater than the maximum suction expected in the experiment. Such a choice will result in an optimum cup conductance for the particular measurements.

(c) Gauge sensitivity S. For the equipment under discussion this could more precisely be described as transducer sensitivity. It is defined as the pressure change per unit volume displacement of the diaphragm. Units: p.s.i./cc.

(d) Response Time Constant $\tau = \dfrac{1}{KS}$ This is a measure of the general response of the tensiometer-transducer system to soil moisture changes at the cup surface. It has the dimensions of time and is

dependent upon the cup conductance and the
transducer sensitivity.

For the measurement of rapidly changing suctions it is
necessary to have a response time as small as possible keeping in
mind the air-entry value requirement. The strain gauge type pressure
transducer has excellent volume displacement-pressure characteristics
and accordingly facilitates a system having a small response time.

Table 4.1 summarizes the operating characteristics of the
system for four different grades of ceramic.

| Nominal Pore Size (microns) | Air-Entry Value (cm. of water) | Cup Conductance K (cc./sec./p.s.i.) | Gauge Sensitivity S (p.s.i./cc.) | Response Time $\tau$ (sec.) |
|---|---|---|---|---|
| 1 | 1300 | $2.3 \times 10^{-4}$ | $1.47 \times 10^2$ | 29.6 |
| 5 | 400 | $4.1 \times 10^{-4}$ | $1.47 \times 10^2$ | 16.6 |
| 10 | 270 | $5.9 \times 10^{-4}$ | $1.47 \times 10^2$ | 11.5 |
| 25-30 | 86 | $6.8 \times 10^{-2}$ | $1.47 \times 10^2$ | 0.1 |

Table 4.1 - Summary of Operating Characteristics

The most porous ceramic in the above table was specially
chosen for the experiments of this study. During the early stages of
the drying and wetting cycles the pressure changes occur very
rapidly and it is most necessary to have a very rapid response system.
The height of the column is 57 cm. and this represents the maximum
suction that has to be measured during an experiment. It is therefore

satisfactory to use a tensiometer cup with pores in the 25-30 micron
range, having an air-entry value of 86 cm. and a response time of
1/10 sec. As will be explained in the next section, if under these
conditions a suddenly applied step input of suction is applied to the
external face of the tensiometer, the transducer will record 99.9% of
the applied suction in 0.69 seconds. Since the recorder gives a dot
record for each channel every 4 seconds exactly, a step input, applied
as one dot is impressed on the chart, is completely recorded by the
position of the following dot. Such fast response enables rapid suction
changes to be accurately recorded with a minimum of correction being
necessary.

Since the tensiometer-transducer system is not a null-type
system and requires moisture transfer to and from the soil to allow
displacement of the transducer diaphragm, it is necessary to check
whether this moisture transfer is liable to upset the moisture condition
at the tensiometer face. From the value of the gauge sensitivity
given in Table 4.1 it can be estimated that for a suction change of 50 cm.
of water there would be a transfer of water into the soil of approximately
0.0003 cc. The area of the tensiometer in contact with the sand is
approximately 0.6 cm$^2$. Accordingly, the volume of water at saturation
in the sand pores for a distance of 1 mm. (3-4 grain diameters) around
the cup is 0.021 cc. The volume of water transfer is thus small compared
with the water in the sand voids in the immediate vicinity of the tensio-
meter face and could be expected to have a negligible effect on the flow
pattern and pressure measurement. The validity of this conclusion is shown
very clearly by the chart record when the transducer is switched from a
particular tensiometer to the open-ended reservoir for an atmospheric
pressure reading and then back to the tensiometer. During such switching
there is a transfer of water across the cup appropriate to the pressure
difference; however, this causes no disturbance in the pressure output

curve as given by the dot record.

## 4.3   Response Theory

Miller (1951) in discussing the dynamic properties of the measuring system he devised for rapidly changing suctions specified the differential equation of flow across the tensiometer cup and solved the equation in terms of the volume of water transferred across the cup wall.  Klute and Gardner (1962) looked at tensiometer response from the viewpoint of "instrument limiting" and "soil limiting" and for the former case corrected the tensiometer reading for an idealized sinusoidal suction variation.  In this section the theory of tensiometer response where the instrument is the limiting factor is briefly given and three solutions of interest outlined.

Let   $\psi_e$     = suction at the external surface of the cup

$\psi_i$     = suction at the internal surface

From the definition of cup conductance   K
Flux of water across cup

$$\frac{dq}{dt} \quad = \quad K(\psi_e - \psi_i) \quad \ldots \ldots \ldots (4.1)$$

Inherent in this equation is the assumption that the flow across the cup obeys Darcy's Law.

Equation (4.1) may be rewritten as

$$\frac{1}{K} \cdot \frac{dq}{d\psi_i} \cdot \frac{d\psi_i}{dt} \quad = \quad \psi_e - \psi_i$$

Now        $\dfrac{dq}{d\psi_i} = \dfrac{1}{S}$

Hence $\quad \tau \dfrac{d\psi_i}{dt} = \psi_e - \psi_i \qquad \ldots\ldots\ldots$ (4.2)

Where $\quad \psi_e$ and $\psi_i$ are both functions of $t$.

The solution of (4.2) is

$$\psi_i = e^{-\frac{t}{\tau}}\left[\int \frac{1}{\tau}\, \psi_e\, e^{\frac{t}{\tau}}\, dt + C\right] \qquad \ldots\ldots\ldots\ldots \text{(4.3)}$$

It is apparent that the final form of this equation is dependent on the manner in which $\psi_e$ varies with time. Three simple cases may be considered.

(a)     An instantaneously applied step input $\psi_e = \psi_o$ at time $t = 0$. It is assumed that the suddenly applied external suction follows an equilibrium condition in which $\psi_i = \psi_e$ . In this instance $\psi_o$ may be considered as a constant coefficient and the solution of (4.3) is

$$\psi_i = \psi_o (1 - e^{-\frac{t}{\tau}}) \qquad \ldots\ldots\ldots\ldots \text{(4.4)}$$

For

$$
\begin{array}{ll}
t = \tau & \psi_i = 0.63\psi_o \\
t = 2.3\tau & \psi_i = 0.90\psi_o \\
t = 3.0\tau & \psi_i = 0.95\psi_o \\
t = 4.6\tau & \psi_i = 0.99\psi_o
\end{array}
$$

(b) A linearly applied increase in $\psi_e$ during period $t = o$ to $t = \beta$.

For $t > \beta$ the value at $t = \beta$ is maintained.

Let $\dfrac{d\psi_e}{dt} = m$

For $t \le \beta$

$$\psi_i = \psi_e - m\tau(1 - e^{-\frac{t}{\tau}}) \qquad \ldots \ldots (4.5)$$

The suction correction $\varepsilon$ which must be applied to the recorded suction $\psi_i$ to give the suction on the external surface of the tensiometer is

$$\varepsilon = m\tau(1 - e^{-\frac{t}{\tau}}) \qquad \ldots \ldots (4.6)$$

$$t > \beta \qquad \psi_i = m\left[\beta - \tau(e^{-\frac{t-\beta}{\tau}} - e^{-\frac{t}{\tau}})\right]$$

$$= (\psi_e)_\beta - m\tau(e^{-\frac{t-\beta}{\tau}} - e^{-\frac{t}{\tau}}) \qquad \ldots (4.7)$$

$$\therefore \varepsilon = m\tau(e^{-\frac{t-\beta}{\tau}} - e^{-\frac{t}{\tau}}) \qquad \ldots \ldots (4.8)$$

The distributions of $\psi_e$, $\psi_i$ and $\varepsilon$ against time are shown in Figure 4.2 for $m = 1$ cm./min., $\beta = 1$ min., $\tau = 1$ min.

(c)    A step input  $\psi_0$  at  t = 0 together with a linearly applied increase in  $\psi_e$  to  t = β when the value  $(\psi_e)_\beta$  is maintained. This is simply a superposition of (a) and (b)

For   t ≤ β

$$\psi_i = \psi_e - m\tau - e^{-\frac{t}{\tau}}(\psi_0 - m\tau) \quad \ldots \ldots \ldots \quad (4.9)$$

giving   $\varepsilon = m\tau + (\psi_0 - m\tau)e^{-\frac{t}{\tau}} \quad \ldots \ldots \ldots \quad (4.10)$

For   t > β

$$\varepsilon = m\tau e^{-\frac{t-\beta}{\tau}} + (\psi_0 - m\tau)e^{-\frac{t}{\tau}} \quad \ldots \ldots \quad (4.11)$$

The facility of recorder output allows the actual response of the system for a step input of suction to be compared with the well known solution given in (a) above. The recorder chart for a step input using the 1 micron tensiometer is given in Figure 4.3; the step input represented a suction of 30 cm. (60 divisions on chart). The chart speed was 1 inch/min. By finding the times (from the application the step input) for 63%, 90%, 95% and 99% of  $\psi_0$  to be reached it is readily possible for the required comparison to be made.

$t_{0.63}$ = 28 sec.          hence   $\tau$ = 28 sec.

$t_{0.90}$ = 68 sec.                    $\tau$ = 68/2.3 = 29.6 sec.

$t_{0.95}$ = 89 sec.                    $\tau$ = 89/3.0 = 29.6 sec.

$t_{0.99}$ = 136 sec.                    $\tau$ = 136/4.6 = 29.6 sec.
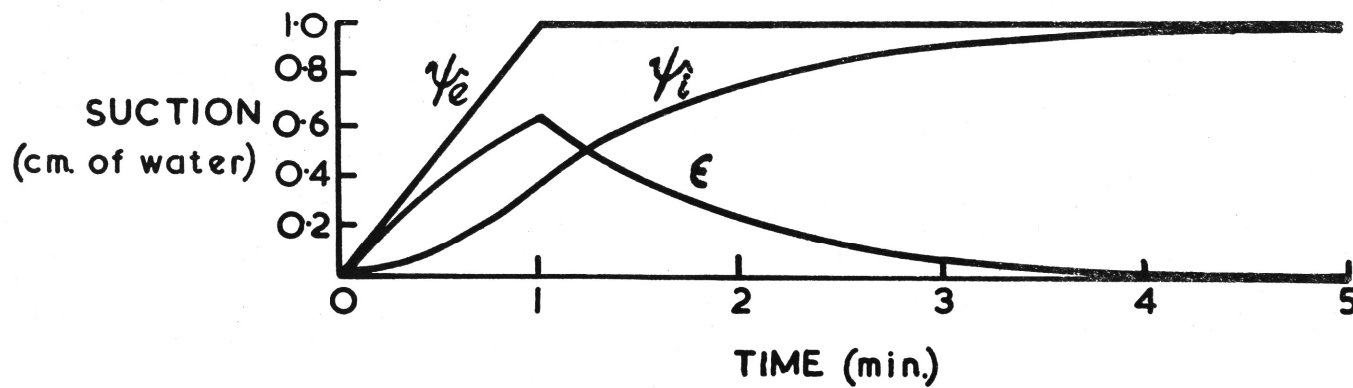
Figure 4. 2: Variation of $\psi_e$, $\psi_i$ and $\epsilon$ with time
for m = 1 cm/min. $\beta$ = 1 min., $T$ = 1 min.
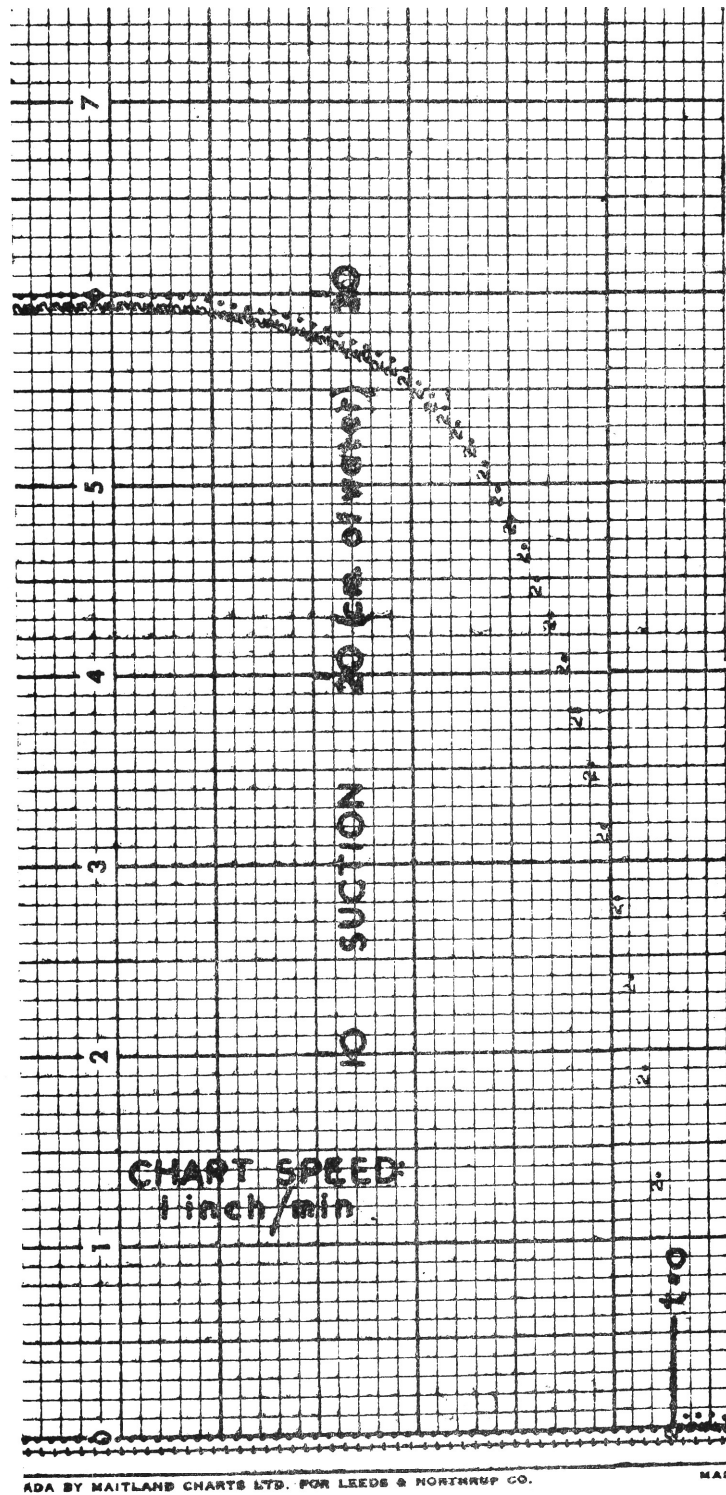
Figure 4.3    Recorder output ($\psi_i$) for a step input of suction
$\psi_0$ = 30 cm. of water at t = 0 ;    $\tau$ = 29.6 seconds.

The above results not only confirm the exponential nature of the transducer output but also suggest a very useful method of determining $\tau$. The use of this method becomes quite necessary when dynamic corrections have to be applied to a series of readings. In such a case it is essential to know the response time constant of the system as operating since the presence of small amounts of entrapped air in the ceramic and the hydraulic lines will alter the time constant as determined by the K and S measurements. However, by applying a step input and calculating $\tau$ from the output a very rapid and accurate $\tau$ determination can be made. Due to the fact that a small time ($\frac{1}{4}$ - $\frac{1}{2}$ sec.) is necessary to apply the step input it is advisable not to base the determination on the $t_{0.63}$ point; similarly, small deviations often occur as the output approaches the $\psi_0$ value making the $t_{c.99}$ point also a little uncertain. Accordingly, it is preferable to use the $t_{c.90}$ and $t_{c.95}$ points in estimating $\tau$. From Table 4.1 it may be noted that the response time constant for this 1 micron tensiometer, as determined by the K and S values, was 29.6 seconds.

## 4.4 Correction Procedure

The previous section has demonstrated that, except for very slow suction changes, the transducer output at any particular time will differ from the suction existent on the external face of the tensiometer cup. It is therefore necessary to establish a technique whereby the transducer output can be corrected to yield the actual external suction. Miller (1951) mentioned the possibility of dynamic correction but since his equipment was of a non-recording nature he took the work no further. Klute and Gardner (1962) suggest that equation (4.2) may be used as the basis of a dynamic method of correction for tensiometer readings.

Since $\psi_i(t)$ is known it is possible to evaluate $d\psi_i/dt$ and thus calculate $\psi_e$. Pilgrim (1965) tried this method in the form of a period by period solution when correcting ratemeter readings for lag errors due to the response time constant RC; the differential equation was of identical form to equation (4.2). He found that convergence was poor with severe fluctuations occurring as the computational process developed. A more accurate approach is the use of a large-molecule finite difference equation. Further reference is made to this method in section 4.5.

An alternative and very satisfactory procedure is possible using equations (4.6) and (4.8) as a basis. Pilgrim (1965) and Watson (1964) have considered such an approach in correcting ratemeter readings. Although the exercise consists in finding the corrections which must be applied to the transducer output $\psi_j(t)$ to give the input suction at the tensiometer face $\psi_e(t)$ the general principles of the method can in the first instance be more easily explained by deriving $\psi_i(t)$ from $\psi_e(t)$.

Equations (4.6) and (4.8) enable the 'standard' error relationship $\varepsilon(t)$ to be computed for particular values of $m$, and $\beta$ as shown in Figure 4.2. The first step in the method is to divide the $\psi_e(t)$ relation into equal increments of time $\beta$; $\beta$ is so chosen initially that the variation of $\psi_e$ during the $\beta$ time periods is approximately linear.

The error relationship based on the first $\beta$ period ($\beta_1$) is computed by determining $m$ for the period $(m_1)$ and, from the 'standard' $\varepsilon(t)$ values for $m$ equal to unity, the $\varepsilon_1(t)$ values for $m_1$, are easily scaled. This computation is made for each $\beta$ period in turn and the results superposed to obtain the total error ordinates for the entire time period. Inherent in the process is the assumption, valid in this case, of a linear system. Pilgrim (1965) has detailed a convenient computational procedure.

The first requirement in establishing the validity of the theoretical approach and the error procedure is to compare a computed and measured $\psi_i(t)$ relationship for a given $\psi_e(t)$ and $\tau$. A tensiometer with a response time constant, as measured by the step input method, of 18.7 seconds was chosen and $\beta$ periods fixed at 8 seconds. The standard error relationship for a $m$ value of 1 cm./sec. applied for the $\beta$ period of 8 seconds is given in Table 4.2.

| Time (Seconds) | 0 | 8 | 16 | 24 | 32 | 40 | 48 | 56 | 64 | 72 | 80 | 88 | 96 |
|---|---|---|---|---|---|---|---|---|---|---|---|---|---|
| $\varepsilon$ (cm.) | 0 | 6.50 | 4.24 | 2.75 | 1.83 | 1.16 | 0.77 | 0.51 | 0.33 | 0.21 | 0.14 | 0.09 | 0.06 |

Table 4.2 - Standard Error Relationship
for $m$ = 1 cm./sec., $\beta$ = 8 sec., $\tau$ = 18.7 sec.

A fairly severe test of the procedure was made by inducing rapid changes in $\psi_e(t)$ in comparison with the time constant value.

For the first 16 seconds $m$ was made 1 cm./sec., for the next 16 seconds ½ cm./sec. and for the next 32 seconds ¼ cm./sec. This variation of suction was achieved experimentally by lowering the calibrating tensiometer down the calibrating rod at the appropriate rate. The only disadvantage in this process was a small instability error in readings during the first 30 seconds caused by the initial contact of the hand with the calibrating unit.

The computation is summarized in Table 4.3. The values $\psi_e$ and $\psi_i$ (by computation) may be readily compared. In addition the $\psi_i$ values as given by the recorded output from the transducer are

listed.  The actual chart record from which these values were obtained is given in Figure 4.4 with $\psi_e(t)$ superimposed for comparison purposes.

The identity of $\psi_i(t)$ (computed) and $\psi_i(t)$ (recorded) is very good indeed and strongly supports the validity of the method, particularly when it is remembered that the movement of the calibrating tensiometer was achieved manually and, although carefully carried out, could have been subjected to small irregularities.

When proceeding from $\psi_i(t)$ to $\psi_e(t)$ it is necessary to resort to an iterative form of solution.  The same general computational method as given in Table 4.3 is used.  A first estimate of the m values for the $\beta$ periods is determined from $\psi_i(t)$ and the error ordinates (now in fact correction ordinates) computed.  These are added to the initial values to give a new and improved $\psi_i(t)$ from which new m values are determined.  The process is repeated until there is no significant change between successive estimates.  The convergence of the process and the labour involved in the solution are dependent on the number of terms in $\varepsilon(t)$ which in turn is related to the values of $\tau$ and $\beta$ .  When, for a particular experiment, these factors are carefully balanced convergence is usually rapid.  In the example given in this study a rather extreme case has been chosen resulting in a tedious iterative process.

In some cases the correction procedure is extremely simple. For example, in using a tensiometer with a 25-30 micron pore size $\tau$ has a value of 0.1 seconds. If $\beta$ is taken as 4 seconds and m as 1 cm./sec.

then  $\varepsilon$ at 4 sec. $= m\tau \left(1 - e^{\frac{-t}{\tau}}\right) \doteqdot m\tau = 0.1$ cm.

| Time (sec.) | External Suction $\psi_e$ (cm.) | Gradient m (cm./sec.) | Error Ordinates $\Delta\varepsilon$ (cm.) Standard Error Values | | | | | | | | | | | | $\Sigma \Delta\varepsilon$ (cm.) | Computed Output $\psi_i$ (cm.) | Recorded Output | |
|---|---|---|---|---|---|---|---|---|---|---|---|---|---|---|---|---|---|---|
| | | | 6.50 | 4.24 | 2.75 | 1.83 | 1.16 | 0.77 | 0.51 | 0.33 | 0.21 | 0.14 | 0.09 | 0.06 | | | Uncorrected (cm.) | Corrected (cm.) |
| 0 | 0 | 1.0 | | | | | | | | | | | | | | 0 | 0 | 0 |
| 8 | 8 | 1.0 | 6.50 | | | | | | | | | | | | 6.50 | 1.50 | 1.8 | 1.6 |
| 16 | 16 | 0.50 | 6.50 | 4.24 | | | | | | | | | | | 10.74 | 5.26 | 6.0 | 5.8 |
| 24 | 20 | 0.50 | 3.25 | 4.24 | 2.75 | | | | | | | | | | 10.24 | 9.76 | 10.6 | 10.4 |
| 32 | 24 | 0.25 | 3.25 | 2.12 | 2.75 | 1.83 | | | | | | | | | 9.95 | 14.05 | 14.7 | 14.5 |
| 40 | 26 | 0.25 | 1.63 | 2.12 | 1.38 | 1.83 | 1.16 | | | | | | | | 8.12 | 17.88 | 18.4 | 18.4 |
| 48 | 28 | 0.25 | 1.63 | 1.06 | 1.38 | 0.92 | 1.16 | 0.77 | | | | | | | 6.92 | 21.08 | 21.5 | 21.5 |
| 56 | 30 | 0.25 | 1.63 | 1.06 | 0.69 | 0.92 | 0.58 | 0.77 | 0.51 | | | | | | 6.16 | 23.84 | 24.1 | 24.1 |
| 64 | 32 | 0 | 1.63 | 1.06 | 0.69 | 0.46 | 0.58 | 0.38 | 0.51 | 0.33 | | | | | 5.64 | 26.36 | 26.4 | 26.4 |
| 72 | 32 | 0 | | 1.06 | 0.69 | 0.46 | 0.29 | 0.38 | 0.26 | 0.33 | 0.21 | | | | 3.68 | 28.32 | 28.2 | 28.2 |
| 80 | 32 | 0 | | | 0.69 | 0.46 | 0.29 | 0.19 | 0.26 | 0.17 | 0.21 | 0.14 | | | 2.41 | 29.59 | 29.4 | 29.4 |
| 88 | 32 | 0 | | | | 0.46 | 0.29 | 0.19 | 0.13 | 0.17 | 0.10 | 0.14 | 0.09 | | 1.57 | 30.43 | 30.0 | 30.0 |
| 96 | 32 | 0 | | | | | 0.29 | 0.19 | 0.13 | 0.08 | 0.10 | 0.07 | 0.09 | 0.06 | 1.01 | 30.99 | 30.6 | 30.6 |
| 104 | 32 | 0 | | | | | | 0.19 | 0.13 | 0.08 | 0.05 | 0.07 | 0.05 | 0.06 | 0.63 | 31.37 | 31.2 | 31.2 |
| 112 | 32 | 0 | | | | | | | 0.13 | 0.08 | 0.05 | 0.04 | 0.05 | 0.03 | 0.38 | 31.62 | 31.4 | 31.4 |
| 120 | 32 | | | | | | | | | 0.08 | 0.05 | 0.04 | 0.02 | 0.03 | 0.22 | 31.78 | 31.6 | 31.6 |

TABLE 4.3.   Error Computation.
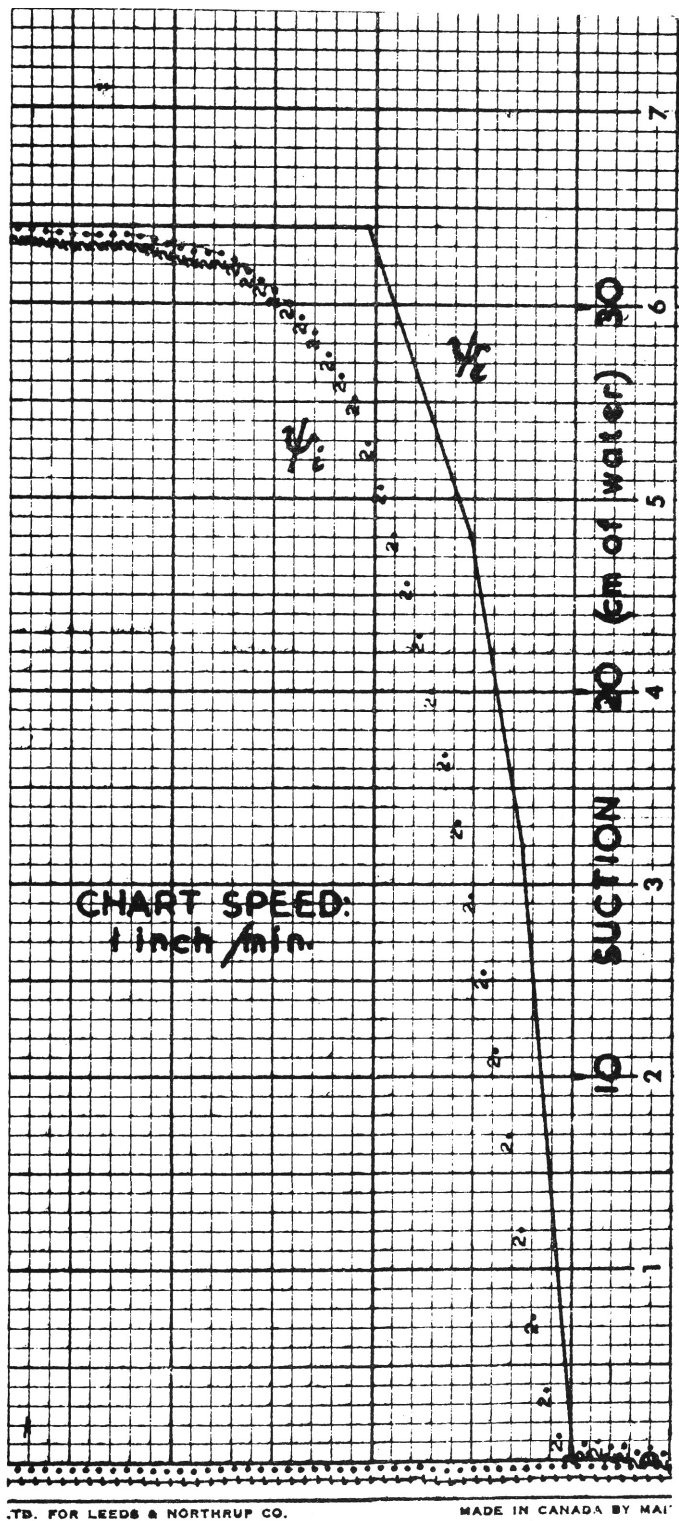
Figure 4.4    Recorder output ( $\psi_i$) for a varying suction

input ( $\psi_e$) ;    $\tau$ = 18. 7 seconds.

Since $e^{-\frac{t}{\tau}} = e^{-40}$ may be neglected.

Accordingly, the $\psi_e$ value at 4 seconds to one decimal place is 4.1 cm. Such a correction may be made by inspection.

## 4.5 Correction Computations

In those cases where the value of the time constant is such that iterative correction computations are necessary it is usual to specify $t$ as an integral number of $\beta$ periods. Hence, for $t = \beta$ it is convenient to write equation (4.6) as

$$\varepsilon = m\beta \cdot \frac{1}{\beta/\tau} (1 - e^{-\frac{\beta}{\tau}})$$

$$= I \cdot \frac{1}{\beta/\tau} (1 - e^{-\frac{\beta}{\tau}}) \quad \ldots \ldots \ldots (4.12)$$

where I = total input (applied linearly) during the $\beta$ period. Equation (4.8) may be similarly rewritten for the following $\beta$ periods. Using this approach the error relationship for a unit input (I = 1) is termed the 'Unit Error Function.' This function is able to be concisely specified for any value of $\beta/\tau$. Table 4.4 lists values of the function for the $\beta/\tau$ range 0.30 to 5.00. These values were extracted from a far more comprehensive list of values which were determined by programming the relationship for computation by a digital computer.

As mentioned in the last section, the iterative correction procedure can be time consuming when done by hand calculations. To eliminate this problem the writer has programmed the correction procedure in 3200 FORTRAN for processing on a Control Data Corporation 3200 Computer. The programme is listed in Table 4.5 and incorporates two correction methods; the unit error function

approach and a finite difference solution. The latter method requires data at intermediate points and consequently only every second value in the output data list is selected for the unit error function analysis.

The following explanations refer to the programme array names:

| | |
|---|---|
| UEF | Computed Unit Error Function |
| OUTPUT | Chart recorded suction values at specified time periods |
| DIFFRNCE | The difference between successive output values |
| SUM | Summation of the row elements in the two-dimensional array. |
| ARRAY | The diagonal two-dimensional array formed during the computation process |
| STORE | An intermediate storage location to simplify programme execution |
| UEFINPUT | The computed input values (that is, the output value plus correction) at the specified time periods using the unit error function procedure |
| FDINPUT | The computed input values using the finite difference solution |

The programme has been written in a general form and requires specification of the following quantities prior to execution.

| | |
|---|---|
| DATASETS | Number of separate sets of output curves to be processed |
| BETA | The basic time period |
| TAU | Time constant of the system |
| RUNL | Number of iterations required |
| M | Number of output values to be operated upon. This must be an odd number. |
| L | The number of terms required in the unit error function calculation |

## Ordinates of Unit Error Function

| $\beta/\tau$ | $t=\beta$ | $t=2\beta$ | $t=3\beta$ | $t=4\beta$ | $t=5\beta$ | $t=6\beta$ | $t=7\beta$ | $t=8\beta$ | $t=9\beta$ | $t=10\beta$ | $t=11\beta$ | $t=12\beta$ | $t=13\beta$ | $t=14\beta$ | $t=15\beta$ | $t=16\beta$ |
|---|---|---|---|---|---|---|---|---|---|---|---|---|---|---|---|---|
| 0.30 | .864 | .640 | .474 | .351 | .260 | .193 | .143 | .106 | .078 | .058 | .043 | .032 | .024 | .017 | .013 | .010 |
| 0.32 | .856 | .621 | .451 | .328 | .238 | .173 | .125 | .091 | .066 | .048 | .035 | .025 | .018 | .013 | .010 | .007 |
| 0.34 | .848 | .603 | .429 | .306 | .218 | .155 | .110 | .078 | .056 | .040 | .028 | .020 | .014 | .010 | .007 | .005 |
| 0.36 | .840 | .586 | .409 | .285 | .199 | .139 | .097 | .068 | .047 | .033 | .023 | .016 | .011 | .008 | .005 | .004 |
| 0.38 | .832 | .569 | .389 | .266 | .182 | .124 | .085 | .058 | .040 | .027 | .019 | .013 | .009 | .006 | .004 | .003 |
| 0.40 | .824 | .552 | .370 | .248 | .166 | .112 | .075 | .050 | .034 | .023 | .015 | .010 | .007 | .005 | .003 | .002 |
| 0.42 | .817 | .537 | .353 | .232 | .152 | .100 | .066 | .043 | .028 | .019 | .012 | .008 | .005 | .003 | .002 | .001 |
| 0.44 | .809 | .521 | .336 | .216 | .139 | .090 | .058 | .037 | .024 | .015 | .010 | .006 | .004 | .003 | .002 | .001 |
| 0.46 | .802 | .506 | .319 | .202 | .127 | .080 | .051 | .032 | .020 | .013 | .008 | .005 | .003 | .002 | .001 | .001 |
| 0.48 | .794 | .491 | .304 | .188 | .116 | .072 | .045 | .028 | .017 | .011 | .007 | .004 | .003 | .002 | .001 | |
| 0.50 | .787 | .477 | .289 | .176 | .107 | .065 | .039 | .024 | .014 | .009 | .005 | .003 | .002 | .001 | .001 | |
| 0.55 | .769 | .444 | .256 | .148 | .085 | .049 | .028 | .016 | .009 | .005 | .003 | .002 | .001 | | | |
| 0.60 | .752 | .413 | .226 | .124 | .068 | .037 | .021 | .011 | .006 | .003 | .002 | .001 | | | | |
| 0.65 | .735 | .384 | .200 | .105 | .055 | .029 | .015 | .008 | .004 | .002 | .001 | | | | | |
| 0.70 | .719 | .357 | .177 | .088 | .044 | .022 | .011 | .005 | .003 | .001 | | | | | | |
| 0.75 | .704 | .332 | .157 | .074 | .035 | .017 | .008 | .004 | .002 | .001 | | | | | | |
| 0.80 | .688 | .309 | .139 | .062 | .028 | .013 | .006 | .003 | .001 | | | | | | | |
| 0.85 | .674 | .288 | .123 | .053 | .022 | .010 | .004 | .002 | .001 | | | | | | | |
| 0.90 | .659 | .268 | .109 | .044 | .018 | .007 | .003 | .001 | | | | | | | | |
| 0.95 | .646 | .250 | .097 | .037 | .014 | .006 | .002 | .001 | | | | | | | | |
| 1.00 | .632 | .233 | .086 | .031 | .012 | .004 | .002 | .001 | | | | | | | | |
| 1.10 | .606 | .202 | .067 | .022 | .007 | .002 | .001 | | | | | | | | | |
| 1.20 | .582 | .175 | .053 | .016 | .005 | .001 | | | | | | | | | | |
| 1.30 | .560 | .153 | .042 | .011 | .003 | .001 | | | | | | | | | | |
| 1.40 | .538 | .133 | .033 | .008 | .002 | | | | | | | | | | | |
| 1.50 | .518 | .116 | .026 | .006 | .001 | | | | | | | | | | | |
| 1.60 | .499 | .101 | .020 | .004 | .001 | | | | | | | | | | | |
| 1.70 | .481 | .088 | .016 | .003 | .001 | | | | | | | | | | | |
| 1.80 | .464 | .077 | .013 | .002 | | | | | | | | | | | | |
| 1.90 | .448 | .067 | .010 | .001 | | | | | | | | | | | | |
| 2.00 | .432 | .059 | .008 | .001 | | | | | | | | | | | | |
| 2.10 | .418 | .051 | .006 | .001 | | | | | | | | | | | | |
| 2.20 | .404 | .045 | .005 | .001 | | | | | | | | | | | | |
| 2.30 | .391 | .039 | .004 | | | | | | | | | | | | | |
| 2.40 | .379 | .034 | .003 | | | | | | | | | | | | | |
| 2.50 | .367 | .030 | .002 | | | | | | | | | | | | | |
| 2.60 | .356 | .026 | .002 | | | | | | | | | | | | | |
| 2.70 | .345 | .023 | .002 | | | | | | | | | | | | | |
| 2.80 | .335 | .020 | .001 | | | | | | | | | | | | | |
| 2.90 | .326 | .018 | .001 | | | | | | | | | | | | | |
| 3.00 | .317 | .016 | .001 | | | | | | | | | | | | | |
| 3.20 | .300 | .012 | | | | | | | | | | | | | | |
| 3.40 | .284 | .009 | | | | | | | | | | | | | | |
| 3.60 | .270 | .007 | | | | | | | | | | | | | | |
| 3.80 | .257 | .006 | | | | | | | | | | | | | | |
| 4.00 | .254 | .004 | | | | | | | | | | | | | | |
| 4.20 | .235 | .004 | | | | | | | | | | | | | | |
| 4.40 | .224 | .003 | | | | | | | | | | | | | | |
| 4.60 | .215 | .002 | | | | | | | | | | | | | | |
| 4.80 | .207 | .002 | | | | | | | | | | | | | | |
| 5.00 | .199 | .001 | | | | | | | | | | | | | | |

TABLE 4.4    Ordinates of Unit Error Function for $\beta/\tau$ range 0.30 to 5.00.  Ordinates at intermediate values of $\beta/\tau$ may be determined by interpolation.

```
      PROGRAM CORRECTN
C     K.K.WATSON  CIVIL ENGINEERING  UNIVERSITY OF N.S.W.
      DIMENSION UEF(20),OUTPUT(160),DIFFRNCE(80),SUM(80)
      DIMENSION ARRAY(100,20),STORE(80),UEFINPUT(80),FDINPUT(160)
      READ (60,99) DATASETS
   99 FORMAT(F5.1)
      DATASET=1.
  100 READ(60,1) BETA,TAU,RUNL,M,L
    1 FORMAT(F5.1,F6.2,F5.1,I4,I3)
      READ(60,2)(OUTPUT(K),K=1,M)
    2 FORMAT(9F8.3)
      X=BETA/TAU
      DO 3 II=1,L
      Y=II-1
    3 UEF(II)=(EXPF  (-Y*X)-EXPF(-(Y+1.)*X))/X
      N=M-2
      DO 4 K=1,N,2
      I=(K+1)/2
    4 DIFFRNCE(I)=OUTPUT(K+2)-OUTPUT(K)
      MM=(M-1)/2
      DO 5 I=1,MM
    5 SUM(I)=DIFFRNCE(I)
      MMM=MM+L-1
      DO 6 K=1,MMM
      DO 6 II=1,L
    6 ARRAY(K,II)=0.0
      RUN=1.
    7 DO 8 I=1,MM
      DO 8 II=1,L
      K=I+II-1
    8 ARRAY(K,II)=UEF(II)*SUM(I)
      I=K
      DO 9 I=1,MM
    9 SUM(I)=0.0
      DO 10 I=1,MM
      DO 10 II=1,L
      PARTSUM=ARRAY(I,II)
   10 SUM(I)=SUM(I)+PARTSUM
      WRITE(61,11)(SUM(I),I=1,MM)
   11 FORMAT(17F8.3)
      DO 12 I=2,MM
   12 STORE(I)=DIFFRNCE(I)+SUM(I)-SUM(I-1)
      STORE(1)=DIFFRNCE(1)+SUM(1)
      DO 13 I=1,MM
   13 SUM(I)=STORE(I)
      RUN=RUN+1.
      IF(RUN-RUNL)7,14,14
   14 UEFINPUT(1)=OUTPUT(1)
      NN=MM+1
      DO 15 J=2,NN
      I=J-1
   15 UEFINPUT(J)=UEFINPUT(J-1)+SUM(I)
      WRITE(61,16)(UEFINPUT(J),J=1,NN)
   16 FORMAT(17F8.3)
      FDINPUT(1)=OUTPUT(1)
      FDINPUT(2)=(TAU*(OUTPUT(3)-OUTPUT(1)))/BETA+OUTPUT(2)
      DO 17 K=3,N
      FDINPUT(K)=OUTPUT(K-2)-8.*OUTPUT(K-1)+8.*OUTPUT(K+1)-OUTPUT(K+2)
   17 FDINPUT(K)=(FDINPUT(K)*TAU)/(6.*BETA)+OUTPUT(K)
      K=M-1
      FDINPUT(K)=(TAU*(OUTPUT(K+1)-OUTPUT(K-1)))/BETA+OUTPUT(K)
      K=M
      FDINPUT(K)=(TAU*(OUTPUT(K-2)-4.*OUTPUT(K-1)+3.*OUTPUT(K)))/BETA
      FDINPUT(K)=FDINPUT(K)+OUTPUT(K)
      WRITE(61,18)(FDINPUT(K),K=1,M)
   18 FORMAT(17F8.3)
      DATASET=DATASET+1.
      IF(DATASET-DATASETS)100,19,19
   19 STOP
      END
```

Table 4. 5:  FORTRAN Programme for Response
Correction of Suction Output.

To illustrate the expected accuracy of the correction procedure an analytical input equation of parabolic form has been chosen, and, using this, the output equation determined by solving equation (4.3). Following numerical substitutions and computer analysis the theoretical and computed inputs are compared in Table 4.6.

$$\text{Input Equation} : \quad \psi_e = \alpha t^2 \quad \ldots \ldots \ldots \ldots \quad (4.13)$$

$$\text{Output Equation} : \quad \psi_i = \alpha t^2 - 2\alpha\tau \left( t - \tau + \tau e^{-\frac{t}{\tau}} \right) \quad . \quad (4.14)$$

$$\text{whence} \quad \varepsilon = 2\alpha\tau \left( t - \tau + \tau e^{-\frac{t}{\tau}} \right)$$

At $t = o$ the system is in equilibrium with $\psi_e = \psi_i = 100$ cm.

Let $\tau = 10$ seconds, $\beta = 5$ seconds and $\alpha = \dfrac{1}{25}$ cm. sec$^{-2}$.

The data fed as OUTPUT into the computer is that given in the column 'Theoretical Output' in Table 4.6.

| Time (Seconds) | Theoretical Input (Equation 4.13) $\psi_e$ (cm.) | Theoretical Output (Equation 4.14) $\psi_i$ (cm.) | Computed Input Using Programmed Solution (cm.) |
|---|---|---|---|
| 0 | 100.00 | 100.00 | 100.00 |
| 5 | 101.00 | 100.15 | 100.69 |
| 10 | 104.00 | 101.06 | 103.96 |
| 15 | 109.00 | 103.21 | 108.73 |
| 20 | 116.00 | 106.92 | 115.89 |
| 25 | 125.00 | 112.34 | 124.85 |
| 30 | 136.00 | 119.60 | 135.78 |
| 35 | 149.00 | 128.76 | 148.83 |
| 40 | 164.00 | 139.85 | 163.88 |
| 45 | 181.00 | 152.91 | 180.84 |
| 50 | 200.00 | 167.95 | 199.81 |
| 55 | 221.00 | 184.96 | 220.80 |
| 60 | 244.00 | 203.98 | 243.87 |
| 65 | 269.00 | 224.99 | 268.83 |
| 70 | 296.00 | 248.00 | 295.89 |
| 75 | 325.00 | 273.00 | 324.80 |

Table 4.6. Comparison of Computed and Theoretical Inputs.

The suction increase over the 75 second period is rather large and, in this sense, the input relationship is somewhat idealized. However, such an example serves to emphasize the satisfactory nature of the correction technique. For experimental purposes the correspondence between the theoretical and computed inputs is quite acceptable, the magnitude of the variation generally being 0.1 to 0.2 cm. Using the programmed correction solution and knowing the time constant of the tensiometer-transducer arrangement it is possible therefore for the output from an experimental system to be accurately and rapidly corrected.

# CHAPTER 5

## WATER CONTENT MEASUREMENTS - OPERATING, CALIBRATION AND CORRECTION PROCEDURES.

### 5.1  Theory of Gamma-Ray Absorption Method

For a fixed distance between source and detector the attenuation equation for collimated monoenergetic gamma radiation is:

$$I/I_o = e^{-\mu\rho x} \qquad \dots \dots \dots \dots (5.1)$$

where  $I/I_o$   = ratio of incident & transmitted flux

$\mu$   = mass absorption coefficient $(cm.^2/gm.)$ of the absorber material for the energy of radiation.

$\rho$   = density of the material $(gm./cc.)$

$x$   = thickness of the sample $(cm.)$

As indicated, equation (5.1) is strictly correct only for a radiation having a single energy; this is approximately achieved by using the low-energy source $Cs^{137}$ as emitter. The peak energy of $Cs^{137}$ is 0.662MeV with the majority of the radiation occurring at that energy. This fact and the use of electrical means to limit the energy band measured enable equation (5.1) to be validly used. Equation (5.1) may be rewritten as

$$- \ln I/I_o = \mu\rho x \qquad \dots \dots \dots \dots (5.2)$$

Accordingly, the mass absorption coefficient of a material may be measured by interposing different thicknesses of the material between the source and detector and by measuring the transmitted radiation I. If the system is behaving monoenergetically, then on plotting $- \ln I/I_o$ versus $x$  a straight line should be obtained whose slope is  $\mu\rho$. Knowing  $\rho$, $\mu$   can be determined for that particular energy of radiation.

The equivalent equation to equation (5.1) when the material is a moist soil is:

$$I/I_o = e^{-(\mu_w \cdot w + \mu_s \cdot \rho) x} \qquad \ldots \ldots \ldots \quad (5.3)$$

where

$\mu_s$ and $\mu_w$ = mass absorption coefficients for soil and water respectively.

$w$ = mass of water/unit volume (gm./cc.)

$\rho$ = bulk density of the soil (gm./cc.)

If equation (5.3) is to be used to measure $w$ then it is necessary to know the values of $\mu_w$ and $\mu_s$ accurately and preferably under exactly the same operating conditions as will be used during the flow investigation. For this purpose a small accurately machined container constructed from Perspex is used. This container is without a top and has the dimensions of 15 cm. in length, 6 cm. in width, 2 cm. in depth. One end of the box is movable and can be accurately positioned to give a specimen of 3, 6, 9, 12 or 15 cm. in length. In determining the mass absorption coefficient of water, flux readings are taken with the movable partition in each position yielding $x$ values of 3, 6, 9, 12 and 15 cm. The same procedure is followed with soil, and care should be taken to pack the material in an identical manner each time. Davidson et al. (1963) adopted the alternative procedure and kept $x$ constant while varying $\rho$. The slope of the straight line on the semi-log plot is then $\mu x$ rather than $\mu \rho$. Both methods are satisfactory although, once a packing technique yielding reproducible densities is achieved, the 'box' method lends itself to greater accuracy. An example of a $\mu_s$ determination is given in Figure 5.1.

## 5.2 Selection of Operating Conditions

The pulses received from the scintillation counter are
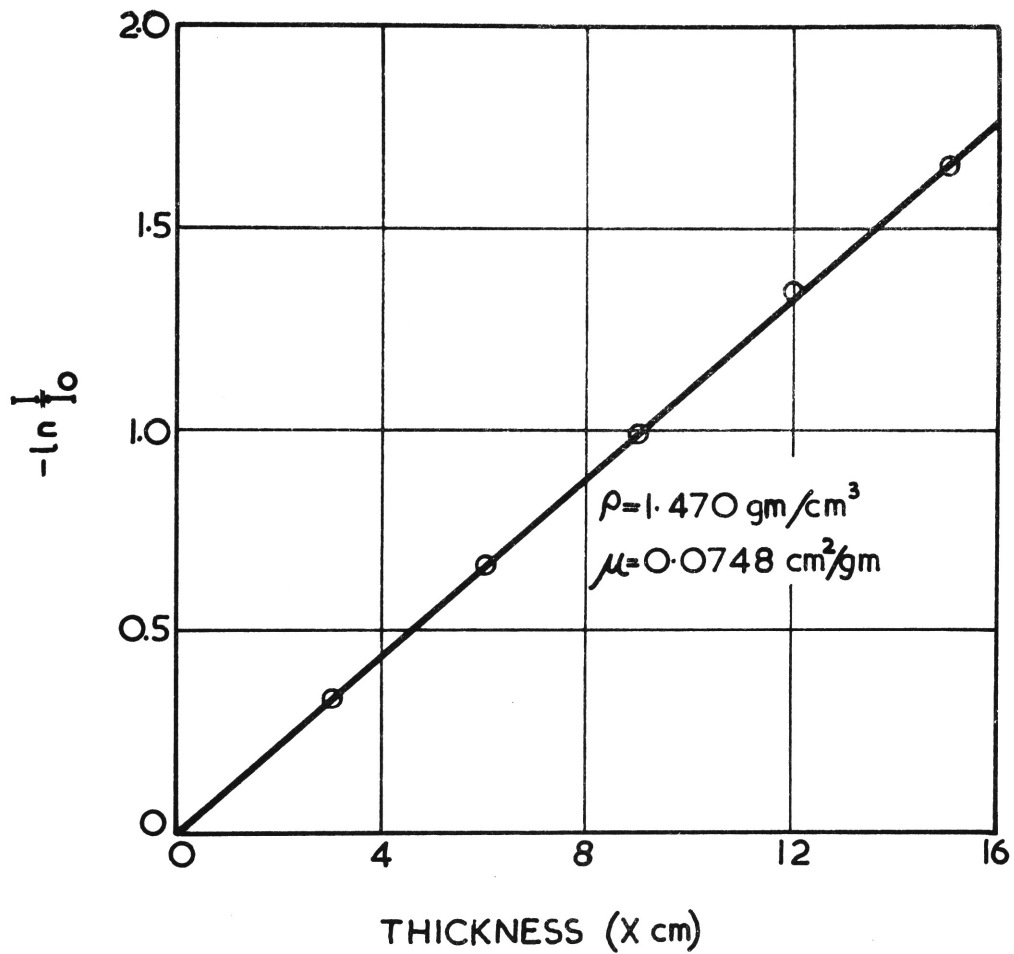
Figure 5. 1: Relation between attenuation and thickness of sample in determining the mass absorption coefficient of sand.

approximately proportional to the energy of the gamma photon that produced the pulses. However, the pulses are only a few millivolts in height and require amplification. The linear amplifier in the ratemeter has gain positions of x25, x50, x100, x250, x500, x1000 and amplifies the pulse from millivolts to tens of volts. Although $Cs^{137}$ is nearly monoenergetic, some dispersion occurs in its pulse height spectrum due to such effects as non-uniformity of the photocathode, escape of some electrons or secondary gamma rays to regions outside the crystal, 'dark noise' in the photocathode, etc. Accordingly, it is necessary to use the pulse height analyser firstly to determine the shape of the pulse height spectrum and then, having determined this, to set limits as to what part of the spectrum will be counted. Basically the analyser unit allows a threshold voltage and a gatewidth to be set. For example, if the threshold is set at 25 volts and the gatewidth at 5 volts, then the ratemeter will count only pulses in the voltage range of 25 to 30 volts.

The determination of the location of the $Cs^{137}$ peak and the spectrum shape is greatly facilitated by a motor driven unit on the analyser. This motor drive enables the pulse range to be scanned automatically at 1 volt/min. A suitable threshold is fixed as the commencing point of the scanning operation and the gatewidth is conveniently made 1 volt. By using the recorder a complete pulse height spectrum is then obtained. An example of such a spectrum is given in Figure 5.2. It should be noted that the shape and location of the spectrum will only be applicable to a particular setting of gain and the HV used. By changing these the shape of the spectrum and the modal position will also change. In general, for any given gain value the spectrum becomes more spread out and the modal voltage increases with increase in HV. Figure 5.3 indicates the varying spectra for a gain of x25. When the pulse height spectrum is known it is then possible to set the threshold and gatewidth

which will determine the counting limits. Ideally, keeping in mind that equations (5.1) and (5.2) are strictly applicable only to monoenergetic rays, the gatewidth would be made quite small and would be symmetrically placed on each side of the peak. However, the peak position changes slightly with density changes and if the energy range is too restricted erroneous readings will be obtained due to this shift. This peak movement effect will usually cause no counting errors with a gatewidth corresponding to $0.66 \pm 0.08$ MeV. With such a setting the count rate for the saturated sand is approximately 650 counts/sec. and for the drained sand at the maximum suction which occurs at the surface, about 950 counts/sec. This range of counts is sufficiently broad to give acceptable accuracy for the water content determinations and has the advantage that it is unnecessary for the scale setting on the ratemeter to be changed.

As mentioned in section 3.2, a standard lead absorber of comparable absorption to the saturated sand section is used to check electronic drift during an experiment and to adjust the ratemeter controls at a standard level for day to day operation. The 'standard' count with the absorber is 650 counts/sec.

The half-life of $Cs^{137}$ is 33 years, therefore its rate of decay is negligibly small over the 2-3 hours duration of the experiments and may be neglected.

## 5.3 Ratemeter Lag.

Whereas a scaler counts all pulses received by it and in general is only subject to error due to its finite resolving time, a ratemeter by its very construction has accuracy drawbacks. Essentially, a ratemeter consists of an RC circuit so designed that each pulse applies a constant charge to the capacitor and this charge is permitted to leak
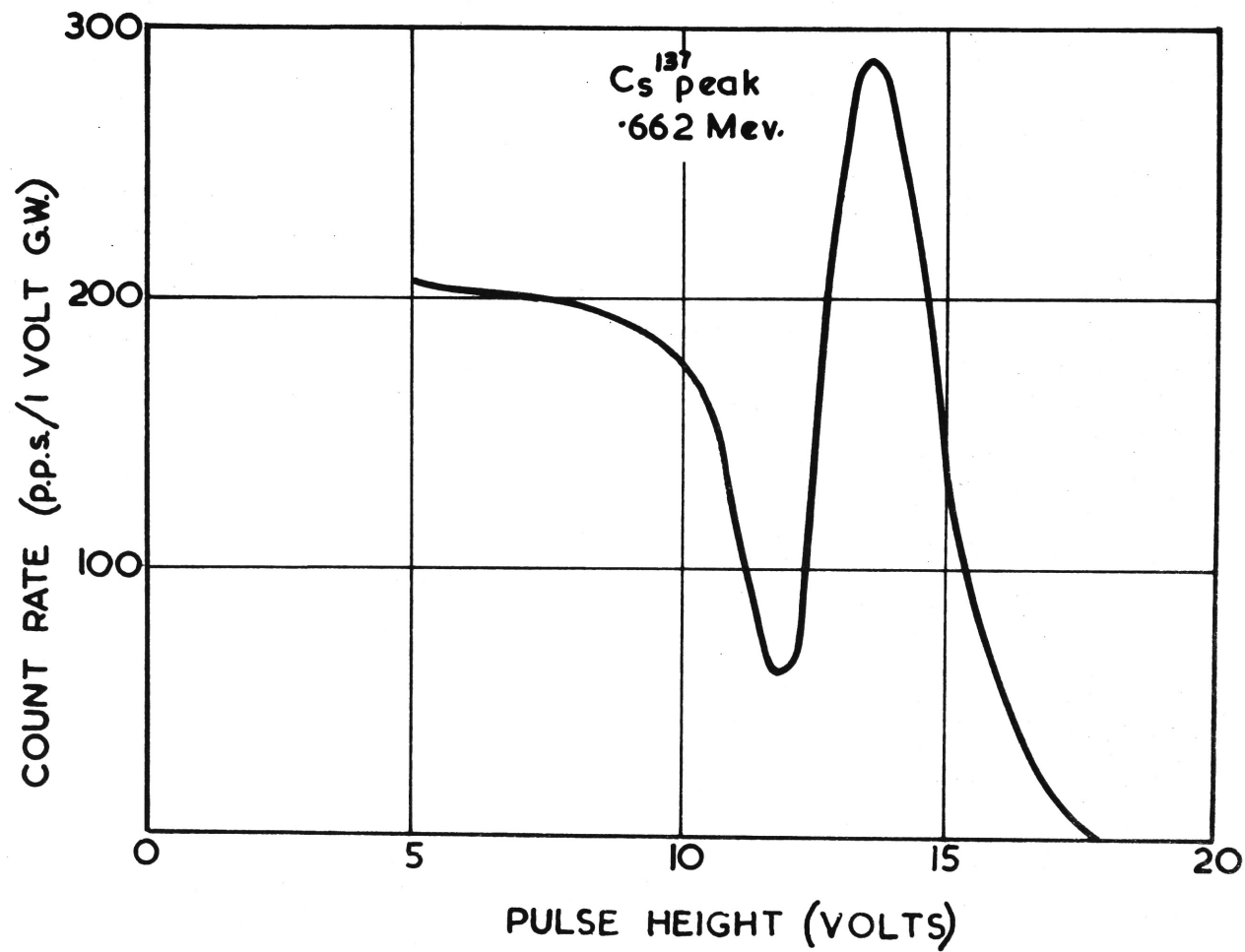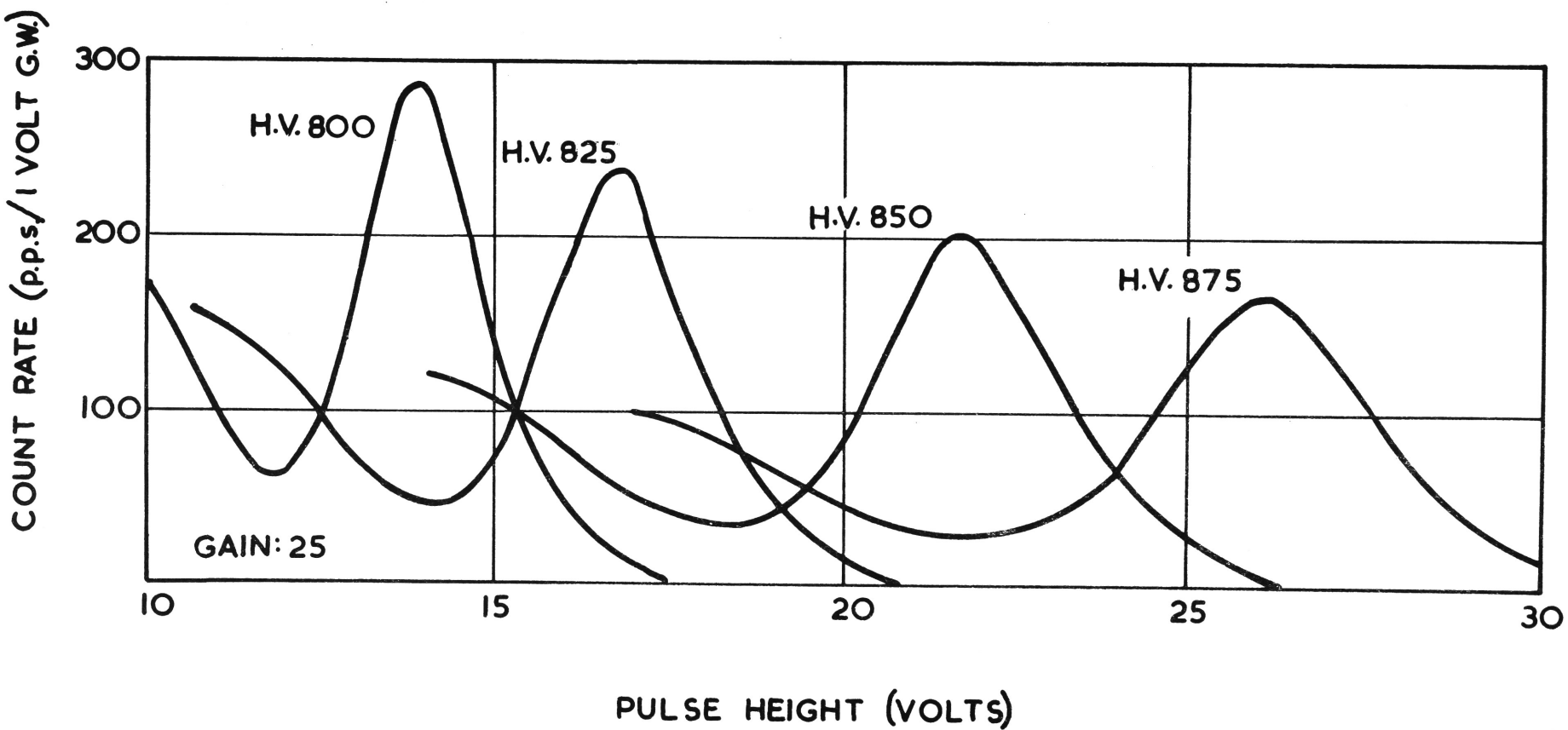
Figure 5. 2:   Pulse height spectrum of $Cs^{137}$.

Figure 5.3:   Variation of pulse height spectra with high voltage change.

away through the resistor at a rate proportional to the arrival of the pulses. In such a circuit, RC is known as the time constant and has the dimensions of time. The appropriate differential equation describing this effect is

$$V_i = V_o + RC \frac{dV_o}{dt} \qquad \dots\dots\dots\dots (5.4)$$

where $\quad V_i$ = input voltage to ratemeter circuit.

$\qquad\qquad V_o$ = output voltage.

This equation is identical in form to equation (4.2) and consequently the response equations developed in section 4.3 are also applicable to the ratemeter. Therefore, the ratemeter reading will lag behind the true reading by an amount dependent on the time constant. By reducing the time constant the response can be made more rapid but this will immediately increase the scatter of the readings about the mean value - an effect which is not paralleled in the hydraulic response pattern of Chapter 4. In using a ratemeter therefore, one is faced with the compromise between the speed of response and the amount of meter or recorder fluctuations that can be tolerated.

Statistically the position is as follows. Due to the random nature of radio-active disintegrations any observed count will fluctuate around a mean value in accordance with the normal law of error. Therefore, assuming that the standard deviation is approximately equal to the square root of the count (y), then :

$$\text{random error } (\%) = \frac{F \sqrt{y}}{y} \times 100 \qquad \dots\dots\dots (5.5)$$

where F = number of standard deviations for the confidence limits desired. For confidence limits of 50, 68.3 and 90 per cent, F has values of 0.675, 1.00 and 1.64 respectively. By comparing the expected standard deviation of a single condenser reading observed at any time with that obtained from a scaler reading for a specified time, it can be shown that

the statistical fluctuations after equilibrium of a single reading on a ratemeter of time constant RC are the same as if the source had been counted on a scaler for a time of 2 x RC. Hence, if y = N.t, where N = number of pulses/sec., and t = duration of counting period = 2RC, then :

$$\text{random error (\%) for 50\% confidence} = \frac{67.5}{\sqrt{2RCN}} \qquad \ldots\ldots\ldots\ldots(5.6)$$

If N = 1000 pulses/sec., RC = 6 sec., then the random error (%) = 0.62.

Because of the above drawbacks, ratemeter use is avoided where the count changes are such that a scaler could be used. However, a ratemeter is essential where it is desired to follow rapid moisture changes, and correction procedures must be worked out to give the desired accuracy.

The N600 ratemeter has a mean probable error (MPE) control which is based on the 50 per cent confidence limit. MPE values of 1, 2, 3, 5 or 10 per cent may be selected and, dependent on the counting range chosen (0-10, 0-30, 0-100, 0-300, 0-1,000, 0-3,000, 0-10,000 pulses/ sec.), the appropriate time constant is brought into the circuit. In addition, the time constant is automatically adjusted to maintain approximately the set MPE value for any reading between 1/3 full scale deflection (FSD) and full scale deflection. Usually the time constant is stated for the FSD position and rises automatically to 3 times this value at 1/3 FSD.

Electronically this is achieved in the following manner. The integrating capacitors in the circuit are connected across the selected measuring resistors via a Miller integrator valve (12AT7). This valve is employed to minimize calibration problems due to leakage when using long time constants and results in the value of the selected capacitor being multiplied by the gain of the valve and the leakage value being

divided by the gain. By means of two resistors in the meter circuit a bias is applied to the Miller valve depending upon the deflection of the meter and this bias is such that the gain on the valve is not linear but is approximately 3:1 over the range 1/3 FSD to FSD. As has been noted, this change of gain changes the effective capacitance of the selected capacitor and accordingly changes the time constant. The inclusion of this effect in equation (5.4) makes the differential equation non-linear and complicates considerably the theoretical aspects of the correction procedure. Two approaches are possible. The development of a correction procedure based on the non-linear differential equation, or the use of the linear approach over small sections of the scale where the time constant may be taken as constant without introducing significant errors. In this study the second approach has been utilized with promising results.

It should be noted that the specification of time constant variation over the range 1/3 FSD to FSD is a very nominal one and depends to a large extent on the precise characteristics of the integrator valve. These vary considerably from valve to valve and for any one valve will change with time causing similar changes in the time constant value. The first requirement therefore is a precise knowledge of the variation of time constant with scale reading. This can only be determined experimentally and requires a source of steady pulses which can be fed as desired into the ratemeter. A portable transistorized pulse generator[*] has been found very satisfactory for this purpose. This instrument provides a stable input and can be used with a range of pulse amplitudes from 0.1 volts to 10 volts.

The most satisfactory manner of determining the time constant is to apply, as previously, an instantaneous step input of pulses

---

[*] DYNATRON, Portable Pulse Generator, Type N 117.

(see section 4. 3) and then to compute the time constant from the recorded output. The difficulty in the present case is that due to the non-linearity of the instrument the time constant must be determined for each 50 unit section of the scale (e. g. 650-700 pulses/sec.) and this cannot be done accurately when the full chart width represents the range 0-1000 pulses/sec. (i. e. 0-100 mV input signal). To magnify the response as presented by the chart record a zero suppression unit attached to the recorder is used to suppress, for example, 600 pulses/sec. (i. e. 60 mV.) and the recorder range then changed to 0-10 mV. In this way the 50 pulses/sec. input, which represents a signal of 5 mV. is recorded across half the chart width. This is repeated in increments of 50 pulses/sec. until the range 400-1000 pulses/sec. is covered. The time constants for the instrument used in these experiments, as determined by the step input method, are given in Table 5. 1. It will be noted that, due probably to the age of the Miller valve, the actual time constants are very much less than those suggested by the specification. At 400 pulses/sec. the expected value would be 15 seconds rather than 8.6 seconds.

| Pulse Range (pulses/sec.) | Time Constant (seconds) |
|---|---|
| 400 - 450 | 8.6 |
| 450 - 500 | 8.4 |
| 500 - 550 | 8.2 |
| 550 - 600 | 8.0 |
| 600 - 650 | 7.8 |
| 650 - 700 | 7.6 |
| 700 - 750 | 7.4 |
| 750 - 800 | 7.2 |
| 800 - 850 | 6.9 |
| 850 - 900 | 6.6 |
| 900 - 950 | 6.3 |
| 950 - 1000 | 6.0 |

Table 5.1.  Time Constants for Ratemeter.

In correcting a recorded output for ratemeter lag the same general correction procedure is utilized as presented in section 4.4. In order to check this correction procedure with the complication of time constant change during pulse rate change a known linearly increasing pulse rate was fed into the ratemeter using the pulse generator, and the recorded output compared with a computed output using the unit error function approach modified to allow for the varying value of the time constant. The input rate (8 pulses/sec./sec.) may be considered very severe in comparison with the pulse rate gradient which occurs in column experiments. For example, in the drainage of the initially saturated sand the gradient was slightly in excess of 1 pulse/sec./sec. The equilibrium position prior to pulse input was 400 pulses/sec. and the input rate was maintained for 32 seconds giving a final expected reading of 656 pulses/ sec. The actual final reading was 655 pulses/sec.; accordingly, in the computations the incremental input during the last second was assumed to be 7 pulses/sec. By observing, from the output record, the number of periods ($\beta$ = 4 seconds) in each range section over which the time constant is assumed constant it is possible to calculate the values of the error ordinates governed by that time constant. This is repeated for each range section falling within the total pulse rate change. The process is a fairly lengthy one since it is necessary to use several unit error functions. The output record with the input superimposed is given in Figure 5.4. The computations are presented in Table 5.2. A study of this table indicates the very good correspondence between the recorded and computed values. The pulse input using the pulse generator was carried out manually over the 32 second period and, although care was taken, slight variations of input gradient could have occurred.

When correcting the chart record for ratemeter lag in column experiments only the output record is available and the iterative process, as discussed in section 4.4, must be used to determine the true input.

However, the position is a good deal less tedious than would be expected because the output record is usually linear over periods of 1/2 minute and accordingly $\beta$ can be taken as 30 seconds. Since this is large compared with the time constant value the error ordinate to be applied in the following $\beta$ period is very small and may be safely neglected. An example of this for an output extending over one period only from a steady state condition is given below.

Assume $\beta$ = 30 sec., $\tau$ = RC = 7.5 sec.

Incremental output (I) = 30 pulses/sec.

Now $\beta/\tau = 4.0$ and from Table 4.4, at $\tau = \beta$, unit error = 0.245

$\tau = 2\beta$, unit error = 0.004

### 1st Iteration

I = 30 pulses/sec. $\therefore$ $\varepsilon$ at 30 seconds = 30 x 0.245 = 7.4 pulses/sec.

$\varepsilon$ at 60 seconds = 30 x 0.004 = 0.1 pulse/sec.

Since the limit of reading of the output chart is 1 pulse/sec. the correction at 60 seconds may be neglected; the decimal place in the correction at 30 seconds is retained for the iterative process only.

### 2nd Iteration

New I = 37.4 pulses/sec.

$\therefore$ $\varepsilon$ at 30 seconds = 37.4 x 0.245 = 9.2 pulses/sec.

### 3rd Iteration

New I = 39.2 pulses/sec.

$\therefore$ $\varepsilon$ at 30 seconds = 39.2 x 0.245 = 9.6 pulses/sec.

### 4th Iteration

New I = 39.6 pulses/sec.

$\therefore$ $\varepsilon$ at 30 seconds = 39.6 x 0.245 = 9.7 pulses/sec.
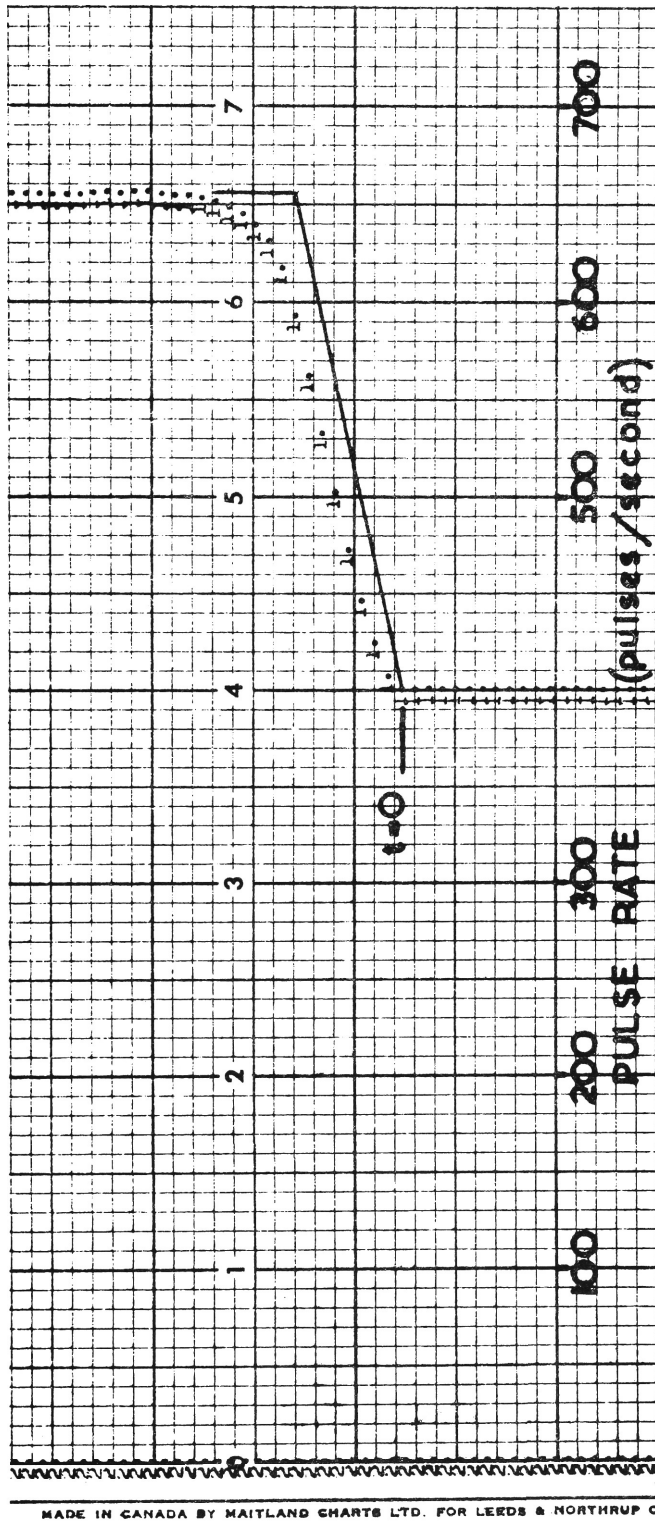
Figure 5.4: Recorder output from ratemeter following a linear input of pulses from the pulse generator.

| Time (sec.) | Input (pulses/sec.) | Incremental Input (pulses/sec.) | Error Ordinates (Δε) (pulses/sec.) | | | | | | | | | | | Σ Δε | Computed Output (pulses/sec.) | Recorded Output (pulses/sec.) |
|---|---|---|---|---|---|---|---|---|---|---|---|---|---|---|---|---|
| 0 | 400 | 32 | | | | | | | | | | | | 0 | 400.0 | 400 |
| 4 | 432 | 32 | 25.58 | | | | | | | | | | | 25.6 | 406.4 | 407 |
| 8 | 464 | 32 | 25.58 | 16.06 | | | | | | | | | | 41.6 | 422.4 | 424 |
| 12 | 496 | 32 | 25.58 | 16.06 | 10.08 | | | | | | | | | 51.7 | 444.3 | 445 |
| 16 | 528 | 32 | 25.46 | 15.81 | 9.82 | 6.10 | | | | | | | | 57.2 | 470.8 | 472 |
| 20 | 560 | 32 | 25.46 | 15.81 | 9.82 | 6.10 | 3.79 | | | | | | | 61.0 | 499.0 | 501 |
| 24 | 592 | 32 | 25.32 | 15.55 | 9.54 | 5.86 | 3.58 | 2.21 | | | | | | 62.1 | 529.9 | 532 |
| 28 | 624 | 31 | 25.18 | 15.26 | 9.25 | 5.62 | 3.41 | 2.06 | 1.25 | | | | | 62.0 | 562.0 | 561 |
| 32 | 655 | 0 | 24.40 | 15.26 | 9.25 | 5.62 | 3.41 | 2.06 | 1.25 | 0.77 | | | | 62.0 | 593.0 | 593 |
| 36 | 655 | 0 | | 14.51 | 8.96 | 5.38 | 3.20 | 1.92 | 1.15 | 0.69 | 0.42 | | | 36.5 | 618.5 | 618 |
| 40 | 655 | 0 | | | 8.68 | 5.38 | 3.20 | 1.92 | 1.15 | 0.69 | 0.42 | 0.26 | | 21.7 | 633.3 | 632 |
| 44 | 655 | 0 | | | | 5.21 | 3.20 | 1.92 | 1.15 | 0.69 | 0.42 | 0.26 | 0.15 | 13.0 | 642.0 | 640 |
| 48 | 655 | 0 | | | | | 3.10 | 1.92 | 1.15 | 0.69 | 0.42 | 0.26 | 0.15 | 7.7 | 647.3 | 646 |
| 52 | 655 | 0 | | | | | | 1.86 | 1.15 | 0.69 | 0.42 | 0.26 | 0.15 | 4.5 | 650.5 | 649 |
| 56 | 655 | 0 | | | | | | | 1.12 | 0.69 | 0.42 | 0.26 | 0.15 | 2.7 | 652.3 | 652 |
| 60 | 655 | 0 | | | | | | | | 0.68 | 0.42 | 0.26 | 0.15 | 1.5 | 653.5 | 654 |
| 64 | 655 | 0 | | | | | | | | | 0.40 | 0.26 | 0.15 | 0.8 | 654.2 | 655 |
| 68 | 655 | 0 | | | | | | | | | | 0.26 | 0.15 | 0.4 | 654.6 | 655 |
| 72 | 655 | | | | | | | | | | | | 0.15 | 0.2 | 654.8 | 655 |

TABLE 5.2.   Error Computation for Ratemeter Correction

## 5th Iteration

New I = 39.7 pulses/sec.

$\therefore$ $\varepsilon$ at 30 seconds = 39.7 x 0.245 = 9.7 pulses/sec.

The correction to be applied to the output reading at 30 seconds is thus 10 pulses/sec. with a negligible correction necessary in the succeeding period. Such a correction procedure can be very rapidly carried out.

The iterations in correcting an actual ratemeter output during the drainage of the sand column are given in Table 5.3. In this example the time constants applicable to the various sections of the meter scale are those given in Table 5.1, $\beta$ is taken as 30 seconds and the unit error functions are interpolated from the values given in Table 4.4.

## 5.4   Calibration

It is now evident that the sources of error in using a ratemeter to measure the changing water content of a soil may be listed as follows:

(a)     Random error due to the nature of radioactive disintegrations and the ratemeter circuitry. This error is given in terms of a single ratemeter reading; however, when a continuous chart record is available a mean curve can be drawn through the fluctuations resulting in improved accuracy of count.

(b)     Error due to lack of calibration in the ratemeter. This can be adjusted using the pulse generator and scaler to equal the limit of reading of the ratemeter dial or, more preferably, the chart record.

(c)     Error caused by electronic drift during the experiment. This can be adequately allowed for using the standard absorber.

| Time (min.) | Ratemeter Output (pulses/sec.) | Incremental Output (pulses/sec.) | Time Constant (seconds) | Unit Error at $t = \beta$ | Input 1st Iteration | Input 2nd Iteration | Input 3rd Iteration | Adopted Input |
|---|---|---|---|---|---|---|---|---|
| 0 | 650 | | | | 650 | 650 | 650 | 650 |
| | | 28 | 7.6 | 0.248 | | | | |
| ½ | 678 | | | | 685.0 | 686.7 | 687.1 | 687 |
| | | 29 | 7.6 | 0.248 | | | | |
| 1 | 707 | | | | 714.2 | 714.2 | 713.8 | 714 |
| | | 23 | 7.4 | 0.243 | | | | |
| 1½ | 730 | | | | 735.6 | 735.2 | 735.1 | 735 |
| | | 20 | 7.4 | 0.243 | | | | |
| 2 | 750 | | | | 754.9 | 754.7 | 754.7 | 755 |
| | | 20 | 7.2 | 0.237 | | | | |
| 2½ | 770 | | | | 774.7 | 774.7 | 774.7 | 775 |
| | | 20 | 7.2 | 0.237 | | | | |
| 3 | 790 | | | | 794.7 | 794.7 | 794.7 | 795 |
| | | 19 | 6.9 | 0.226 | | | | |
| 3½ | 809 | | | | 813.3 | 813.2 | 813.2 | 813 |
| | | 17 | 6.9 | 0.226 | | | | |
| 4 | 826 | | | | 829.8 | 829.7 | 829.7 | 830 |

Table 5.3. Input Computation from actual Ratemeter Output obtained during Drainage Experiments.

(d)    Errors due to ratemeter lag when the count rates are changing rapidly. For the conditions encountered in the column experiments the readings can be corrected as discussed in the last section to a degree better than the limit of reading of the chart.

(e)    Errors which are related to the use of the attenuation equation and the assumption of monoenergetic radiation in calculating the water contents of the sand from the count rate.

In assessing these sources of error it is noted that the first four sources listed are related to the obtaining of an accurate count reading for the density changes occurring and the fifth concerns the basic validity of the method as seen from the accuracy viewpoint. In regard to this latter source of error some progress can be made by studying the accuracy of the various elements in the equation, but since we are dealing with the relevance of a physical law to the process in question it is finally necessary to resort to experimental means to assess the expected accuracy of the method.

This section is concerned with such a calibration procedure and the method used in calculating the moisture content for the conditions existing in this study. Inherent in the statement of errors above must be the assumption for column experiments that variations arising from non-uniform packing of the column are small compared with the other sources of error. For this reason and other very important hydraulic reasons (for example, the sensitivity of the suction-water content relationship to small density variations) it is a necessity to have a uniformly packed column. This can be ensured using the gamma-ray method. By utilizing the electronic timer and scaler over fairly long counting periods it is possible to minimize the random error

and compare the gamma-ray absorption at different levels. Knowing the mass absorption coefficients of soil and water, the densities at each level in the column can be computed; if these densities are not within the allowable experimental limits the column can be repacked until the desired uniformity is achieved.

The procedure used in calculating the water content when the column is initially saturated is very convenient requiring only one mass absorption coefficient, that of water. During the packing of the column careful record is kept of the weight of the dry sand and water used. Since the sand is deposited under water it can safely be assumed that the column is fully saturated. Accordingly the bulk density of the sand and the volumetric water content are determinable. In addition, the accuracy of these values can be checked by comparing the total volume of the added sand and water with the known volume of the column. In the computational procedure given below the bulk density value is not required.

For a constant value of incident flux $I_o$ equation (5.7) may be derived from equation (5.3).

$$\frac{I \text{ dry sand}}{I \text{ moist sand}} = e^{\mu_w \cdot w_m \cdot x} \quad \cdot \cdot \cdot \cdot \cdot \cdot \cdot \cdot \cdot (5.7)$$

where $w_m$ = volumetric water content of moist sand (cc./cc.)

At saturation $w_m = w_{sat.}$

The following data are available :

$$I_{sat..} = 650 \text{ pulses/sec.}$$

$$w_{sat.} = 0.3500 \text{ cc./cc.}$$

$$\mu_w = 0.0841 \text{ cm.}^2/\text{gm.}$$

$$x = 15.00 \text{ cm.}$$

Therefore

$$\log_{10} I_d = \frac{\mu_w \cdot w_{sat} \cdot x}{2.3026} + \log_{10} I_{sat.} \quad \ldots \quad (5.8)$$

The water content $w_m$ for any reading $I_m$ is then

$$w_m = \frac{2.3026}{15.0 \times .0841}(\log_{10} I_d - \log_{10} I_m) = 1.8253 \, (3.00466 - \log_{10} I_m) \quad (5.9)$$

An example of the computation of water content changes during the first ten minutes of the drainage of the saturated column at one elevation is given in Table 5.4. The ratemeter readings listed have been corrected for drift and lag.

| Time (min.) | $I_m$ Corrected (pulses/sec.) | $\log_{10} I_m$ | $\log_{10} \frac{I_d}{I_m}$ | $w_m$ (cc./cc.) |
|---|---|---|---|---|
| 0 | 650 ($I_{sat.}$) | 2.8129 | 0.1918 | 0.350 ($w_{sat.}$) |
| 1 | 718 | 2.8561 | 0.1486 | 0.271 |
| 2 | 762 | 2.8819 | 0.1228 | 0.224 |
| 3 | 792 | 2.8987 | 0.1060 | 0.194 |
| 4 | 813 | 2.9101 | 0.0946 | 0.173 |
| 5 | 830 | 2.9191 | 0.0856 | 0.156 |
| 6 | 842 | 2.9253 | 0.0794 | 0.145 |
| 7 | 853 | 2.9309 | 0.0738 | 0.135 |
| 8 | 861 | 2.9350 | 0.0697 | 0.127 |
| 9 | 869 | 2.9390 | 0.0657 | 0.120 |
| 10 | 875 | 2.9420 | 0.0627 | 0.114 |

Table 5.4. Water Content Calculation.

The comparison between the water contents computed by the attenuation equation and determined by gravimetric means is made using a specially constructed Perspex box of internal cross section

15 cm. x 10 cm. and 15 cm. in height. The box comprises fifteen 1 cm. thick sections, which are screwed together through side brackets. Such an arrangement permits any sample height to be used up to the maximum of 15 cm. The bottom unit consists of a porous stone so set in its base that a vacuum can be applied to the sand through it. The saturated sand is placed in the multi-section box, the necessary scaler readings taken and a vacuum is applied to the porous base. When sufficient moisture has been drawn from the sand to provide a suitable moisture profile in equilibrium, another series of scaler readings is taken and the 'column' sliced along each 1 cm. section to obtain gravimetric moisture content samples.

The arrangement described above is in general very satisfactory but care has to be exercised in interpreting the results. This is principally because the moisture profile varies quite markedly down the sample causing significant changes through the 1 cm. sections. In parts of the profile the change is not linear through the section with the result that a gamma-ray reading taken only in the centre of the section produces an erroneous comparison. The gravimetric moisture content is of necessity an average through the section and to make valid comparisons it is necessary to take at least three gamma-ray readings for each slice and from these determine the average moisture content for the slice. When this procedure is followed comparisons can be validly made.

| Section Number | Average Moisture Content (cc./cc.) | |
| | Gamma-ray Method | Gravimetric Method |
| --- | --- | --- |
| 2 | 0.213 | 0.216 |
| 3 | 0.184 | 0.185 |
| 4 | 0.170 | 0.173 |
| 5 | 0.161 | 0.163 |
| 6 | 0.156 | 0.153 |
| 7 | 0.121 | 0.119 |

Table 5.5.   Moisture Determination Comparisons.

Table 5.5 summarizes the results of a typical calibration experiment. A careful analysis of such experiments together with a consideration of the significance of the other sources of error discussed indicates that in general the accuracy obtained from computed water contents is of the order of 1% or better for the high moisture contents and 2% for the drier values. These accuracies are quite satisfactory for the precise experimentation of the nature discussed in the following chapters.

# CHAPTER 6

## THE DRAINAGE CYCLE

### 6.1 Objectives

The first phase of the column experimentation is concerned with the vertical drainage of the initially saturated sand column. The objectives of this work, which is reported in this chapter, are as follows:-

(a) The determination of the soil suction-moisture content relation under unsteady state conditions and the comparison of this relation with that given by the equilibrium condition existing in the column after extended drainage.

(b) The development of a method for determining the capillary conductivity-water content relation under unsteady state conditions by using the experimental information relating to the change of water content and suction with time at several elevations in the column.

(c) The investigation of the applicability of Darcy's Law to unsaturated unsteady flow using the information evaluated in (b).

(d) The numerical solution of the differential equation of flow for those boundary conditions imposed by the vertical drainage problem using the suction and conductivity parameters determined in (a) and (b) above.

(e) A comparison of the computed and measured moisture profiles.

## 6.2 Experimental

In this section the experimental details not previously outlined in the descriptions of the pressure and water content measuring equipment will be discussed. The discussion is in a condensed form with only those details, necessary to impart a clear concept of the experiment, being included.

The sand fraction used was obtained from Botany Sand and comprised that material passing a No. 50 sieve and being retained on a No. 100 sieve. The grains were well rounded and, as would be expected from the narrow sieving range, were fairly uniform in size. Figure 6.1 is a photograph of some grains from the sand fraction at a magnification of x135.

The base of the column is so constructed that air at atmospheric pressure is always maintained during an experiment on the underside of the screen (100 mesh) supporting the sand. The lowest elevation in the sand column is thus a fixed piezometric surface at atmospheric pressure; this surface is conveniently taken as the datum in gradient measurements.

The sand is always placed in the column assembly in small quantities with 2 or 3 inches depth of excess water continuously available over the surface of the sand already deposited. In this way a fully saturated sand column is obtained. Compaction in thin layers by surface tamping is continued until a uniform density as determined by gamma-ray attenuation is obtained over the full column length of 57 cm. Prior to the commencement of an experiment 'standard' readings are taken against the standard lead absorber and the standard water column, whose surface is positioned at the transducer diaphragm level.

The temperature in the laboratory is controlled by a room conditioning unit which regulates the temperature to $69^{\circ}F \pm 1.5^{\circ}F$. Since in these experiments the study of water movement under evaporative

demand is not involved humidity control is unnecessary and the above unit is quite satisfactory.

A steady state condition is achieved at the start of the experiment by supplying excess water (distilled and boiled) to the surface of the column such that a very small head of water (1 mm.) is maintained there. This condition is continued for approximately 10 minutes during which time the rate of volume outflow from the bottom of the column is measured. Under these conditions the hydraulic gradient is known and, from the rate of volume outflow, the hydraulic conductivity is able to be determined. In the above work care has to be exercised to ensure that the sand surface receives a minimum of disturbance; in addition to this precaution, continuous compaction of the surface is carried out during this preparatory part of the experiment.

The steady state saturated flow condition just described also allows the tensiometers to reach an equilibrium condition prior to the commencement of drainage. This is not of critical importance in the present experiments due to the very porous ceramic used (25-30 micron pore size); however, if a much finer ceramic is used an initial equilibrium condition is essential.

The drainage cycle commences the moment the ponded water disappears through the upper soil surface. The pressure change at this time is so rapid that it is very clearly defined on the recorder chart. Although in principle it is possible by using the traversing mechanism and the multi-inlet valve to cover moisture and suction changes through-out a full column length without replication, this is not possible with the sand fraction due to the speed at which it drains. In forming the replicate columns careful control using the gamma-ray equipment is exercised to obtain a bulk density corresponding to that in the first column. Using the methods described in the last chapter the saturated moisture content for the column was $0.3500 \pm .0005$ cc./cc. and the
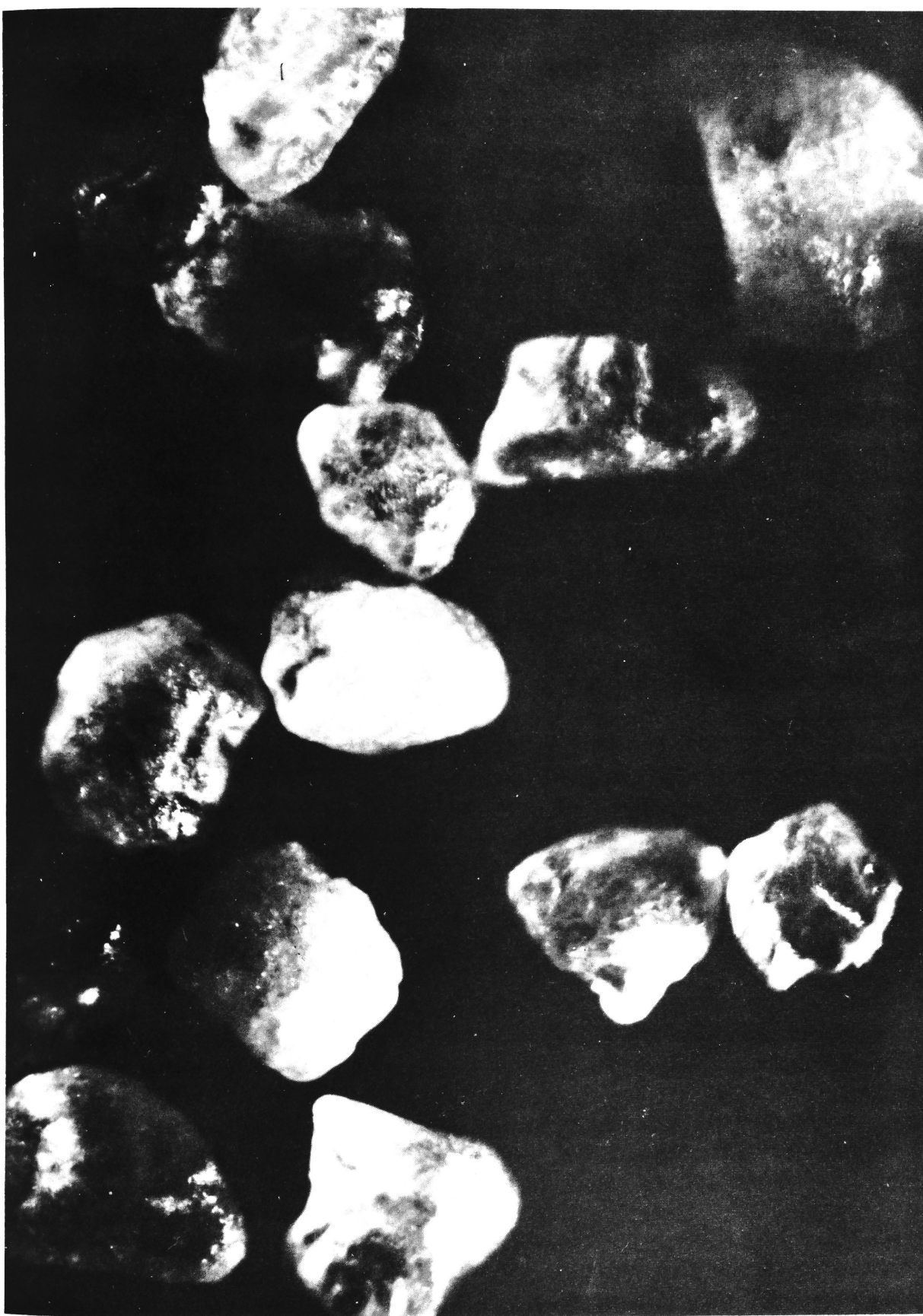
Figure 6.1:   Photograph of Sand Fraction Grains,
Magnification x135.

bulk density 2.080 $\overset{+}{-}$ .002 gm./cc.

Figure 6.2 is a reproduction of the chart record for the first five minutes of the draining cycle, the measurements of both suction and moisture content being taken at an elevation of 54 cm. Channel 1 records the gamma-ray attenuation with the full chart width representing the 0-1000 pulses/second ratemeter range. The output from the strain gauge measuring bridge is recorded by Channel 2 with 21.8 chart divisions representing 10.0 cm. suction for this experiment. The strain gauge bridge is balanced (that is, zero reading on the recorder chart) against the standard water column, whose surface is held constant at transducer diaphragm level. Relative to this position, the recorded pressure during the steady state saturated condition for any point in the column <u>above</u> transducer diaphragm level is positive. This is illustrated in Figure 6.2 where the recorded pressure due to the elevation difference between the tensiometer and the transducer diaphragm is 31.7 divisions during the steady state condition. This rapidly changes to a negative pressure (see Figure 6.2) as soon as drainage commences; the change to a negative pressure is accommodated experimentally by changing the output terminal on the bridge from +ve to -ve as the dot record approaches the zero reading. A study of the chart record in Figure 6.2 emphasizes the very steady nature of the suction record (Channel 2). In contrast, the ratemeter output fluctuates somewhat due to the random nature of radioactive disintegrations; the dots are usually joined and a mean curve drawn through the fluctuating readings. Regular readings are taken during the experiment against the standard lead absorber and the standard water column. The outflow-time relation is determined by piping the outflow to the pan of the automatic balance. The surface of the column is protected against evaporation whilst the equilibrium position is being reached over an extended time.

## 6.3    The Draining Moisture Characteristic

The experimental information obtained from the corrected pressure and water content measurements is summarized in Figures 6.3 and 6.4.  Figure 6.3 indicates the variation of soil water suction with time at several elevations in the column for the first 20 minutes of drainage. The experimental points from which the curves have been drawn have been omitted for clarity since their inclusion would, in fact, entail the reproduction of the dot record output as illustrated in Figure 6.2.  In a similar manner Figure 6.4 gives the water content changes with time at the same column elevations.  Where replicate columns have been used the results are extremely consistent with those plotted, the variations being too small to indicate graphically.  Not all the experimental information has been summarized in these figures since suction and water content readings were taken at intermediate elevations to those shown and at elevations less than 45 cm.  In addition, the total period of reading was in excess of 20 minutes, being usually 1 to 2 hours.  Not all the columns tested were permitted to drain to equilibrium.  It was not possible to record suction and water content changes at the upper surface of the soil column, but readings were taken 2 mm. below the surface and these were extrapolated to give the surface ($z = 57$ cm.) values shown by the dashed line.

The position of the drainage front (defined as that plane at which drainage is just commencing) at any elapsed time may be easily determined from the curves in Figure 6.4.  For example, the sand at elevations of 49 and 43 cm. commences to drain at 4 and 16 minutes respectively.  From such information Figure 6.5 may be drawn; this gives the relation between the time and the position of the drainage front for the first 20 minutes.

The draining moisture characteristic under unsteady state conditions is derived by plotting, for a particular elevation, the water content against the soil suction both values being taken at the same elapsed
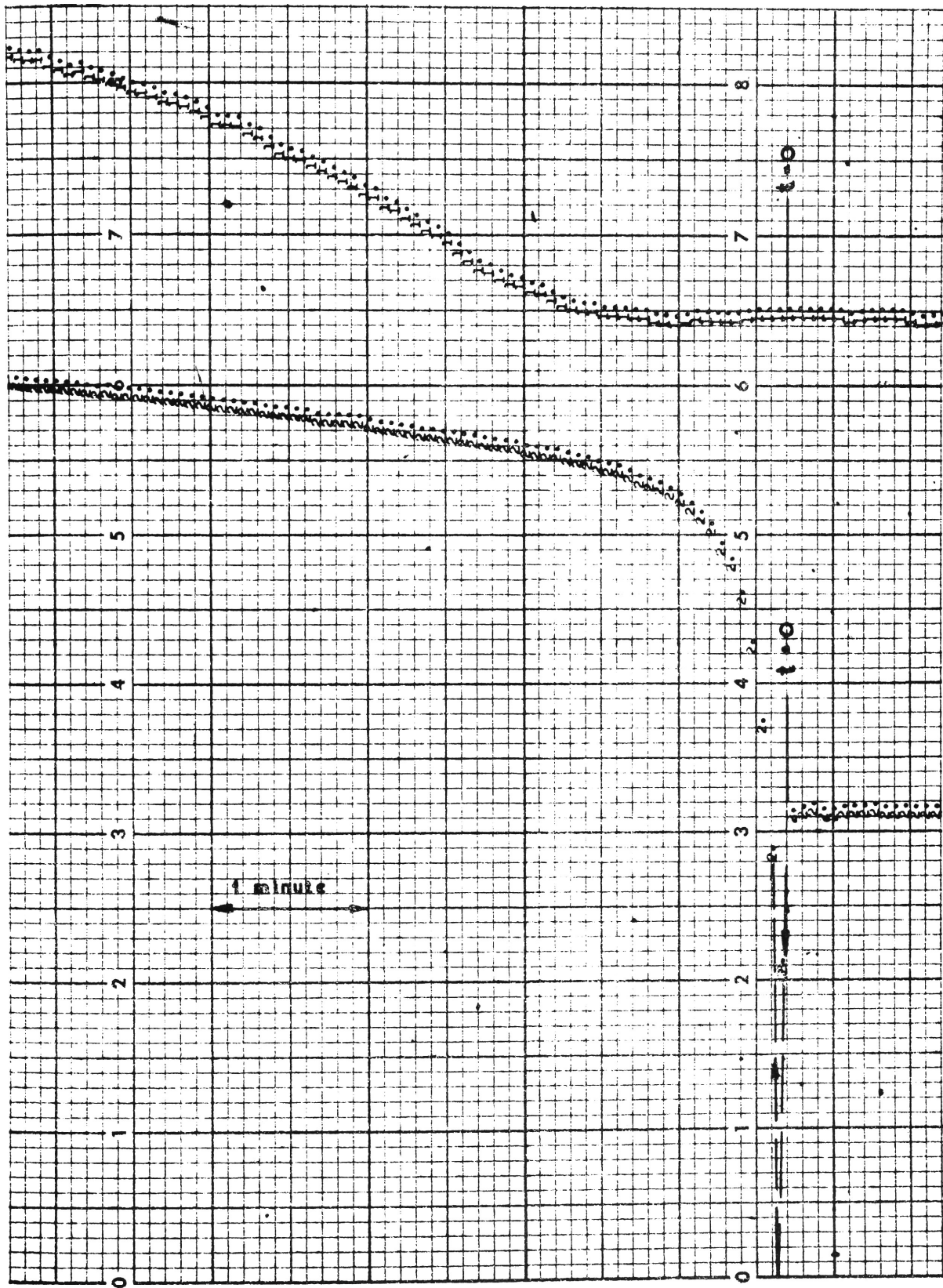
Figure 6. 2:   Typical chart record at commencement of drainage.
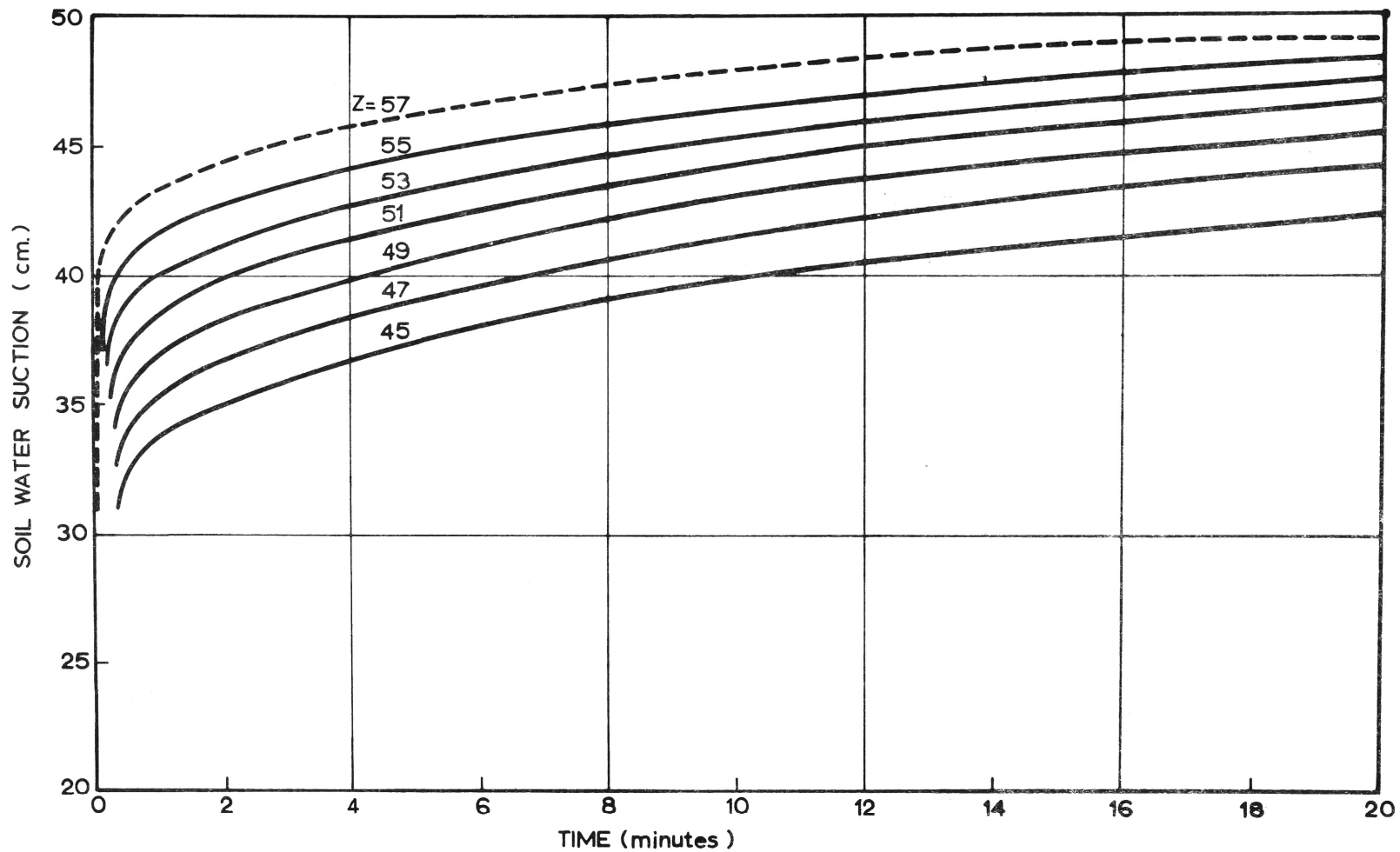
Figure 6. 3:   Variation of soil water suction with time at several column elevations.
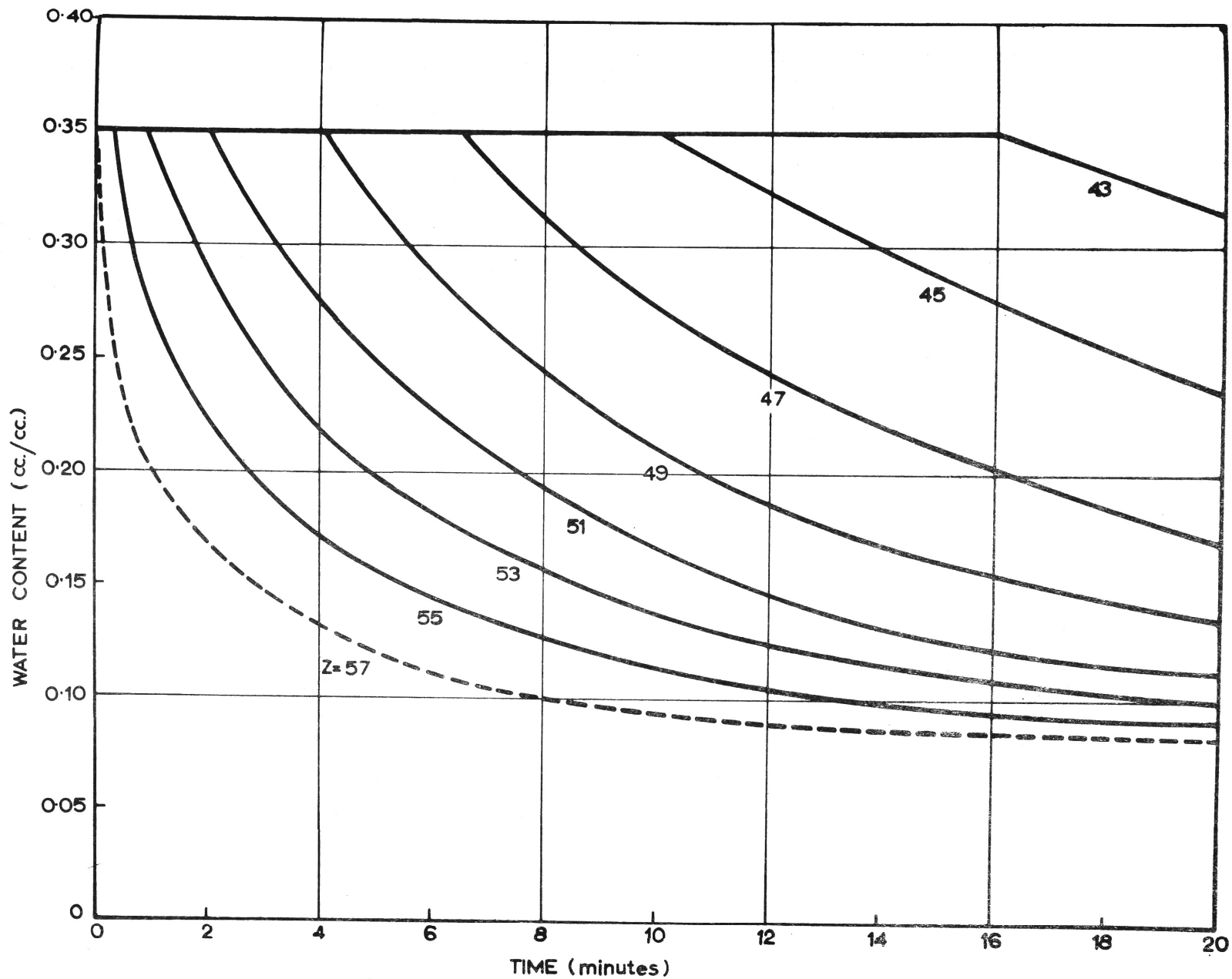
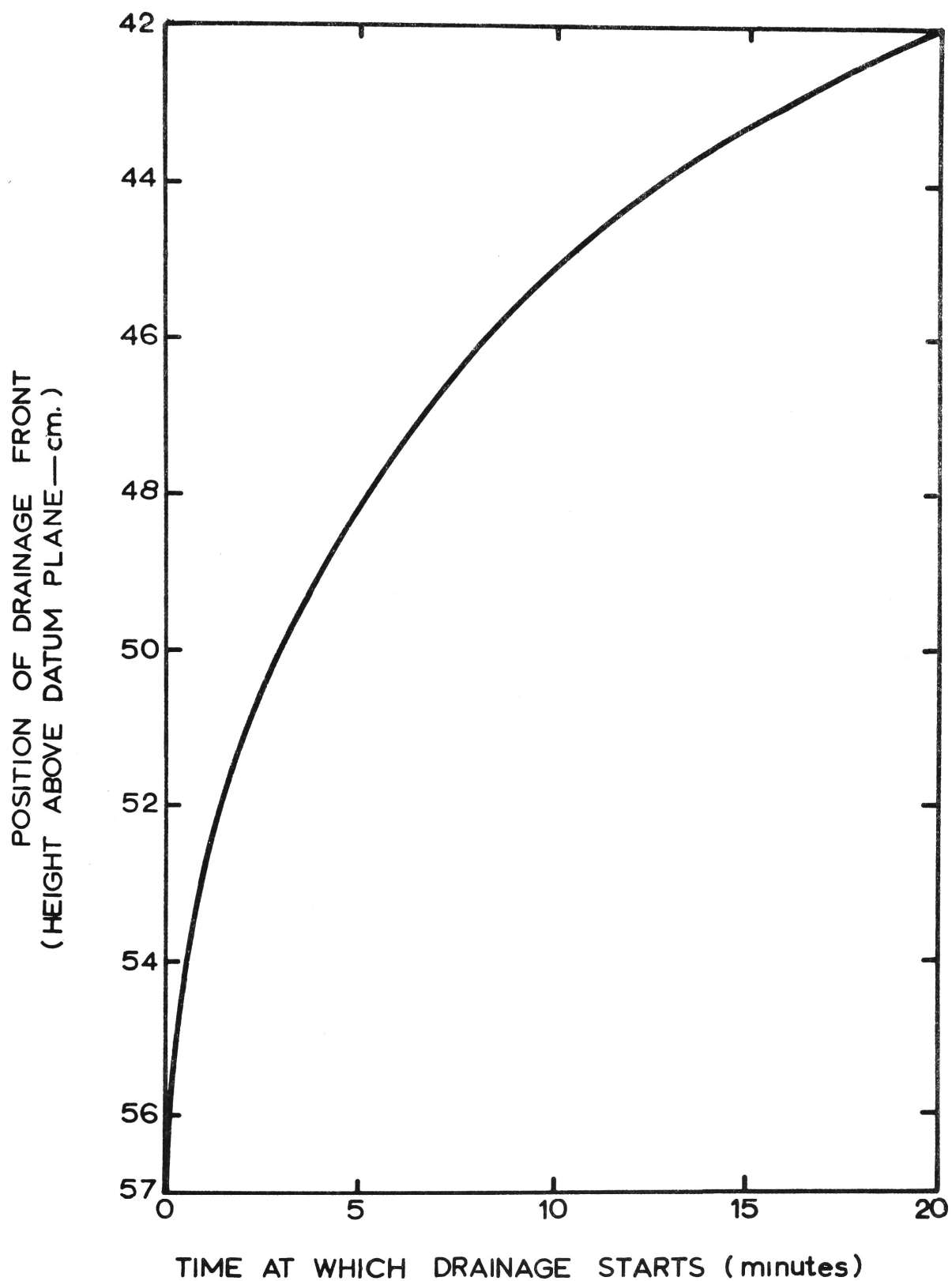Figure 6. 4:   Variation of moisture content with time at several column elevations.

Figure 6.5: Relation between time and position of the drainage front.

times. This may be repeated for several different times. The results of
this procedure are given in Figure 6.6 where the relationship is plotted for
elevations of 55, 53, 51 and 49 cm. The numerals beside the plotted plots
represent the times at which the moisture content and soil suction were
read. The points closely follow a common curve and this has been drawn
in Figure 6.7. The most significant aspect of this curve, apart from the
excellent correspondence of points at different elevations, is the very
distinct air-entry value of 39.8 cm. It is evident from all the chart records
taken that no moisture change occurs in this sand fraction at the compacted
density until a suction pressure of 39.8 cm. is reached; when this suction
value is attained drainage immediately commences as illustrated in Figure
6.2 by the distinct upward trend in the ratemeter reading. The critical
nature of the air-entry value is difficult to determine with such precision
by the more normal equilibrium methods usually used in moisture
characteristic determinations. In addition there are other very real
advantages in the method. Due to its non-destructive nature a complete
moisture characteristic can be obtained on a single soil cross section;
this can be achieved rapidly and in a dynamic draining situation. Another
significant feature of the moisture characteristic is the narrow suction
range over which considerable moisture changes occur; an increase of
suction from 39.8 to 44.8 cm. decreases the water content from 0.35 to
0.15 cc./cc. The correspondence between the relationships obtained at
different elevations is indicative of the close density control attained.

In the equilibrium condition after extended drainage (with the
column protected against evaporation) the suction at any elevation is
equal to the height of that point above the datum plane. By measuring
the moisture contents at various elevations the moisture characteristic
under the equilibrium condition may be plotted. This information is
also included in Figure 6.6. There is good agreement between these
points and the unsteady state points over the majority of the curve.

However, near the air-entry value the equilibrium moisture profile becomes a little diffuse and a sharp cut-off there is not accurately discernible or measurable, although if its existence can be assumed it can be obtained by extrapolating the lower section of the curve backwards.

## 6.4    The Method of Instantaneous Profiles

The experimental information of Figures 6.3 and 6.4 provides a powerful and instructive means of determining the capillary conductivity-water content relation. The approach has been termed by the writer, the method of instantaneous profiles. In essence, the method consists of determining down the column, the profiles of the macroscopic flow velocity, the potential gradient and the water content at any instant of time after the commencement of drainage. Once these are known for a particular time it is then possible to find the capillary conductivity for each elevation by dividing the appropriate velocity value by the potential gradient value. Since the moisture profile is known at this same time a series of points on the capillary conductivity-water content relation is available.

The first step in the method is to find from Figure 6.4 the relations between $\partial w / \partial t$ and z at several required times.   w represents the volumetric moisture content (cc./cc.) and z is the elevation above the datum plane defined as positive in the upward direction. In this analysis, profiles at times of 1, 3, 5, 10 and 20 minutes have been considered. Since the equation of continuity for an unsaturated soil in a one dimensional flow system is

$$\partial w / \partial t = - \partial v / \partial z \qquad \dots\dots\dots (6.1)$$

where  v   is the velocity in cm./sec., the velocity profiles are obtained by integrating graphically with respect to z the $\partial w / \partial t$  profile curves. This has been carried out for the above times and the resulting velocity
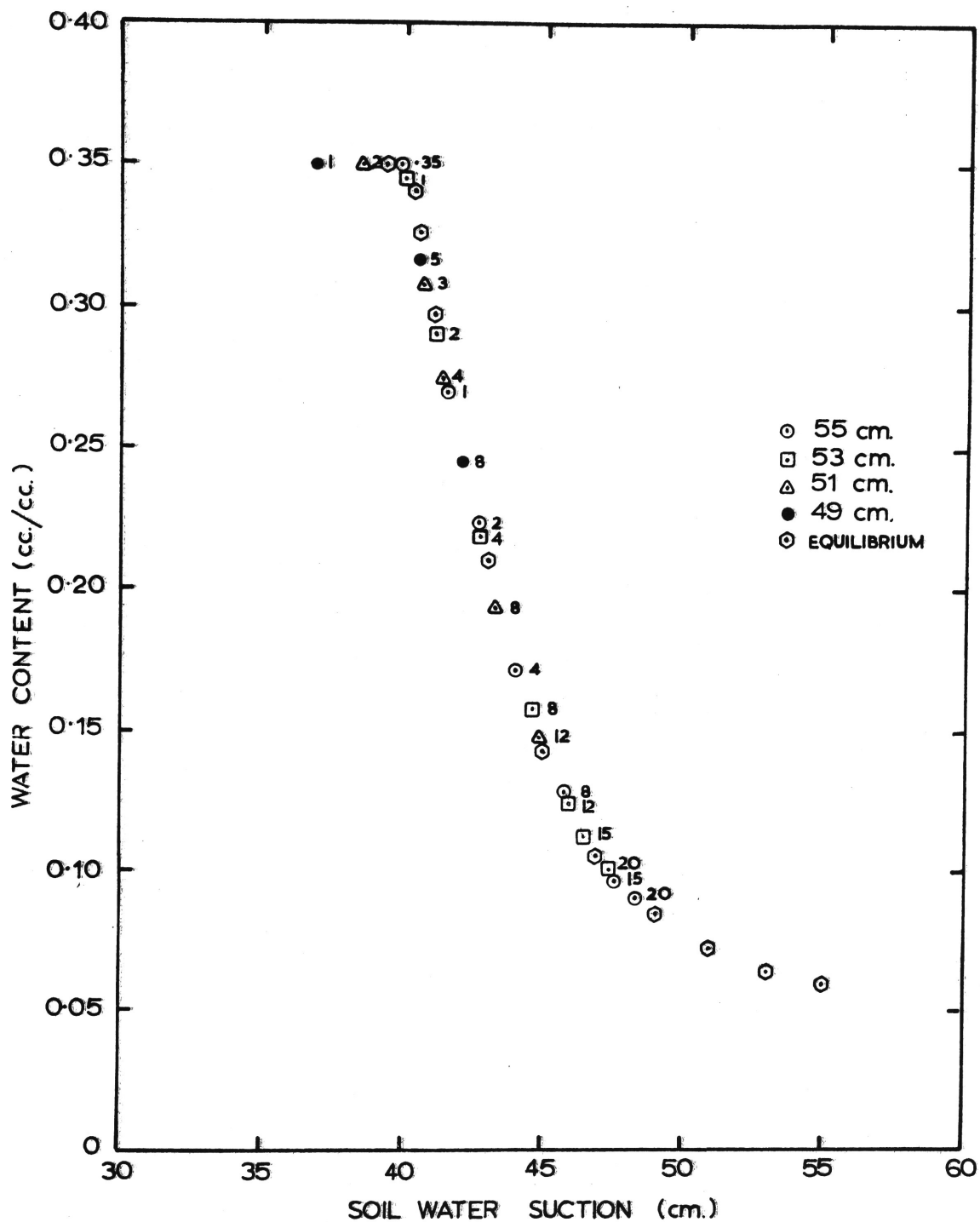
Figure 6.6:

Experimental points for moisture characteristic determination.
The numerals beside the plotted points represent the time in
minutes at which the water content and suction readings were taken.
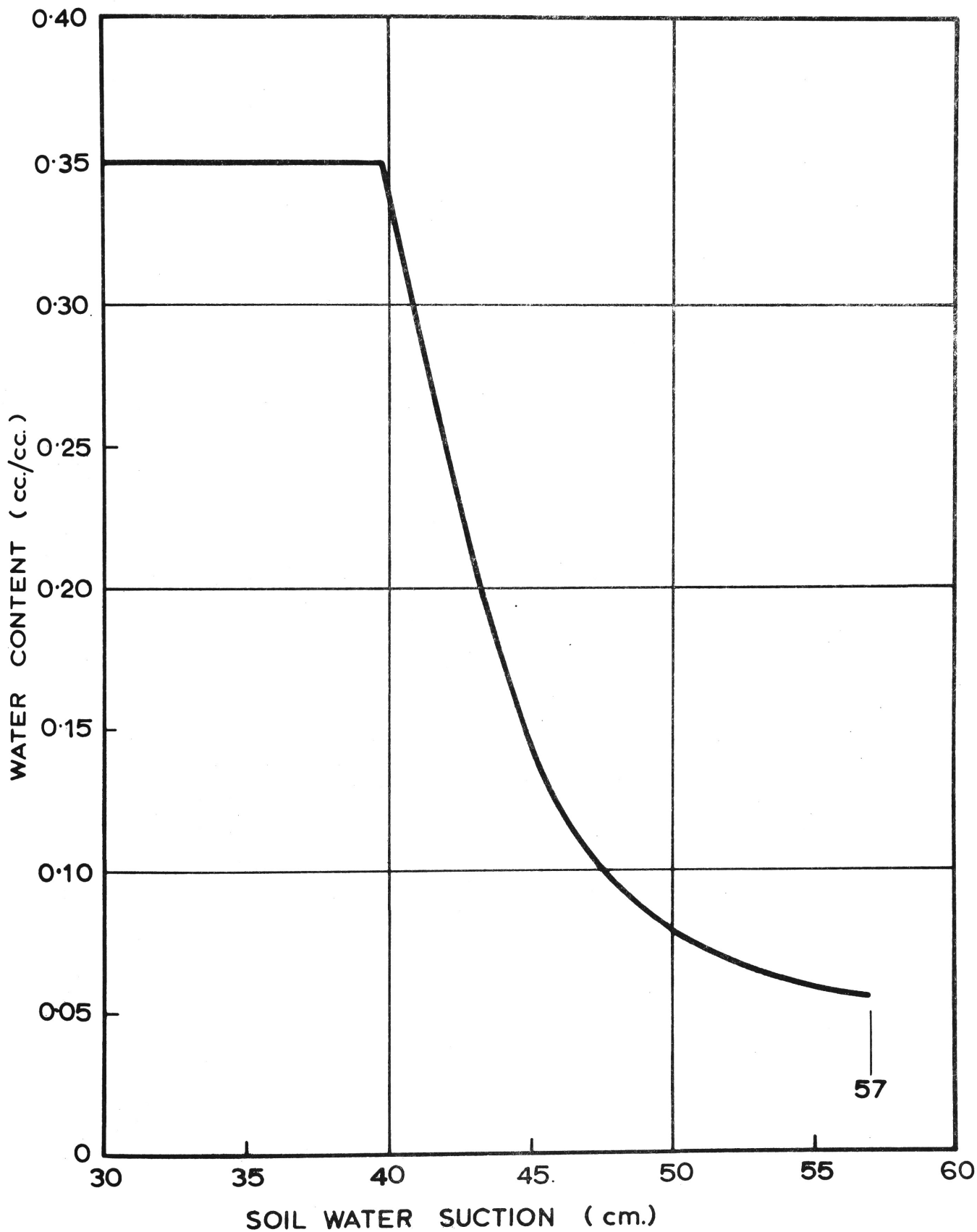
Figure 6.7: The draining moisture characteristic determined under unsteady state conditions.

profiles are given in Figure 6.8. These profiles represent the instantaneous velocities down the column at the times stated. For consistency with the sign convention adopted these velocities are negative. The instantaneous velocity is constant throughout the still-saturated zone of the column.

The first part of the next step is the determining of the soil suction profile values at 1, 3, 5, 10 and 20 minutes from Figure 6.3. Since the total potential $\varphi$ is equal to the negative suction component $\psi$ and the gravitational component z, the total potential profiles at the above times, may be readily plotted. These are presented in Figure 6.9. These curves may be differentiated graphically to give the positive potential gradient $(\partial \varphi / \partial z)$ profiles, these being presented in Figure 6.10. In the graphical differentiation the total potential curves were redrawn to a much larger scale.

From Figures 6.8 and 6.10 it is a relatively simple matter to determine the capillary conductivity K for any elevation and time by dividing the velocity value at that point in space-time by the corresponding potential gradient value, due note being taken of the signs. The final requirement is the water content profiles at the selected times. These profiles are read directly from Figure 6.4 and are presented in Figure 6.11 for times of 1, 3, 5, 10, 20 minutes and for equilibrium. The last step in the method is the plotting of the K (w) curve using the w and K values just obtained. This relationship is given in Figure 6.12 where the conductivity scale is logarithmic to enable the smaller conductivities to be accurately presented. It should be noted that, in Figure 6.12, the points plotted for the different elapsed times form a single relationship with only small experimental departures occurring. This relationship has been replotted in Figure 6.13 in its more usual form with a natural scale being used for the capillary conductivity.

The single relationship evidenced in Figure 6.12 from data taken at different times and more importantly at widely different gradients for any given moisture content is of fundamental importance. Childs

and Collis-George (1950) showed that for steady state flow in an unsaturated porous material and for any given moisture content there was a linear relationship between velocity and gradient; or, that Darcy's Law (keeping in mind the limitations of moisture dependence) was valid for steady flow in unsaturated materials. It has been customary to extend the relationship to unsteady flow conditions by developing the differential flow equation which implies that the very reasonable assumption has been made that the acceleration terms and other possible dynamic effects have a negligible effect on the relationship. However, up to this time, no experimental evidence of the validity of this assumption has been forthcoming. This is now provided by Figure 6.12 since all the data plotted were measured under transient conditions. Basically, Figure 6.12 means that the linear relationship between velocity and potential gradient at a given moisture content is valid under unsteady state conditions. This is of fundamental interest particularly as the sand fraction is a free-draining material with the dynamic effects being of a magnitude as large as likely to occur under most conditions.

In addition to the advantage of determination under unsteady state conditions the method is able, at the larger times, to span a wide range of capillary conductivity values. For example, at 20 minutes the values derived vary from 0.000015 to 0.01860 cm./sec. This obviates one of the difficulties in steady state measurements of capillary conductivity where a small constant flow to the surface is difficult to maintain.

The aspect of the method which is sensitive to error and which must be closely watched concerns the graphical differentiations. Since the result of one of these is integrated and then divided by the other to give the $K$ value small errors can result in much larger $K$ variations.

## 6.5 The Numerical Solution

The experimental measurements summarized in Figures 6.3 and 6.4 and the derived $\psi$ (w) and $K$ (w) relationships provide the required data for carrying out a numerical solution of the vertical drainage problem
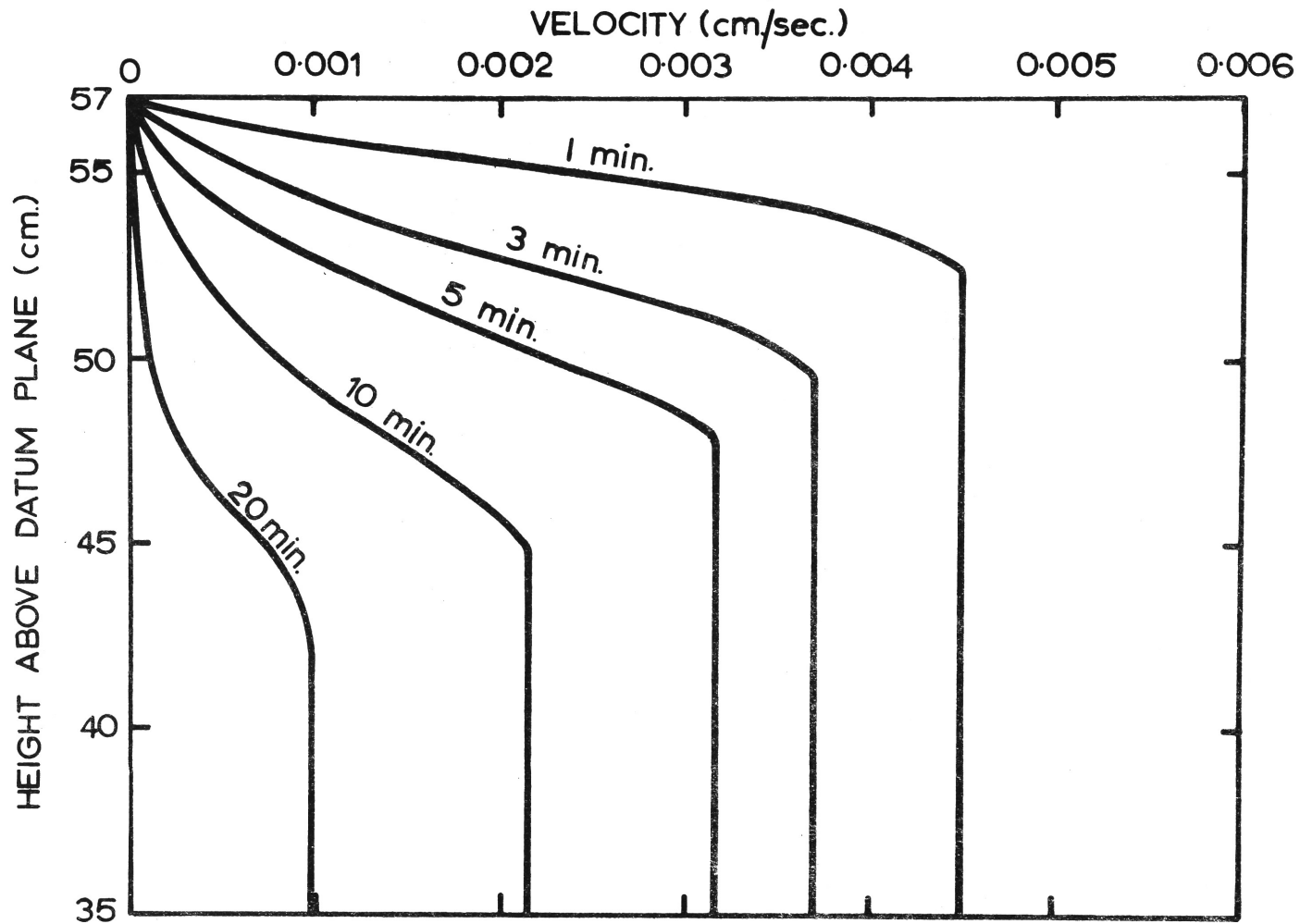
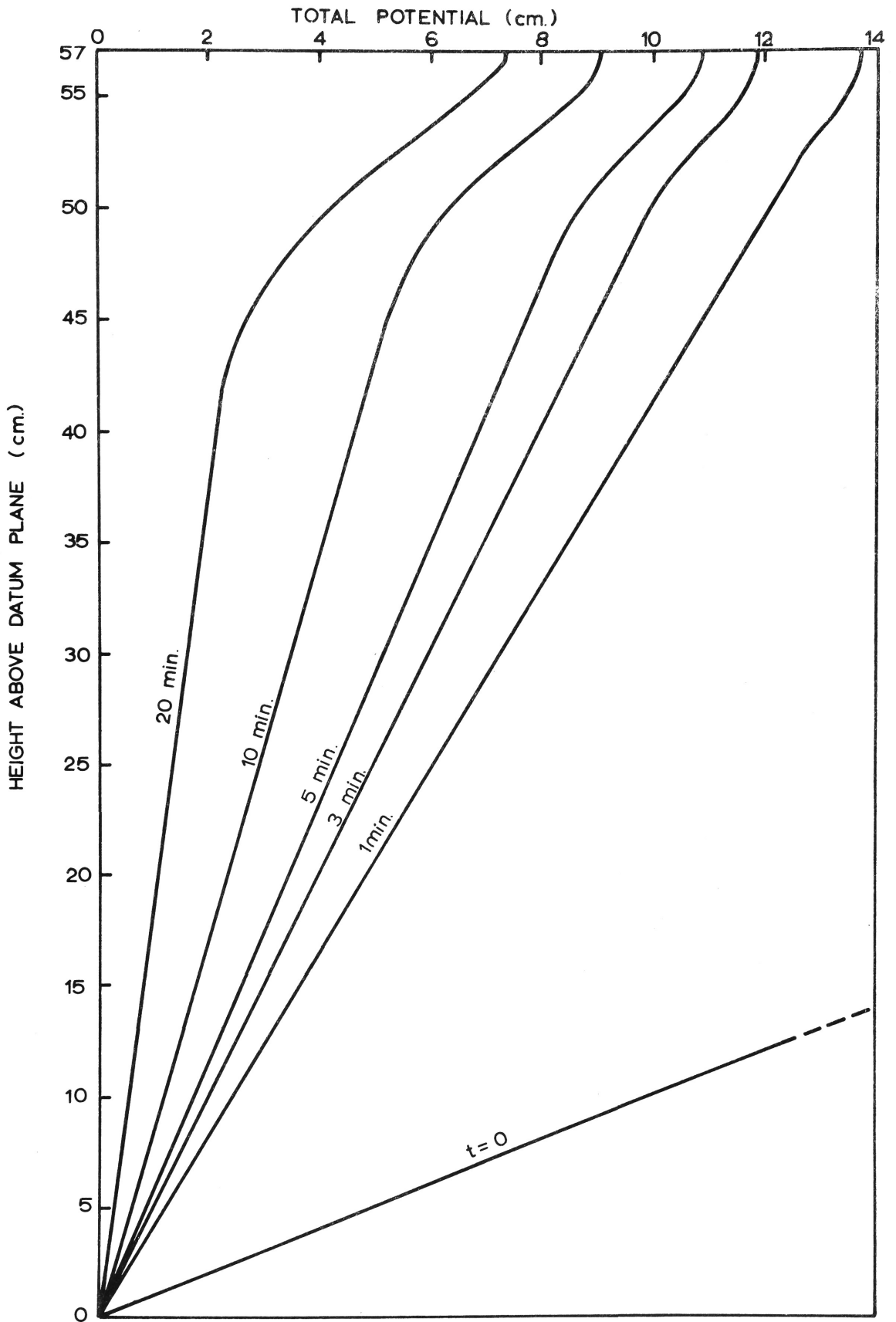Figure 6.8:   Instantaneous velocity profiles.

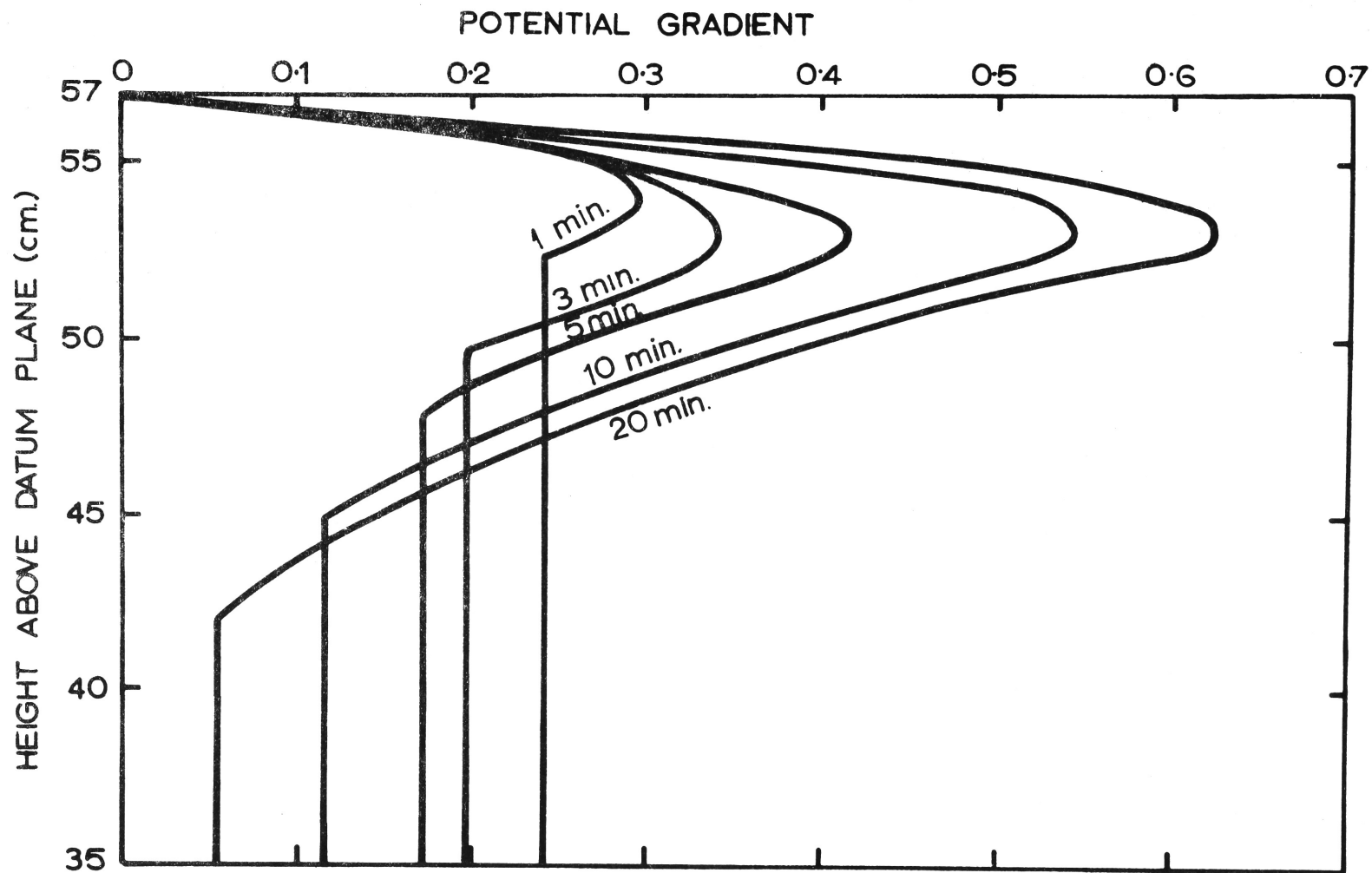Figure 6.9:   Instantaneous total potential profiles.

Figure 6.10: Instantaneous potential gradient profiles.
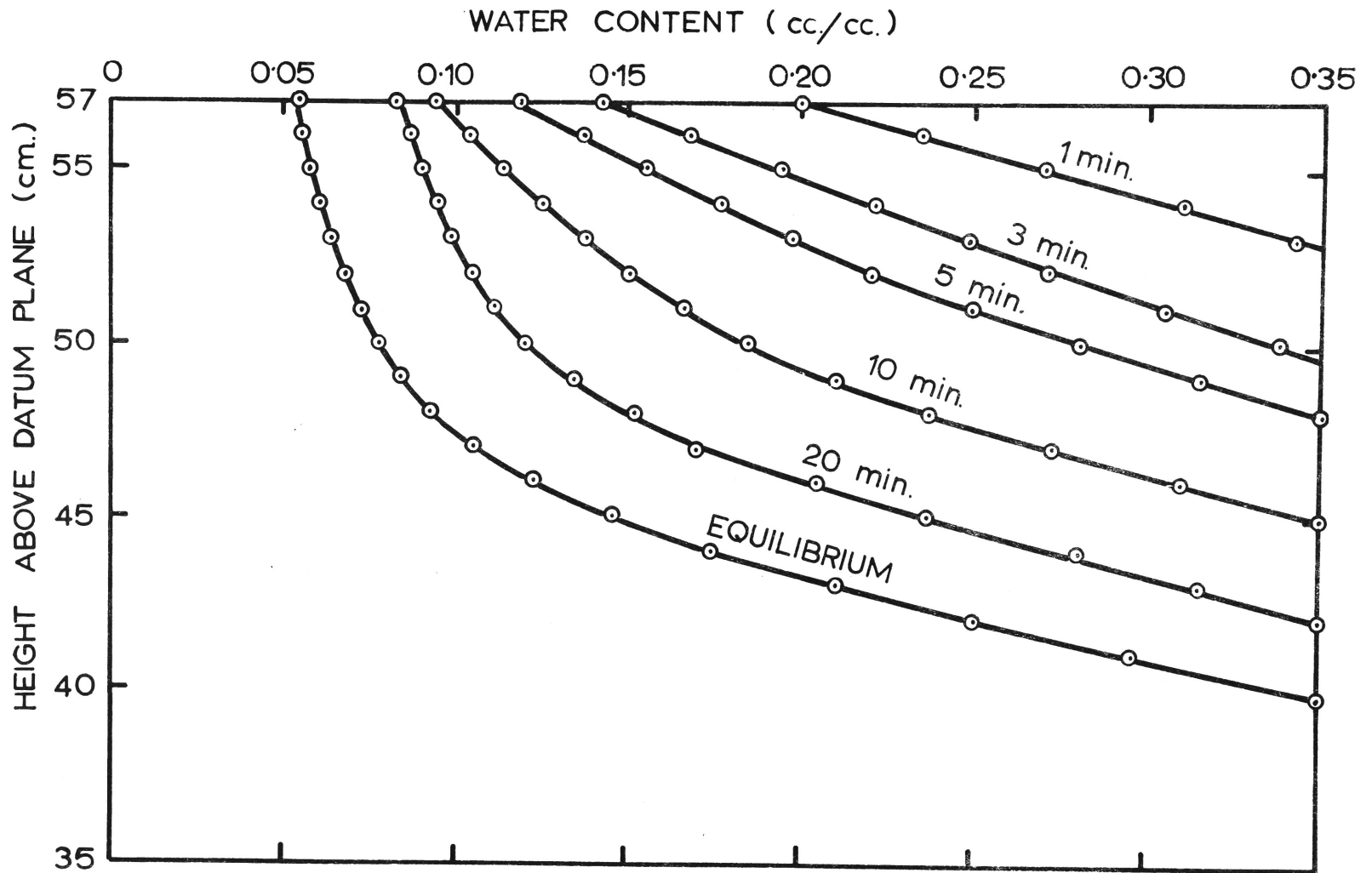
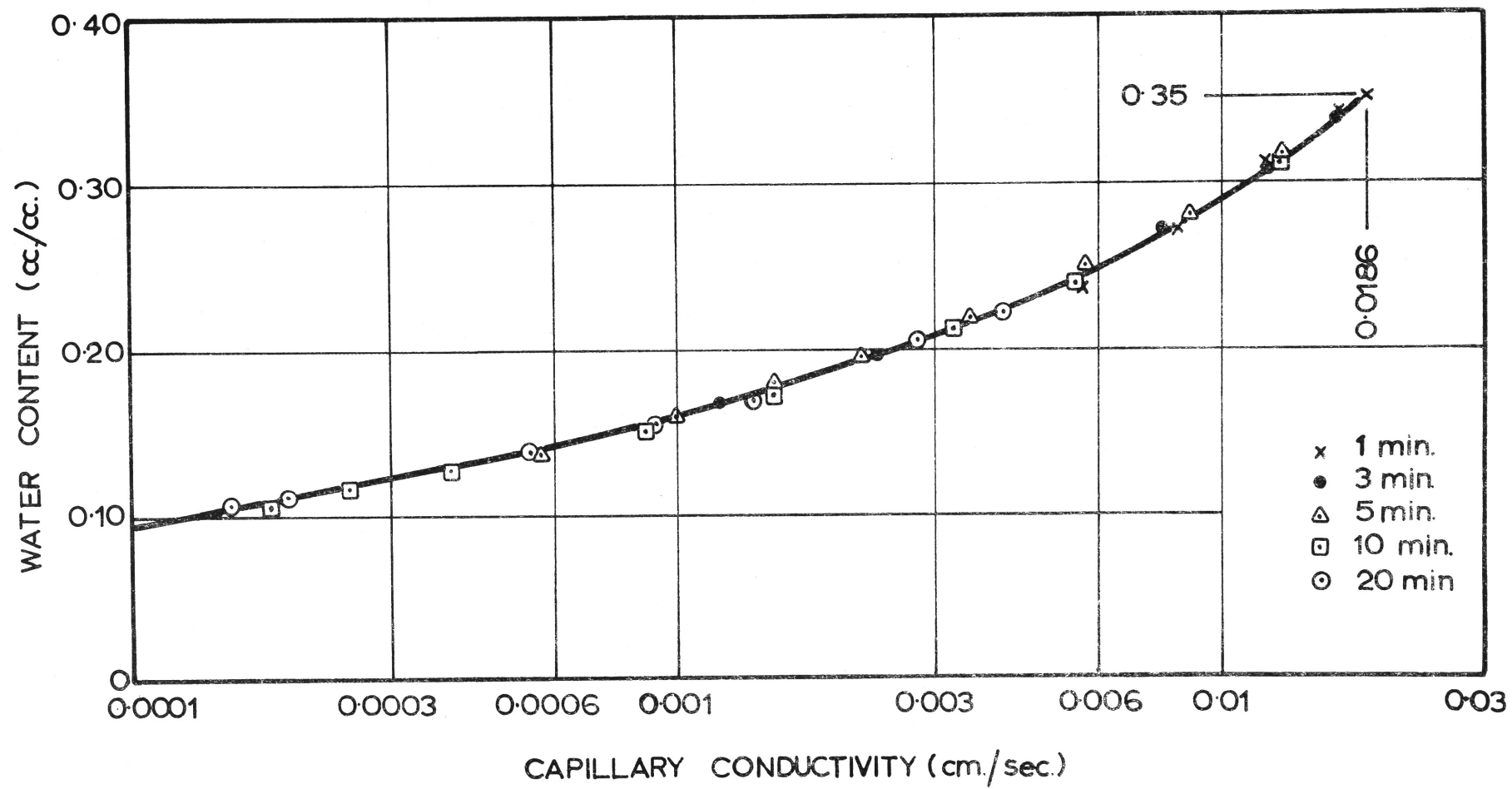Figure 6.11:   Instantaneous water content profiles.

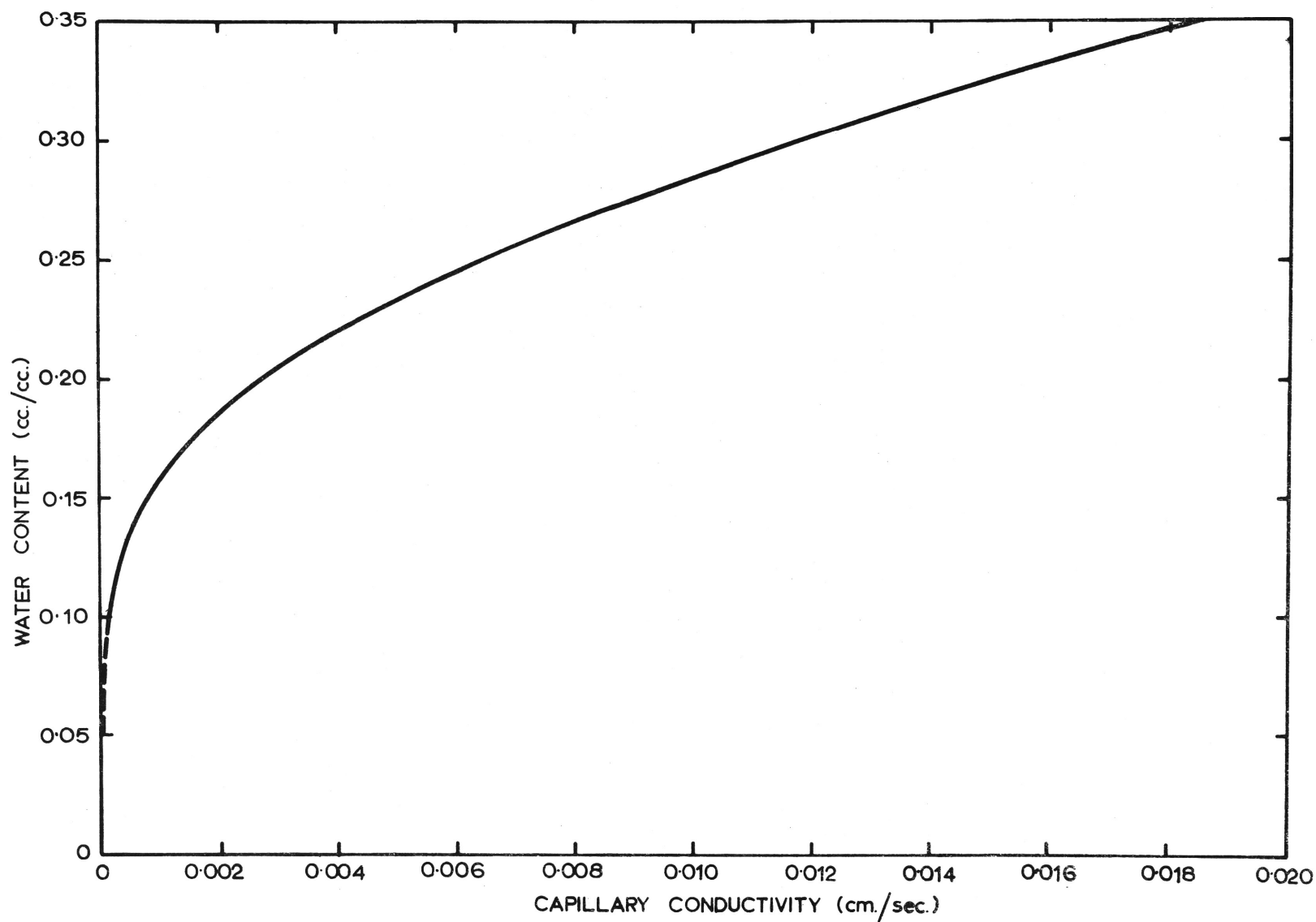Figure 6.12: The water content - capillary conductivity relation showing the computed values.

Figure 6.13: The water content - capillary conductivity relation plotted to natural scales.

and a comparison of the computed and experimentally obtained moisture profiles. If the hydrologic characteristics of the material have been accurately determined and if a precise numerical analysis can be developed, a large measure of self-consistency should be evidenced in the results.

The first question which must be answered prior to detailed work on the numerical solution is the form of the differential equation to be used. The basic differential flow equation for one dimensional flow may be represented as

$$\frac{\partial w}{\partial t} = \frac{\partial}{\partial z}\left(K\frac{\partial \varphi}{\partial z}\right) \qquad \ldots\ldots\ldots(6.2)$$

where $K$ is the moisture dependent capillary conductivity and $\varphi$ is the total potential. In general this equation has not been widely used to date since its form is not readily amenable to solution by 'hand' numerical methods. The far more popular equation and one which has received a great deal of research attention is the diffusion form which, for a vertical system, may be written

$$\frac{\partial w}{\partial t} = \frac{\partial}{\partial z}\left(D\frac{\partial w}{\partial z}\right) + \frac{\partial K}{\partial z} \qquad \ldots\ldots\ldots(6.3)$$

where $D = K(\partial \psi/\partial w)$. For certain boundary conditions some elegant numerical solutions of the equation have been developed. Some of these have converged rapidly and have required only a small number of iterations; this has been very convenient for hand solutions.

Although it must be acknowledged that equation (6.3) lends itself to more elegant solutions than (6.2) and allows the explicit statement of $t$ it would appear that, with the ready availability of digital computers and the increasing complexity of the problems requiring numerical solution (for example, those involving hysteresis and pore-air compression) many of the advantages of equation (6.3) are greatly diminished. In these more complex cases it seems decidedly preferable

to carry through the numerical solution by working simultaneously with the pressure and moisture variables rather than set up a series of the somewhat artificial (from a physical viewpoint) $D(w)$ relations as required with hysteresis complications. Accordingly, in this study equation (6.2) has been used in the numerical solution.

The finite difference form of equation (6.2) is developed in the following manner.

Let A, B, C be three points in a vertical line with A at the highest elevation. The points are equally spaced with the interval being $\Delta z$; the suction pressures at the points are $\psi_A$, $\psi_B$ and $\psi_C$ and the corresponding capillary conductivities are $K_A$, $K_B$ and $K_C$. The datum plane may be considered to pass through B. We require equation (6.2) to be expressed at B in terms of the pressures and conductivities at A, B and C.

$$\partial\varphi/\partial z \quad \text{midway between A and B} = (\varphi_A - \varphi_B)/\Delta z$$

$$\partial\varphi/\partial z \quad \text{midway between B and C} = (\varphi_B - \varphi_C)/\Delta z$$

If the conductivity midway between A and B be assumed to be $(K_A + K_B)/2$ and that midway between B and C as $(K_B + K_C)/2$

then

$$\frac{\partial}{\partial z}\left(K\frac{\partial\varphi}{\partial z}\right) = \frac{1}{\Delta z}\left[\frac{(K_A + K_B)}{2}\cdot\frac{(\varphi_A - \varphi_B)}{\Delta z} - \frac{(K_B + K_C)}{2}\cdot\frac{(\varphi_B - \varphi_C)}{\Delta z}\right]$$

$$\therefore \partial w/\partial t = \left[(K_A + K_B)\varphi_A - (K_A + 2K_B + K_C)\varphi_B + (K_B + K_C)\varphi_C\right]/2(\Delta z)^2$$

now $\quad \varphi_A = \psi_A + \Delta z \qquad \varphi_B = \psi_B \qquad \varphi_C = \psi_C - \Delta z$

$$\therefore \partial w/\partial t = \left[(K_A + K_B)(\psi_A + \Delta z) - (K_A + 2K_B + K_C)\psi_B + (K_B + K_C)(\psi_C - \Delta z)\right]/2(\Delta z)^2$$

This expression is identical to that given by Day and Luthin (1956). In the following analysis $\partial w / \partial t$ has been estimated from the water content changes and the equation is used to successively improve the pressure term at the B location. The finite difference form is then conveniently written as

$$\psi_B = \frac{(K_A + K_B)(\psi_A + \Delta z) + (K_B + K_C)(\psi_C - \Delta z) - 2(\Delta z)^2 \, \partial w / \partial t}{(K_A + 2K_B + K_C)} \quad \ldots \text{(6.4)}$$

The general form of the solution is similar to that presented by Day and Luthin (1956); however, the top boundary condition and the saturated lower profile of the column have been treated differently. The steps in the solution are set out below:-

(a)　The column is divided into one hundred and fourteen ½ cm. sections. A pressure head at the soil surface is assumed and the pressure distributed in a linear manner to zero pressure at $z = 0$. At each ½ cm. section the water content and capillary conductivity appropriate to the pressure head are determined. It should be noted that $t$ is the dependent variable and emerges as part of the solution.

(b)　The decrease of water content at each elevation is determined by subtracting the approximate profile calculated in (a) from the initial moisture profile. By summing these incremental volumes, the total volume over the time interval, which is not yet known, is determined. The rate of outflow is determined from the lower saturated section of the column, and $\partial w / \partial t$ at each elevation determined by multiplying the incremental water content decrease by the ratio of the average discharge rate to the outflow volume.

(c)  Equation (6.4) is then applied to the top two sections to improve the value of $\psi_B$ and this process repeated down the column. For $t > o$ the boundary conditions are as follows where L is the height of the column.

$$z = o , \qquad \varphi = o$$
$$z = L , \qquad \partial\varphi/\partial z = o$$

The boundary condition $\partial\varphi/\partial z = o$ may be alternatively stated as $\partial\psi/\partial z = -1$. This latter form of the boundary condition is satisfied in the analysis by fixing the surface value of pressure (after the first iteration) from the pressure value one node below the surface. Thus, if A represents the surface level and B the first node then

$$\psi_A = \psi_B + \Delta z$$

By 'freeing' the surface pressure head in this manner and because z is so small the upper boundary condition is satisfied. Since equation (6.4) is only applicable to the partly saturated section of the profile it is necessary to adopt a means of correcting the pressure distribution in the saturated column zone. This is achieved by finding the elevation where the pressure is equal to the air-entry value of 39.8 cm. and then distributing the pressure linearly from this point to the base of the column. The entire procedure was repeated until convergence occurred. The number of iterations required for this varied depending on the initial surface pressure value assumed. Usually 20 iterations were carried out with this number being increased if necessary.

(d)   When a converged profile has been obtained the average
discharge rate is then calculated and, from the outflow
volume, the time interval determined. The process is
then repeated for other assumed pressure profiles.
For convenience in calculation, the suction pressure
values and the water content changes with time are
assumed positive. This is quite a satisfactory
computational device but care must be then taken with
signs when gradients are calculated and equation (6.4)
set up in the computer programme.

The above procedure has been programmed by the writer in
3200 FORTRAN. The programme has been written in general terms so
that any height of column and any data can be used; it is presented in
Figure 6.14. The array and other variable names are explained below.

| | |
|---|---|
| WCON | Water content values at which the suction and capillary conductivity values are listed. |
| PSI | Soil suction values for the above water contents. |
| COND | Capillary conductivity values for the above water contents. |
| PSIS | The suction values assumed at the column surface. |
| WCONI | Initial water content at beginning of each time increment. |
| PSIZ | Soil suction at any elevation z. |
| WCONZ | Appropriate water content at elevation z. |
| CONDZ | Appropriate capillary conductivity at elevation z. |
| THICK | Height of column. |
| ENSTP | Number of height intervals in column. |
| N | Number of pieces of data for WCON, PSI and COND. |
| M | Number of values of PSIS. |
| RUNL | Number of iterations. |

RATEL     Outflow rate at end of last time increment.

RATEC     Average outflow rate for current time increment.

AIRENTRY Air-entry value

VOLIN     Water content decrease for each height interval.

TOVOL     Cumulative water content decrease down column
          during time increment.

TTOVOL    Summation of volume outflows over successive
          time increments.

GRADW     $\partial w / \partial t$

TIME      Time increment.

TOTIME    Summation of time increments commencing from
          zero time.

As previously discussed, the time at which any computed moisture profile occurs emerges with the solution in the type of analysis used in this study. Figure 6.15 gives the computed moisture profiles up to 1204 secs. The numerals on the curves represent the time in seconds from the start of drainage at which the profiles are established. On comparing these curves with the experimentally determined moisture profiles as given in Figure 6.11 the excellent correspondence is immediately apparent. The computed discharge rate-time relationship is given in Figure 6.16, the circled dots representing the computed points. The rapid decrease of drainage rate at early times is clearly demonstrated in this Figure.

The results of the numerical analysis are extremely encouraging. There is now no doubt that, if the hydrologic characteristics of the material are accurately known, the computer programme presented in Figure 6.14 enables the moisture and pressure profiles to be easily and precisely obtainable.

```
      PROGRAM DRAINAGE
C     VERTICAL DRAINAGE PROBLEM    K.WATSON  CIVIL ENGINEERING
      DIMENSION WCON(60),PSI(60),COND(60),PSIS(40)
      DIMENSION WCONI(300),PSIZ(300),WCONZ(300),CONDZ(300)
      READ(60,1)THICK,ENSTP,N,M,RUNL,RATEL,AIRENTRY
    1 FORMAT(2F6.1,2I3,F5.1,F8.5,F6.2)
      READ(60,3)(WCON(II),II=1,N)
      READ(60,3)(COND(II),II=1,N)
      READ(60,4)(PSI(II),II=1,N)
    3 FORMAT(9F8.5)
    4 FORMAT(12F6.2)
      READ(60,6)(PSIS(K),K=1,M)
    6 FORMAT(18F4.1)
      NN=ENSTP
      NNN=NN+1
      DLZTA=THICK/ENSTP
      DO 7 I=1,NNN
    7 PSIZ(I)=0.0
      READ(60,8)(WCONI(I),I=1,NNN)
    8 FORMAT(9F8.5)
      TTOVOL=0.0
      TOTIME=0.0
      DO 25 K=1,M
      DO 9 I=2,NNN
      Z=I-1
    9 PSIZ(I)=(PSIS(K)*(ENSTP-Z))/ENSTP
      PSIZ(1)=PSIZ(2)+DLZTA
      RUN=1.
   10 DO 13 I=1,NNN
      DO 11 II=2,N
      IF(PSIZ(I)-PSI(II))12,12,11
   11 CONTINUE
   12 FACTO=(PSI(II)-PSIZ(I))/(PSI(II)-PSI(II-1))
      WCONZ(I)=WCON(II)+(FACTO*(WCON(II-1)-WCON(II)))
   13 CONDZ(I)=COND(II)+(FACTO*(COND(II-1)-COND(II))   )
      TOVOL=0.0
      DO 14 I=2,NNN
      VOLIN=((WCONI(I)+WCONI(I-1)-WCONZ(I)-WCONZ(I-1))/2.)*DLZTA
   14 TOVOL=TOVOL+VOLIN
      RATEC=(RATEL+COND(1)*((10.*DLZTA-PSIZ(NNN-10))/(10.*DLZTA)))/2.
      DO 15 I=2,NN
      GRADW=((WCONI(I)-WCONZ(I))*DLZTA*RATEC)/TOVOL
      PSIZ(I)=(CONDZ(I-1)+CONDZ(I))*(PSIZ(I-1)-DLZTA)
      PSIZ(I)=PSIZ(I)+(CONDZ(I)+CONDZ(I+1))*(PSIZ(I+1)+DLZTA)
      PSIZ(I)=PSIZ(I)-2.*(DLZTA**2)*GRADW
   15 PSIZ(I)=PSIZ(I)/(CONDZ(I-1)+2.*CONDZ(I)+CONDZ(I+1))
      PSIZ(1)=PSIZ(2)+DLZTA
      DO 16 I=2,NNN
      IF(PSIZ(I)-AIRENTRY)17,17,16
   16 CONTINUE
   17 DISTANCE=((AIRENTRY-PSIZ(I))/(PSIZ(I-1)-PSIZ(I)))*DLZTA
      L=I
      ZZ=NNN-L
      DO 18 I=L,NNN
      ZZZ=NNN-I
   18 PSIZ(I)=(AIRENTRY*ZZZ*DLZTA)/((ZZ*DLZTA)+DISTANCE)
      WRITE(61,19)(PSIZ(I),I=1,NNN,2)
   19 FORMAT(20F6.2)
      RUN=RUN+1.
      IF(RUN-RUNL)10,20,20
   20 RATEC=(RATEL+COND(1)*((10.*DLZTA-PSIZ(NNN-10))/(10.*DLZTA)))/2.
      RATEL=COND(1)*((10.*DLZTA-PSIZ(NNN-10))/(10.*DLZTA))
      TOVOL=0.0
      DO 21 I=2,NNN
      VOLIN=((WCONI(I)+WCONI(I-1)-WCONZ(I)-WCONZ(I-1))/2.)*DLZTA
   21 TOVOL=TOVOL+VOLIN
      TTOVOL=TTOVOL+TOVOL
      TIME=TOVOL/RATEC
      TOTIME=TOTIME+TIME
      WRITE(61,22)TIME,TOTIME,TOVOL,TTOVOL,RATEC,RATEL
   22 FORMAT(2F8.1,2F7.4,2F8.5)
      WRITE(61,23)(PSIZ(I),I=1,NNN,2)
      WRITE(61,24)(WCONZ(I),I=1,NNN)
      WRITE(61,24)(CONDZ(I),I=1,NNN,2)
   23 FORMAT(20F6.2)
   24 FORMAT(15F8.5)
      DO 25 I=1,NNN
   25 WCONI(I)=WCONZ(I)
      STOP
      END
```

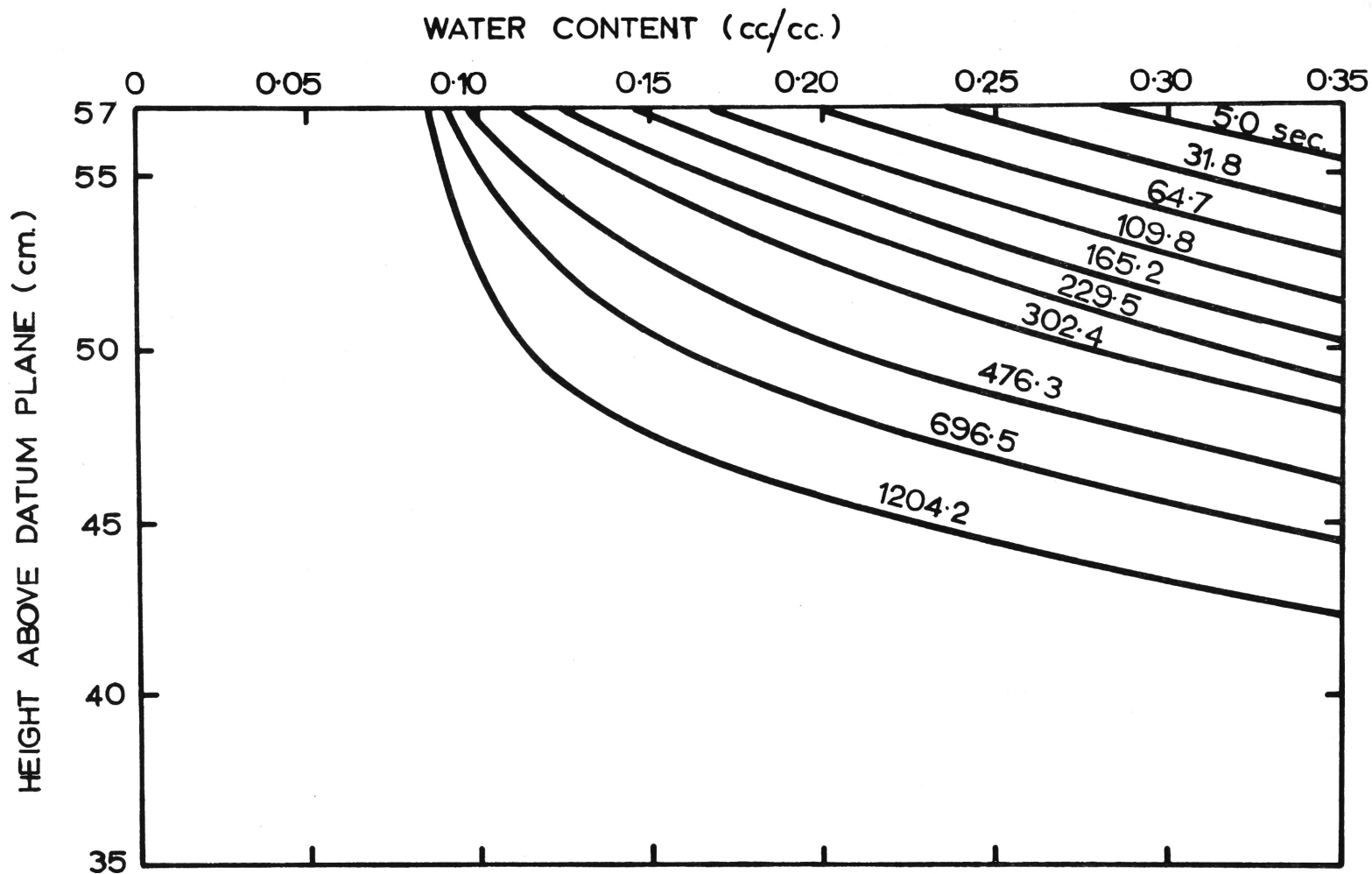Figure 6.14:   Computer programme for vertical
drainage problem.

Figure 6.15: Computed moisture profiles. The numerals represent the time in seconds from the start of drainage.
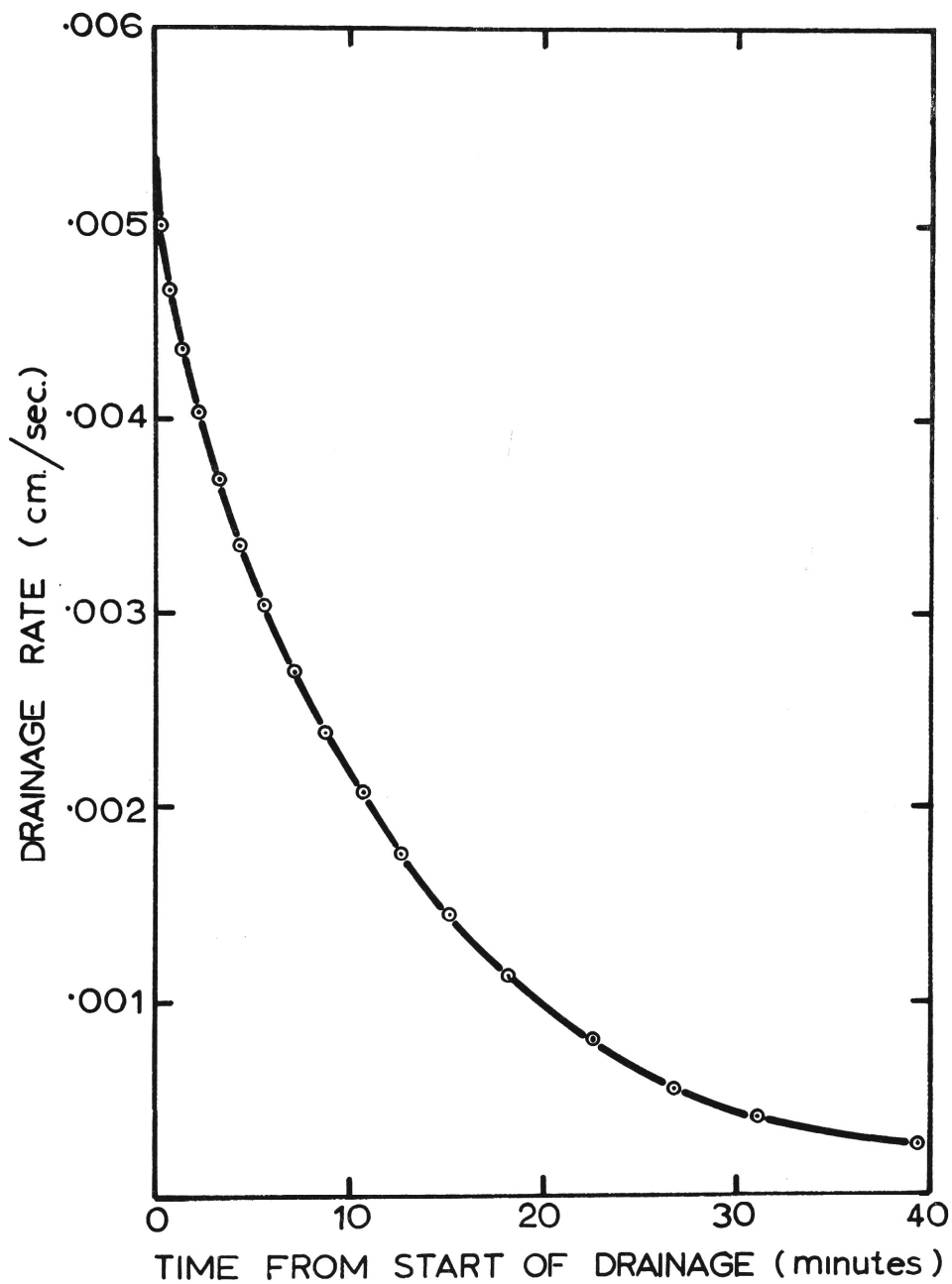
Figure 6.16:   Computed outflow - time relation.

# CHAPTER 7.

## THE REWETTING CYCLE

### 7.1 Objectives

During the rewetting cycle a number of complex and intractable problems arise and, in this chapter, approaches are presented which meet the experimental demands of the present situation and allow some progress towards a sound numerical solution. Before listing the specific objectives of the chapter the physical conditions occurring in the column during the rewetting cycle are briefly restated.

When water in excess of the infiltration capacity is applied to the upper surface of the column following a period of drainage the wetting up of the drained profile takes place along primary scanning curves. In addition, the downward movement of the wet front causes compression of the air in the voids. This pore-air compression is time dependent and results in the rapid draining of the profile in the vicinity of the saturated-unsaturated interface. The vertical infiltration is also inhibited by the increased air pressure in the voids and this effect must be included in numerical solutions based on the differential flow equation. The specific objectives of this chapter then emerge as follows:-

(a) The construction of controlled flow equipment to enable the wetting up of the sand to be carried out at a controlled rate. With such control the hysteresis loop characteristics can be accurately determined.

(b) The measurement of primary and secondary hysteresis loop scanning curves.

(c) The experimental determination during rewetting under excess surface water, of moisture and pressure profiles and of pore-air pressure changes in the column.

(d)    The development of a method which will provide
a theoretically sound framework for a numerical
analysis of the rewetting cycle. In such an
analysis the experimental information described
in the following section would provide the basic
data.

## 7.2   Hysteresis Loop Characteristics

The sand fraction used in these experiments wets up so rapidly
that it is not possible to provide a controlled flow (as required in the
determination of primary-secondary scanning curve sequences) by simply
supplying water in excess to the upper surface of the column. In the
present experiment the desired flow control is achieved by using a
multiple hypodermic needle device. A brass container of rectangular
cross section (15 cm. x 10 cm.) and 18 cm. in height with open top was
constructed from 1/8" brass plate. 48 tapered brass fittings, designed
to mate with Record type hypodermic needles, were inserted through the
base. The fittings were positioned in 6 rows (8 per row) and were
uniformly spaced over the column area; the end of the fitting inside the
box could be easily sealed off if required. Using this box a wide range
of flows is possible by an appropriate selection of needle gauge, head of
water in box and number of needles in use. In determining the hysteresis
loop characteristics of the sand fraction 48 needles of No. 21 gauge are
used under approximately 10 cm. head of water. The brass box, with
its spine-like projections, is supported on a stand held rigidly to the
top of the column. Sufficient space is allowed between the sand surface
and the hypodermic needles to clean the needles from below if clogging
occurs during an experiment.

The moisture condition in the column at the commencement
of the experiment is again full saturation. The sand in the column drains

along its boundary draining curve until the suction at which reversal is required is reached at the measuring elevation. The controlled flow box, which is prepared and dripping steadily is then quickly placed in position on the supporting stand and the wetting-up process is commenced. In some cases, particularly where measurements are taken near the surface, the flow is continued until excess water appears on the surface and the elevation in question can be considered saturated. In other cases a primary wetting scanning curve is 'followed' for a short period and then the box is removed causing the suction-water content relation to be represented by a secondary draining scanning curve. In order to avoid compression of the pore air several of the Perspex plugs on the column face are removed during the wetting-up process.

Figure 7.1 is a reproduction of the chart record at the reversal point which occurs when the wetting up (primary wetting scanning curve in this case) is suddenly stopped and drainage commences (secondary draining scanning curve). The tensiometer used in this experiment was made from 25-30 micron ceramic. The equipment response to the change from wetting to draining is almost instantaneous and permits a very accurate plotting of the hysteresis loop characteristics.

Figure 7.2 represents graphically the results of some of the hysteresis loop determinations. Many characteristic features of the hysteresis relationship are shown in this figure. The relationship ABC represents a portion of the boundary draining curve for a fully saturated sand. Upon rewetting the primary wetting scanning curve CDEF, for an elevation near the surface, is obtained. This curve shows clearly two characteristics at its wet extremity. Firstly, a constant moisture content is reached at a suction of 22 cm.; this suction value in the wetting cycle is analogous to the air-entry value in the draining cycle and is the suction which corresponds to the average maximum interfacial radius in the pores. Peck (1965a) has termed this value the

air-exit value. Secondly, the sand on rewetting is not able to reach the same moisture content as initially due to the presence of entrapped air. From a pressure viewpoint the sand may be considered saturated with all that this implies, but the presence of small pockets of air trapped in the pores, probably during the final stages of the wetting-up process, naturally reduces the moisture content and, in addition, the capillary conductivity at saturation. If sand which has been wetted up to saturation is allowed to drain the draining curve, shown in Figure 7.2 as FGC, is obtained. It may be noted that the air-entry value is unchanged but, for suctions greater than this value, a reduced moisture content occurs at any particular suction compared with the draining curve ABC. This is again due to the presence of entrapped air. For illustrative purposes two primary wetting scanning curves at smaller reversal suctions are shown. One of these (HJE) is wet up to saturation and exhibits the same air-exit value as the first scanning curve. The wetting-up process for the other is reversed after a short period at M and a secondary draining scanning curve MKC is obtained.

## 7.3   Measurement of Rewetting Profiles

In the first section of this chapter the complex conditions existing in the column upon rewetting under a small surface head were discussed. In this section the experimental determination of the moisture content, suction and pore-air pressure in the column under the above boundary condition will be considered.

The technique for measuring the pore-air pressure has already been discussed in Chapter 3, but the related matter, the effect of the pore-air compression on the recorded suction reading has not yet been considered. Not only is the magnitude of the pore-air compression a physical requirement in its own right but, in addition, unless it is accurately measured it is not possible to interpret from the chart record the true suction at the tensiometer face since the excess pressure (relative
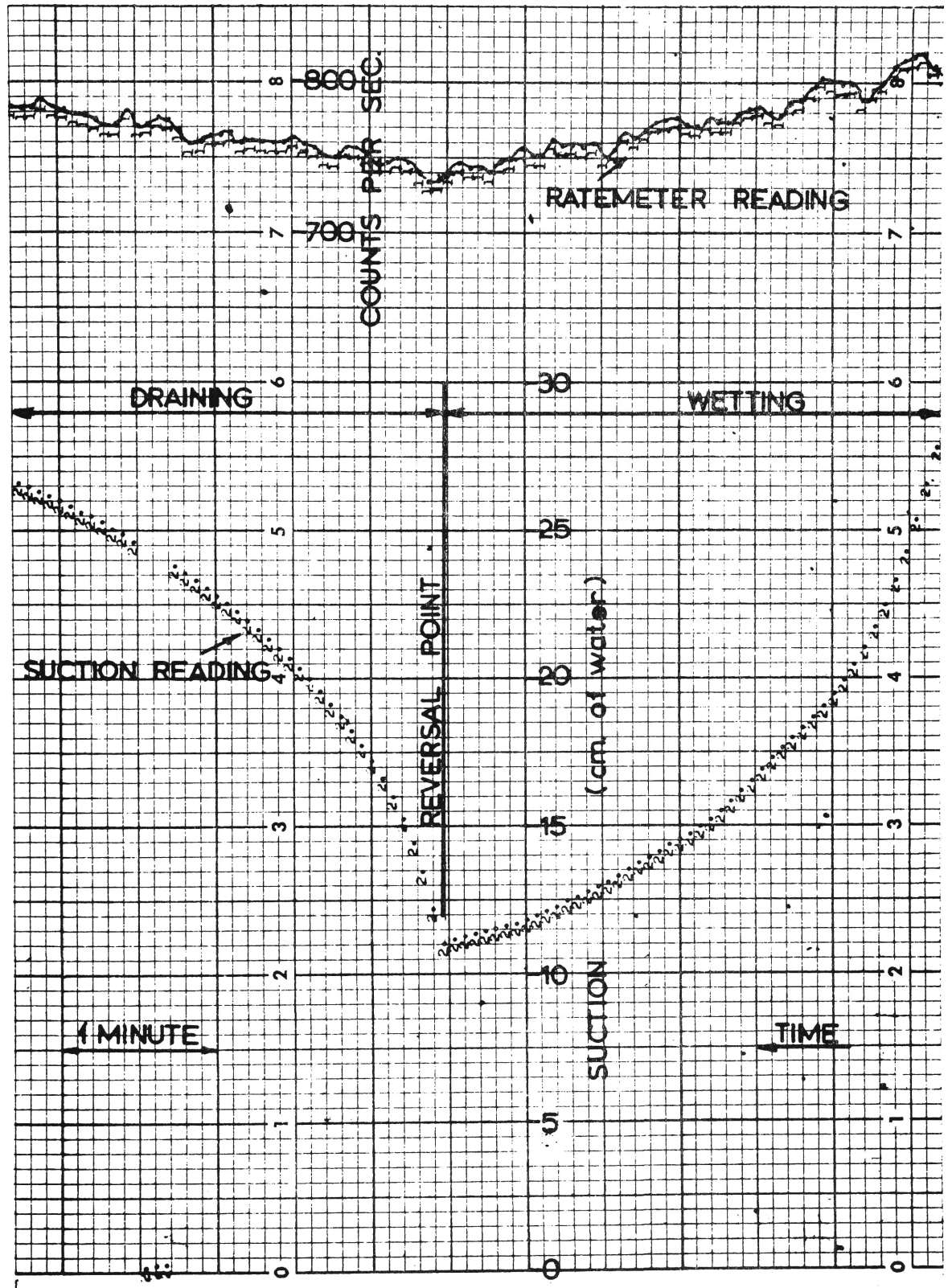
Figure 7.1: Chart record showing suction and water content
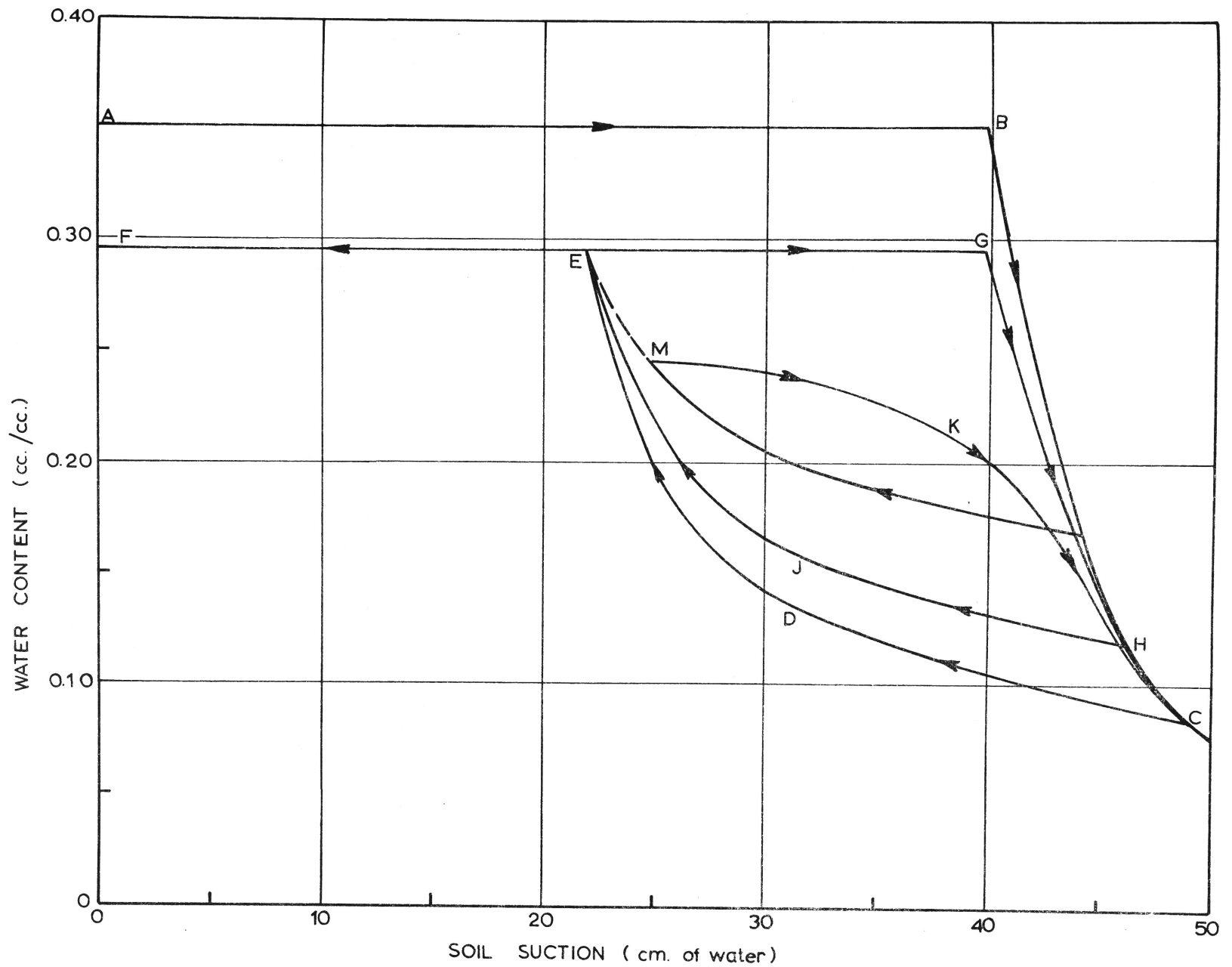changes at reversal point in hysteresis loop
measurement.

Figure 7. 2:   Hysteresis characteristics of the sand fraction.

to atmosphere) of the pore air against the saturated cup wall reduces the 'true' transducer reading by the magnitude of the pressure excess. Since both the excess pore-air pressure and the suction changes are time dependent it is a matter of some complexity to determine the actual suction variation.

Figure 7.3 is a reproduction of the chart record at an elevation of 40 cm. and covers the period immediately prior to and following the commencement of rewetting. This occurred after 20 minutes of drainage. The elevation in question is in the zone which was saturated before rewetting and which drains rapidly under the additional potential gradient caused by the increased pressure of the pore air. Since the sand at this elevation is passing from a saturated to a partly saturated condition the suction there must be increasing and the water content decreasing. The water content decrease is clearly depicted by the increasing ratemeter reading (Channel 1); however, the pressure record (Channel 2) shows an immediate and sudden decrease due to the increased air pressure against the tensiometer cup. Before discussing the method for correcting the suction reading, the nature and significance of the air pressure increase will be discussed.

Ideally, the air pressure changes should be measured at the same time and with the same column as the suction measurements; however, the changes in both variables are so rapid in these experiments with the sand fraction that accurate chart records for both cannot be obtained in the one experiment even when particular attention is paid to the switching schedule. A replicate column therefore has been used for the pore-air pressure changes and these are recorded in Figure 7.4. Similar measurements on several columns resulted in a high degree of reproducibility. In Figure 7.4 the zero reading on the chart again represents atmospheric pressure at transducer diaphragm level and the steady positive pressure reading prior to wetting represents the

hydrostatic pressure of the water in the nylon tubing due to the elevation difference between the measuring point and the standard surface. In effect, this reading (11.1 div.) is the zero for the pore-air pressure increase, that is, it is a reading which represents the atmospheric pressure at the time of the test, and changes, relative to this reading, give the air pressures in excess of atmospheric. From the above detail it will be realized that the method used for measuring the pore-air pressures is the alternative one described in Chapter 3; that is, only one transducer is used. In the rewetting phase of this experiment great care is exercised to ensure that all screwed plugs are airtight and that no air can escape through the tensiometer assemblies.

Figure 7.4 reveals the extremely rapid nature of the air pressure increase in these experiments. Approximately 4-6 seconds after the addition of excess water to the column surface the air pressure has risen to a steady value in excess of atmospheric pressure, represented by 50 divisions on the chart (that is, 25.0 cm. of water). The rapid nature of the increase is not surprising when the small volume change necessary to cause the increase is calculated. Assuming isothermal conditions, this calculation is possible by applying Boyle's Law to the process and determining the relationship between air volume decrease and air pressure increase. If atmospheric pressure is represented by $P_a$ and the pore-air volume at this pressure $V_o$ then the volume decrease $\Delta V$ under a step-input pressure increase $\Delta P$ is given by

$$\Delta V = \frac{\Delta P \cdot V_o}{P_a + \Delta P} \qquad \ldots\ldots\ldots 7.1$$

In the present case the volume of air in the pores for each square centimetre of column area, after draining has progressed from the saturated condition for 20 minutes, is 2.94 cc. If $\Delta P = 25.0$ cm., then from equation (7.1) $\Delta V = 0.07$ cc. If we assume for the moment
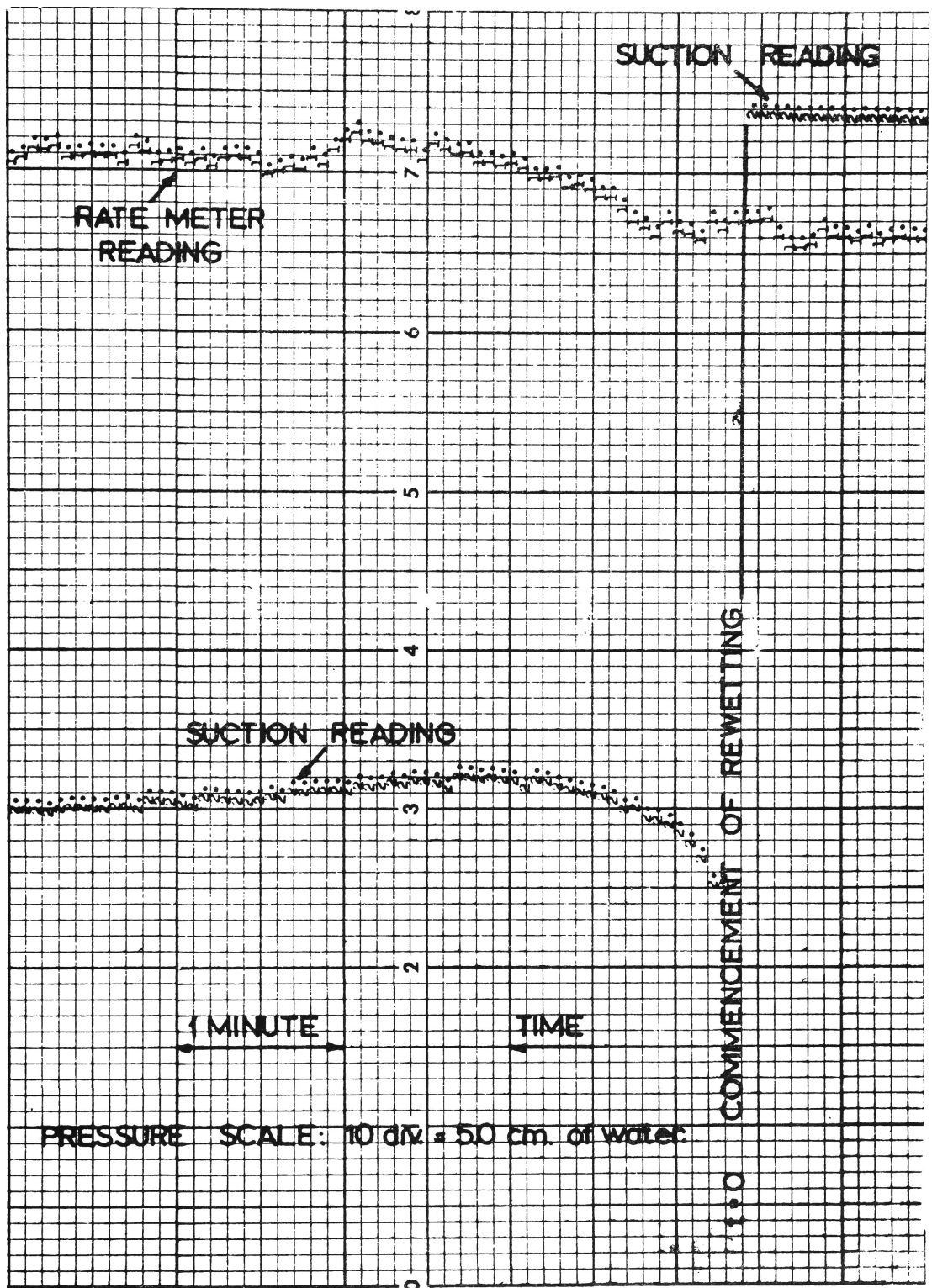
Figure 7. 3: Chart record at commencement of rewetting at an elevation of 40 cm. A small ratemeter time constant was used in this experiment.
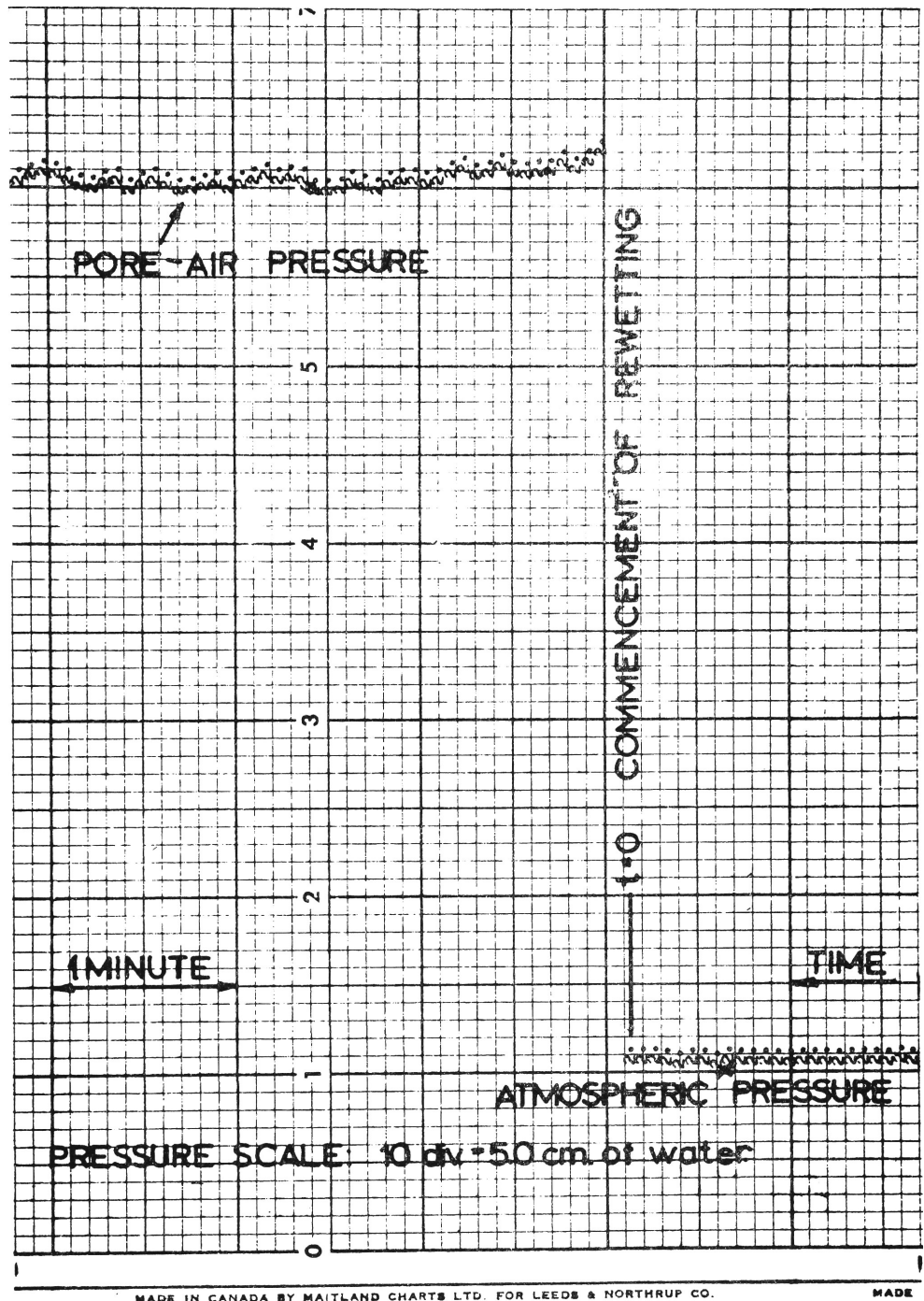
Figure 7. 4:   Chart record of pore-air pressure changes during rewetting.

that there is no volume outflow in these first few seconds of rewetting, then the depth of the wet front to produce the above volume decrease is easily calculable. The moisture content in the top few centimetres of the column after drainage is very close to 0.09 cc./cc.; if the wetted-up moisture content is assumed to be 0.30 cc./cc. then the volume of water used in wetting the top centimetre is 0.21 cc. From this calculation it is seen that the volume decrease is achieved by a rewetting of 0.33 cm. of the column.

For the sand column the mechanism of the air pressure increase appears to be as follows. Due to the high permeability of the sand and the large gradients involved in the very early stages of infiltration the near-surface sand wets up extremely rapidly. This results in an almost immediate air pressure increase. As may be seen in part from Figure 7.4 this immediate air pressure value is not exceeded during the remainder of rewetting; this has been continued for 30 minutes and during that time the air pressure has remained almost constant. A drop in pressure of 0.5 cm. of water over the 30 minute period has been noticed and this has been assumed to be due to a small volume of air dissolving in the air-free water. It would appear therefore that after the first few seconds of rewetting, when the air pressure and air volume have reached their constant values, a wetting-draining balance exists in the column under the air pressure excess of 25 cm.

It should be noted that, since the air pressure increase is considerably less than the air-entry value of the sand, no escape of air to the surface, by bubbling through the pores, occurs. However, column fracture due to the pore-air compression does tend to occur and to prevent this a special device is used which weights the surface slightly yet allows infiltration to proceed over the entire surface area. Since the compacted sand can be considered as a rigid material, the surface weighting has no effect on the hydraulic process.

When the air pressure increase has been measured it is possible to make the necessary corrections to the recorded suction changes. In the present case the correction is not a difficult one due to the rapidity of the air pressure change. The true suction reading is obtained by simply adding the air pressure reading to the recorded suction value. Figures 7.3 and 7.4 have been reproduced in Figure 7.5 and the true suction variation shown.

For porous materials of a finer grain size than the sand the air pressure increase will build up much more slowly, and a time-dependent pore-air compression over a more extended time (as distinct from the 4-6 seconds in the sand) will be recorded. In such circumstances the true suction at any instant is determined by adding the recorded pore-air compression at that instant to the suction value.

From a number of chart records similar to Figure 7.3 the wetting and draining water content profiles at different times can be determined. These are given in Figure 7.6 for times of 10, 20, 60 and 120 seconds.

The mechanism of profile development in the column can be explained most clearly by considering the wetting-draining sequence at particular elevations as given by the chart records.

50 cm.    At this level (and all elevations above it) there is no perceptible drainage under the pore-air compression. At 20 secs. water from the surface reaches this level and the sand commences to wet up.

48 cm.    The chart record shows an extremely small amount of drainage here and then a very gradual increase in moisture content. The moisture changes in the vicinity of this point are the smallest in the column.
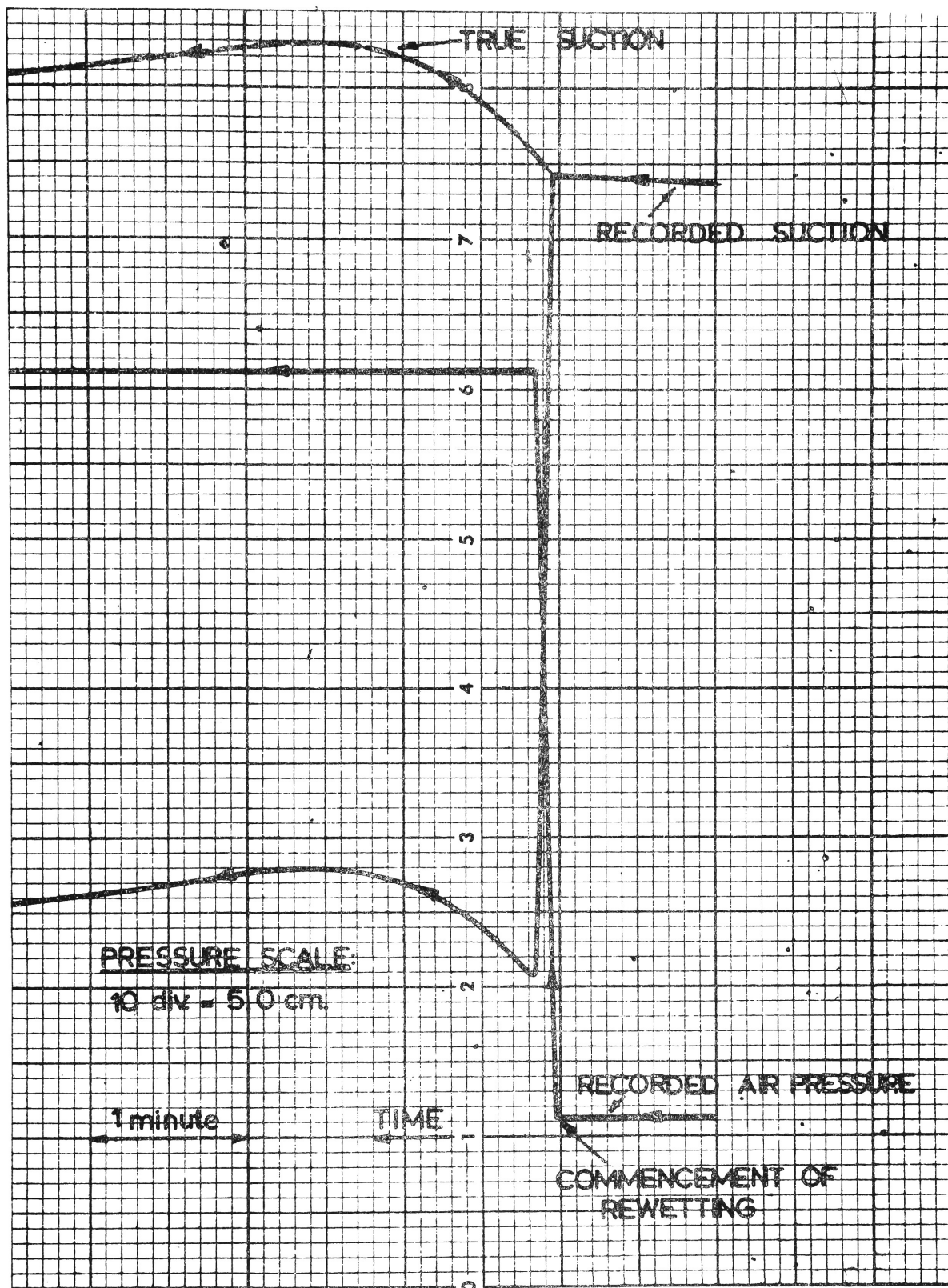
Figure 7.5: Adjustment of suction record for pore-air pressure changes.
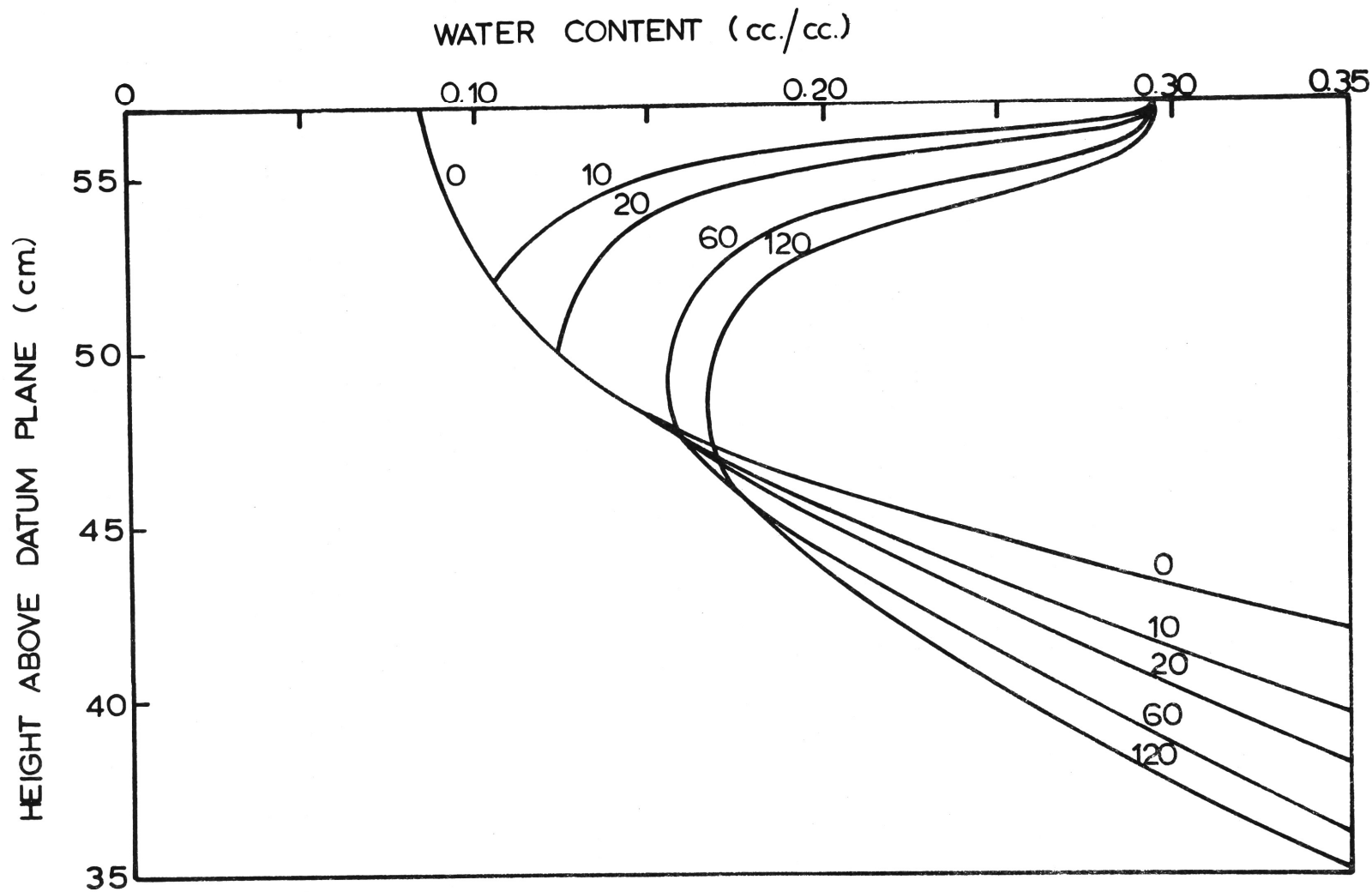
Figure 7.6:  Water content profiles during rewetting.   The numerals on the profiles represent the time in seconds from the commencement of rewetting at which the profiles were established.

46 cm.     At this elevation the moisture content decreases quite markedly under the pore-air compression. When the wetting front reaches this elevation at about 50 secs. a reversal of suction occurs and the suction gradually decreases. However, due to the flat gradient on the wetting scanning curve the moisture increase in the period 50-120 secs. is negligible.

40 cm.     The wetting front reaches this elevation at approximately 110 secs. Prior to this time drainage from a saturated condition had been progressing. Again the suction decrease is very small after this time and the moisture content remains sensibly constant.

After rewetting has been in progress for approximately 15 minutes the moisture profile reaches a stable form which is very similar to that shown for 120 secs. After this time steady state flow may be safely assumed. This condition suggests a useful method of steady state capillary conductivity measurement.

The wetting and draining history of the sand, coupled with the pore-air compression effect, produces the rather unusual bell-shaped moisture profile as shown in Figure 7.6. For the sand fraction the final stable profile covers the fairly wide range of water content of 0.17 to 0.35 cc./cc. If during the steady state flow the potential gradients and moisture contents are measured then the water-content capillary conductivity relationship can be readily obtained. Such measurements can be obtained very easily with the rapid response equipment of this study; however, the method also lends itself for use with more usual tensiometer techniques, and column sectioning methods of moisture determination. The steps in the procedure would be:

(a)     Once the stable moisture profile is obtained the outflow velocity and the pore-air pressure are measured.

(b)     The tensiometer readings are then taken and potential gradients determined.

(c)     The column must be rapidly sliced to determine the gravimetric moisture contents.

The minimum moisture content could be decreased either by increasing the initial drainage time or by increasing the length of the column. If the latter course is followed care must be taken that the pore-air pressure increase does not exceed the air-entry value.

In addition, the method has possibilities for determining hysteresis effects in the capillary conductivity relationship. The section of the profile above an elevation of 48 cm. wets up quite extensively from a drained condition and that below drains from a wet condition with negligible change of water content as the stable profile is reached. Therefore the capillary conductivity determination for the upper profile represents wetting values and that of the lower profile, draining values. Detailed work on this approach does not constitute a phase of this study, but the method would appear to have particular usefulness.

## 7.4   A Numerical Approach

In this section a general approach for determining the time-dependent pore-air compression (and the related moisture and pressure profiles) for the rewetting boundary conditions of this chapter is suggested. In principle the method is applicable to the sand fraction although the rapid nature of the development of the air pressure increase in that material would require a computer programme using very fine mode spacing. In the suggested analysis no allowance has been made for the possible effects of air pressure gradients.

The major difficulty in finding the relation between the pore-air pressure increase and time during the rewetting cycle is the simultaneous inflow-outflow process. The following procedure appears to satisfactorily meet this condition, although the method is approximate in so far as incremental inflows and outflows are assumed to occur over time periods during which the incremental air pressure increase is considered constant.

The steps in the method would be as follows:-

(a)     An incremental pore-air pressure increase would be assumed (say 5 cm. head of water).

(b)     Computer programmes using the finite difference form of the differential equation of flow and incorporating the effect of the pore-air compression would then be compiled separately for infiltration inflow and drainage outflow. It is valid to consider the two processes separately (up to the time when the entire profile is wetting up) if allowance is made for the decreasing height of the drainage zone as the wet front descends from the upper surface.

(c)     Under the incremental air pressure excess, the inflow into the column at times, which emerge with the solution, would be computed and an inflow-time relation determined. In this procedure the data must be so presented that each elevation wets up along its own scanning curve. In addition, for the second and successive air pressure increments a draining effect in the upper part of the wetting zone (as discussed by Youngs and Peck (1964)) will occur. The programme must therefore include a test to determine the position

of the transition point ($\partial \psi / \partial t = 0$ ); the soil above the transition point will commence draining along secondary scanning curves and the soil below will continue wetting up. Due to the almost horizontal form of many secondary scanning curves the amount of water actually draining will be very small. The moisture and pressure profiles will also be obtained from this analysis.

(d) A procedure similar to (c) would then be carried out for the draining of the lower section of the profile and an outflow-time curve obtained.

(e) If the outflow-time curve is then subtracted from the inflow-time curve a curve of pore-air volume decrease against time would be obtained.

(f) Since the volume of air in the pores at the beginning of the increment is known and the assumed pressure increase is known it would be possible by using equation (7.1) to determine the air volume decrease under the incremental pressure increase.

(g) This decrease would then be read against the curve determined in (e) from inflow-outflow information to find the time at which the pressure increase would occur.

(h) The process would then be repeated for further air-pressure increments. In each case the initial moisture and pressure conditions would be those existing in the column at the computed time (as found in (g)) for the previous increment.

# CHAPTER 8.

## CONCLUSION

In the Introduction the first phase of this study was stated to be the design and construction of measuring equipment to allow investigation in long laboratory columns of non-continuous flow phenomena. This involves the non-destructive measurement with rapid response of the water content, soil suction and pore-air compression. This very demanding objective has been satisfactorily met in the instrumentation described in Chapters 3, 4 and 5.

In Chapter 3 the mechanical design features of the traversing mechanism have been discussed. This mechanism is a necessary prerequisite to the attainment of the overall objective since flexibility and speed in the positioning of the radioactive source and the scintillation counter allow efficient use of the non-destructive water content measuring equipment. Extended use of the traversing equipment has established the satisfactory nature of its design and construction in meeting the requirements of the experiment. In particular, the microswitch unit works extremely well in stopping automatically the traversing head at any selected elevation.

The tensiometer-pressure transducer system, as discussed in Chapters 3 and 4, provides a flexible and reliable means of soil-water suction measurement. When careful attention is paid to the choice of the ceramic in the tensiometer, in relation to the overall suction demands of the experiment, an efficient measuring system is available. This system, in combination with that of water content measurement by gamma-ray absorption (Chapters 3 and 5), provides the necessary simultaneous rapid response readings. The more the writer uses the equipment the more impressed he becomes with its potential for solving a wide range of time-dependent moisture movement problems. The dual channel

chart record not only provides the required quantitative information but, in a general qualitative sense, it is most instructive to note the simultaneous graphical reproduction of the changes in the variables.

Considerable space has been devoted to calibration and correction procedures. This has been deemed necessary since sophisticated instrumentation requires careful calibration. The methods described in Chapters 4 and 5 permit adequate calibration of both measuring systems and, in addition, the correction during an experiment for electronic drift and other external changes. In practice these methods have proved both sufficient and satisfactory. It is rather fortuitous, yet very convenient, that the basic response equations for the two systems are of identical form. This has provided encouragement for a careful study of correction techniques for response lag. In this study numerical correction procedures have been developed and then checked against controlled experiments with known inputs. The use of these procedures enables an unknown input to be determined with very acceptable accuracy from a recorded output.

Although the measuring equipment was specifically designed for non-continuous flow experiments, the rapid and simultaneous nature of the suction and water content measurements has made possible interesting studies on the nature of the draining moisture characteristic and the capillary conductivity relationship. This latter parameter has been determined by a new method called the method of instantaneous profiles. This method permits the determination of the water content - capillary conductivity relationship over a wide range of water contents under transient conditions. In addition, the significant conclusion has been reached that, keeping in mind the moisture dependence of the relationship, Darcy's Law is applicable to unsteady unsaturated flow in rigid porous materials. Good correspondence has been obtained for the drainage experiment between the measured moisture content profiles and those obtained by computer analysis.

In the complicated rewetting phase the effect of pore-air compression on the tensiometer readings has been considered and corrections for this distortion satisfactorily made. The ease with which the hysteresis loop characteristics of a material can be determined with the equipment has been illustrated in Chapter 7 where full hysteresis information on the sand fraction has been presented. Finally, the moisture profiles during rewetting have been determined and a suggested numerical approach presented.

# REFERENCES

ADRIAN, D.D. (1964). The influence of capillarity on the flow of air and water in a porous medium. Tech.Report No.38, Dept. of Civil Engineering, Stanford University.

CHILDS, E.C. and COLLIS-GEORGE, N. (1950). The permeability of porous materials. Proc.Royal Soc., 201A: 392-405.

CRONEY, D. (1952). The movement and distribution of water in soils. Geotechnique, 3: 1-16.

DAVIDSON, J.M., BIGGAR, J.W. and NIELSEN, D.R. (1963). Gamma-radiation intensity for measuring bulk density and transient water flow in porous materials. J. Geophysical Res., 68: 4777-4783.

DAY, P.R. and LUTHIN, J.N. (1956). A numerical solution of the differential equation of flow for a vertical drainage problem. Soil Sci. Soc.Am., Proc., 20: 443-447.

FERGUSON, A.H. (1959). Movement of soil water as inferred from moisture content measurements by gamma-ray absorption. Ph.D. Thesis. Washington State University.

FERGUSON, A.H. and GARDNER, W.H. (1962). Water content measurements in soil columns by gamma-ray absorption. Soil Sci. Soc. Am., Proc., 26: 11-14.

FREE, G.R. and PALMER, V.J. (1940). Inter-relationship of infiltration, air movement and pore size in graded silica sand. Soil Sci. Soc. Am., Proc., 5: 390-398.

FUJIOKA, Y. and KITAMURA, T. (1964). Approximate solution of a vertical drainage problem. J. Geophysical Res., 69: 5249-5255.

GARDNER, W.R. (1962). Approximate solution of a non-steady-state drainage problem. Soil Sci. Soc. Am., Proc., 26: 129-132.

GRAECEN, E.L. (1960). Water content and soil strength. J. Soil Sci., 11: 313-333.

GURR, C.G. (1962). Use of gamma rays in measuring water content and permeability in unsaturated columns of soil. Soil Sci., 94:224-229.

GURR, C.G. (1964). Calculation of soil water contents from gamma ray readings. Aust. J. Soil Res., 2: 29-32.

KLUTE, A. and GARDNER, W.R. (1962). Tensiometer response time. Soil Sci., 93: 204-207.

KLUTE, A. and PETERS, D.B. (1962). A recording tensiometer with a short response time. Soil Sci. Soc. Am., Proc., 26: 87-88.

LEONARD, R.A. and LOW, P.F. (1962). A self-adjusting, null-point tensiometer. Soil Sci. Soc.Am., Proc., 26: 123-125.

LINSLEY, R.K. (1964). Report of AGU Committee on Status and Needs in Hydrology. Trans. Am. Geophysical Union, 45: 693-698.

MILLER, R.D. (1951). A technique for measuring soil-moisture tensions in rapidly changing systems. Soil Sci., 72: 291-301.

PECK, A.J. (1965a). Moisture profile development and air compression during water uptake by bounded porous bodies: 2. Horizontal Columns. Soil Sci., 99: 327-334.

PECK, A.J. (1965b). Moisture profile development and air compression during water uptake by bounded porous bodies: 3. Vertical Columns. Soil Sci., In press.

PHILIP, J.R. (1957). The theory of infiltration: 1. Soil Sci., 83: 345-357.

PHILIP, J.R. (1964). Similarity hypothesis for capillary hysteresis in porous materials. J. Geophysical Res., 69: 1553-1562.

PILGRIM, D.H. (1965). Correction of ratemeter readings with varying count rates for response time lag. J. App. Rad. and Isotopes, 16: 461-472.

POULOVASSILIS, A. (1962). Hysteresis of pore water, an application of the concept of independent domains. Soil Sci., 93: 405-412.

POWERS, W.L. (1934). Soil water movement as affected by confined air. J. Agric. Res., 49: 1125-1133.

RAWLINS, S.L. (1961). A theoretical and experimental examination of the validity of diffusion analysis as applied to unsaturated flow of water. Ph.D. Thesis. Washington State University.

REMSON, I., DRAKE, R.L., McNEARY, S.S. and WALLO, E.M. (1965).
Vertical drainage of an unsaturated soil. J. Hyd. Div., ASCE,
91, HY1, 55-74.

RICHARDS, L.A. (1949). Methods of measuring soil moisture tension.
Soil Sci., 68: 95-112.

WANG, Flora G., HASSAN, N.A. and FRANZINI, J.B. (1964). A method
of analyzing unsteady, unsaturated flow in soils. J. Geophysical
Res., 69: 2569-2577.

WATSON, K.K. (1963). An apparatus for studying the non-continuous
transient flow of water in unsaturated soil columns. Proc. Fourth
Aust. - N.Z. Conf. Soil Mech. and Foundation Eng., 244-246.

WATSON, K.K. (1964). The measurement of rapidly changing moisture
contents by gamma-ray absorption using the ratemeter recorder
instrumentation. Proc. Second Biennial Conf., Aust. Road Res.
Board, 2: 951-962.

WILSON, L.G. and LUTHIN, J.N. (1963). Effect of air flow ahead of
the wetting front on infiltration. Soil Sci., 96: 136-143.

YOUNGS, E.G. (1960). The hysteresis effect in soil moisture studies.
Trans. Intern. Congr. Soil Sci., Seventh Congr., Madison, 1:107-113.

YOUNGS, E.G. (1960). The drainage of liquids from porous materials.
J. Geophysical Res., 65: 4025-4030.

YOUNGS, E.G. (1964). An infiltration method of measuring the
hydraulic conductivity of unsaturated porous materials. Soil Sci.,
97: 307-311.

YOUNGS, E.G. and PECK, A.J. (1964). Moisture profile development
and air compression during water uptake by bounded porous bodies:
1. Theoretical introduction. Soil Sci., 98: 290-294.

## ACKNOWLEDGEMENTS